Design of a wideband conformal array antenna system with beamforming and null steering, for application in a DVB-T based passive radar

Master of Science Thesis

Vedaprabhu Basavarajappa

Student number: 4121910

03-July-2012

Supervisors:

Dr. Massimiliano Simeoni and Dr. Peter Knott

Delft University of Technology

Department of Telecommunications

The undersigned hereby certify that they have read and recommend to the Faculty of Electrical Engineering, Mathematics and Computer Science for acceptance a thesis entitled "**Design of a wideband conformal array antenna system with beamforming and null steering, for application in a DVB-T based passive radar**", by **Vedaprabhu Basavarajappa** in partial fulfilment of the requirements for the degree of Master of Science in Electrical Engineering.

Dated: 03-July-2012

Committee members

____

Prof. Dr. A. Yaravoy (Chair)

____

Dr. M. Simeoni

____

Dr. P. Knott

____

Dr. Ir. B. J. Kooij

____

Dr.ing. I.E. Lager

Acknowledgments

I would like to express my sincerest thanks to Dr. Peter Knott who was my supervisor at Fraunhofer FHR for his constant support and encouragement. I am very grateful to my supervisor at TU Delft, Dr. Massimiliano Simeoni for having provided this opportunity and for his constant support and motivation and for providing valuable feedback to my work at Fraunhofer FHR. I would also like to extend my heartiest thanks to my graduation professor Prof. Dr. Alexander Yaravoy for his support and for his valuable feedbacks. I would also like to thank Dr. Daniel O' Hagan of PSK group at FHR for his valuable inputs.

I would like to extend my thanks to my friends at Fraunhofer FHR for having provided me with a wonderful atmosphere where I could carry out my thesis. I also thank my friends at TU Delft for their support.

Last but not least, I would like to offer my heartiest thanks to my family whose constant encouragement and support played a vital role.

Finally, I would like to thank everyone involved both directly and indirectly in the completion of my thesis.

Vedaprabhu Basavarajappa

Wachtberg, Germany

04 June, 2012

Abstract

The use of radars in detecting low flying, small targets is being explored for several decades now. However radar with counter-stealth abilities namely the passive, multistatic, low frequency radars are in the focus recently. Passive radar that uses Digital Video Broadcast Terrestrial (DVB-T) signals as illuminator of opportunity is a major contender in this area. A DVB-T based passive radar requires the development of an antenna array that performs satisfactorily over the entire DVB-T band. At Fraunhofer FHR, there is currently a need for an array antenna to be designed for operation over the 450-900 MHz range with wideband beamforming and null steering capabilities. This would add to the ability of the passive radar in detecting covert targets and would improve the performance of the system. The array should require no mechanical adjustments to inter-element spacing to correspond to the DVB-T carrier frequency used for any particular measurement. Such an array would have an increased flexibility of operation in different environment or locations.

The design of such an array antenna and the applied techniques for wideband beamforming and null steering are presented in the thesis. The interaction between the inter-element spacing, the grating lobes and the mutual couplings had to be carefully studied and an optimal solution was to be reached at that meets all the specifications of the antenna array for wideband applications. Directional beams, nulls along interference directions, low sidelobe levels, polarization aspects and operation along a wide bandwidth of 450-900 MHz were some of the key considerations.

Table of Contents

List of Figures

List of acronyms

ADC	Analog to Digital Converter
AF	Array Factor
CORA	COvert RAdar
CST	Computer Simulation Technology
DAB	Digital Audio Broadcast
DOA	Direction Of Arrival
DVB-T	Digital Video Broadcast –Terrestrial
FFT	Fast Fourier Transform
FIT	Finite Integration Technique
FM	Frequency Modulation
FPGA	Field Programmable Gate Array
GPU	General Processing Unit
HF	High Frequency
LMS	Least Mean Squares
LNA	Low-Noise Amplifier
MoM	Method of Moments
MWS	Microwave Studio
NEC	Numerical Electromagnetic Code
NLMS	Normalized Least Mean Squares
PCL	Passive Coherent Location
PCR	Passive Covert Radar
RCS	Radar Cross Section
RDE	Radar Data Extractor
RLS	Recursive Least Squares
RF	Radio Frequency
SIR	Signal to Interference Ratio
SLL	Side Lobe Level
SMI	Sample Matrix Inversion
TR	Transmit-Receive
UCA	Uniform Circular Array
UHF	Ultra High Frequency
VHF	Very High Frequency

List of symbols

β	Phase difference
d	Spacing between antenna elements
$\vec{\mathrm{E}}_{\mathrm{t}}$	Total electric field
κ	Wavenumber
θ	Elevation angle
ϕ	Azimuthal or horizontal angle
λ	Wavelength
AF	Array factor
M	Number of elements on *x*-axis of planar array
N	Number of elements on *y*-axis of planar array
D_0	Maximum directivity
a	Circular ring radius
$u_N(t)$	Received signal in the N^{th} antenna
R(t)	Covariance matrix
$\hat{R}$	Correlation matrix
$e(n)$	Error function
$E(x)$	Expectation of *x*
μ	Step size
$M_L(u)$	Lower mask
$M_U(u)$	Upper mask
E	Field matrix

Chapter 1- Introduction

Radars have long been used for detection and tracking of flying targets. There are numerous examples in the literature to substantiate the fact that a successful detection and tracking of the target is possible to the highest accuracies. However many of these active radars are prone to be detected as they inherently have to transmit signals to detect a target. Thus active radars are vulnerable to localisation due to the fact that they cannot operate without transmitting energy, though their need in the military as means to detect enemy air or naval targets cannot be undermined. A radar location could be determined by receiving the radar signals and using triangulation. The location being known could lead to jamming and destruction of radar systems. Thus the advantage of silent operation without revealing ones position was obvious and therefore the idea to have passive radars was implanted in construction during the early days of radars itself [1].

A classical monostatic radar is shown in Figure 1. An electromagnetic pulse is sent by the radar transmitter towards the target. The reflected pulse is measured by the radar receiver. The transmitter and the receiver are collocated. The accurate position of the target can be detected with the help of directional antennas. The velocity and Doppler of the target can also be estimated.

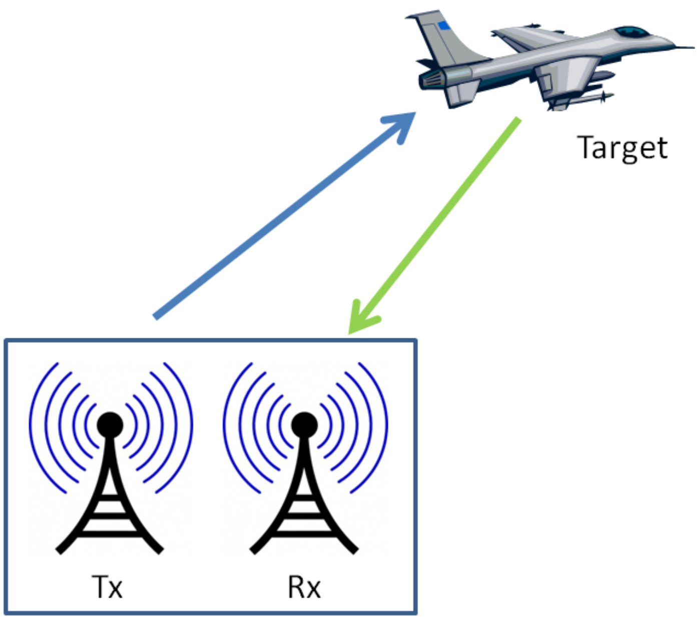

Figure 1. Classical monostatic radar principle

Passive radars operate on the principle of using either transmitters of opportunity or co-operative transmitters. The signal received directly from a transmitter of opportunity is cross correlated with its reflections from a target. Using a passive radar receiver and an independent transmitting antenna, a target can be located along an ellipse. The antennas are located at the foci of the ellipse. To resolve a target's location without much uncertainty, multiple such transmitter receiver pairs are needed, allowing the target to be tracked at the intersection of the resulting ellipses [4]. The accuracy of the target position strongly depends on the bandwidth of the used signal and the receiver antenna beam width.

A classical passive radar scenario with a single target is shown in Figure 2. It is assumed that the moving target is illuminated by multiple transmitters of opportunity and the reflected signal is received by the passive radar. The direct signal from the transmitter is also received at the reference antenna in the passive radar. These two signals are cross correlated to detect and track the target efficiently.

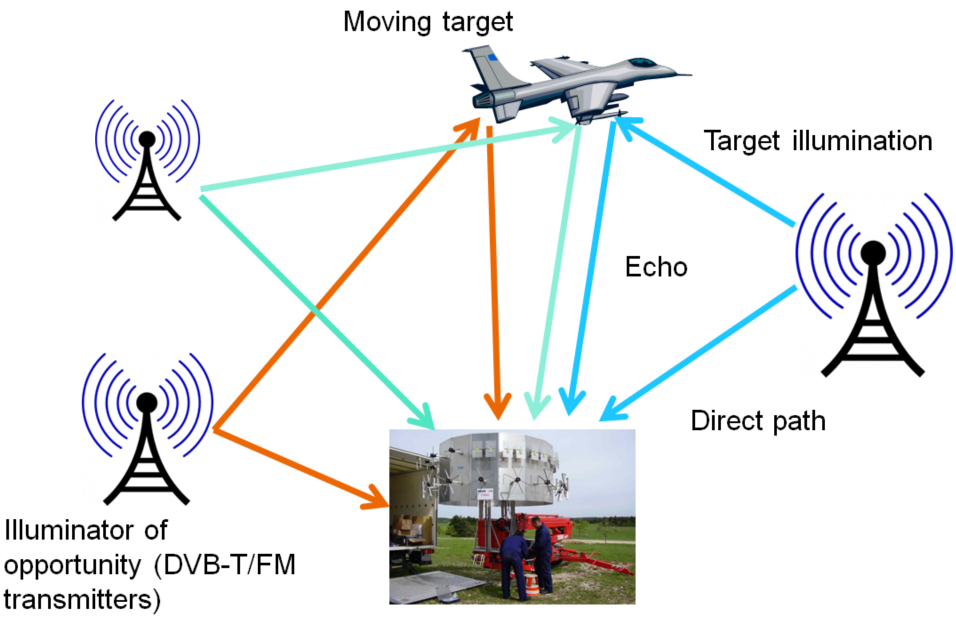

Figure 2 . A passive radar operating with single target and multiple transmitters.

1.1 About passive radar - A Brief history of passive radar

The passive radar was first built before the World War II. It dates back to 1935 when Sir Robert Watson-watt conducted an experiment to detect a Heyford bomber aircraft by the illumination from a shortwave BBC Empire transmitter at Daventry which is shown in Figure 3

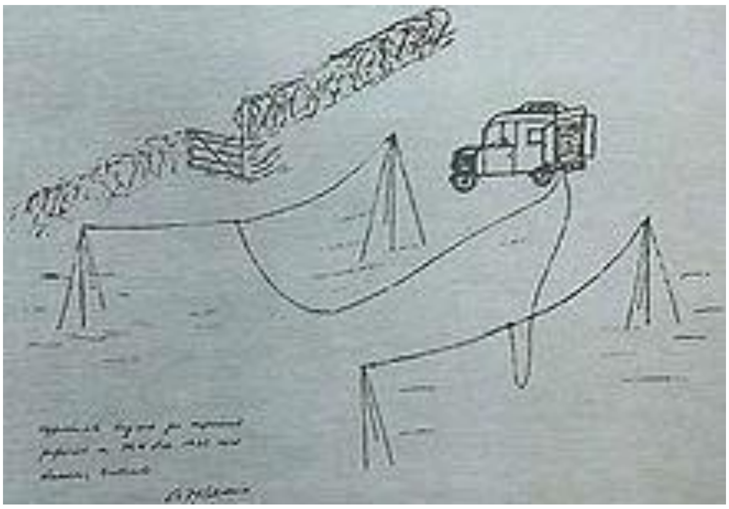

Figure 3. Daventry experiment [5]

Robert Watson-Watt and his assistant Arnold Wilkins conducted the experiment and as the Heyford bomber flew overhead the signal of the transmitter which was being received and displayed on the oscilloscope began to fluctuate indicating that a measurable and variable amount of radio signal was being reflected from the flying bomber. Thus the successful implementation of passive radar was first demonstrated [2].

After World War II, and recently many studies on passive radar have been done. The first commercial Passive radar using FM radio broadcast emissions was developed by Lockheed and Martin and called the "Silent Sentry" [3]. Thales developed a HA100 antenna for this purpose. The group at UCL, London has been investigating use of analogue TV transmission for detection of aircrafts. Fraunhofer FHR have recently developed PCR sensor CORA for exploitation of DAB and DVB-T signals as shown in Figure 4.

Figure 4. PCR sensor CORA of Fraunhofer FHR [5]

Benefits of passive radar

The passive radar has many benefits. Some of them are listed here:

- **Cost**: The receivers use passive components which are usually cheaper. Operations and maintenance costs are also low due to lack of transmitters and moving parts. Also passive radars use a third party's transmitter and hence is cheaper and more reliable to run
- **Stealth operation**: The opponent being detected is unaware that they are being scanned.
- **Wide area**: Passive radar can detect targets over a wide area often measured in several kilometres.
- **Continuous detection**: Passive radars detect targets continuously, typically once in a second.
- **No frequency allocation** is required for the radar frequency though it is required in the DVB-T signal.
- **Environment friendly**: Allowing the radar to be setup in areas where normal radars would not be allowed to as there is no exposure to extra EM radiation
- **Relatively inexpensive**: as they require nothing more than a digital receiver system, stable oscillators and an adequate signal processing capability

1.2 Motivation for the type of antenna design for passive radar

There are several illuminators of opportunity available. DVB-T is one such digital TV signal that is widely in use across Europe. Such multi-static transmitter networks are found in the digital broadcast service nets for radio (DAB) and television (DVB-T) with bandwidths ranging from 1.5 to 7 MHz and transmit powers between 1 and 10 kW. The receiver becomes difficult to locate when the DVB-T signals are employed for radar purposes. The VHF/UHF frequency range has anti-stealth capability i.e the ability to counter stealth. Radars that use these frequencies can counter the threat of stealth aircraft as stealth shaping does not help against low frequency waves due to half-wave resonance effects. These are returns generated when the wavelength of the wave is roughly twice the size of the target, thus returning one full wavelength of measurement to the receiver antenna allowing a picture to be obtained [6] Simultaneous multistatic illuminations under different aspect angles can be done. Increased multistatic coverage adds to the detection of low flying targets. Passive, multi-static, low frequency radars are thus of tremendous use in anti-stealth and detection of low flying objects.

A passive radar that operates in the DVB-T frequency range requires an antenna that should have beamforming capabilities like main beam steering and null steering in order to be able to direct a main beam pointing in the desired signal's direction and nulls along the direction of interference. This can be best realized by using an array antenna. The array antenna element should be operational over a wideband of DVB-T namely the 450MHz to 900 MHz. Such an antenna element was built at the Fraunhofer FHR. It uses a Discone element. This Discone element is to be arranged in a suitable array geometry.

One option in design of an array would be to have an array operating at 450 MHz, another array optimized for 900 MHz and another possibly for 675 MHz. It would necessitate a mechanically adjustable array one in which the inter element spacing can be adjusted with the frequency of operation or to switch between the individually designed arrays. To have an array capable of providing satisfactory performance without requiring mechanical adjustment would be of great value for use in DVB-T based passive radar. Digital waveforms like DVB-T signals offer wide bandwidth channels which allow achieving good spatial resolution. Moreover, they have spectral properties which are nearly independent of the signal content [7]. During the course of the thesis the design and implementation of such an antenna array was aimed at.

1.3 Identification of the problem

Considering the scenario described above, the problem can be identified as to design a circular cylindrical antenna array for a passive radar system in the DVB-T frequency range using Discone antenna element and to find the optimum array geometry that would allow for beamforming and null steering to be performed on it. An investigation of the performance of the design is eventually done.

The element to be used in the array was designed at Fraunhofer FHR earlier. The goal is to adopt the existing element in an array to achieve wideband capabilities for the array. It is required to find array dimensions allowing for beam steering with low side-lobes / deep nulls of required bandwidth and to specify parameters for antenna fabrication such as the polarization and the type of array grid.

Approach adopted:

Step 1: Literature review of the general properties of antenna arrays, beam forming techniques and adaptive null steering and implementation of algorithms for beamforming and null steering in MATLAB.

Step 2: Used simplified NEC-2 model of Discone antenna for principal array analysis (proof-of-concept). The 4NEC2 Discone model to be used was to operate in the 450 -900 MHz. The Discone model available in the Library of NEC2 was operable in the 7 MHz range. This model had to be adopted to operate in the 450 -900 MHz range.

Step 3: Full wave analysis using CST of arrangement of the Discone element in the circular array fashion with the appropriate radius of the array and inter element spacing. This was done by a series of parametric studies at different positions of the elements.

Step 4: The Discone array was simulated to get the radiation pattern in the azimuthal plane at steps of 5 MHz between 450-900 MHz using full wave analysis using CST. The data of the simulation was read into Matlab and then processed to perform the beam forming and null steering.

Step 5: Investigation of the influence of support structure and improvement of antenna mount.

Step 6: Fabrication and testing of the designed array antenna (to be performed in near future)

1.4 Challenge of the work and methodology adopted

Within the framework outlined in detail above the challenge was to find a suitable antenna array topology for application in the DVB-T range that would also additionally allow for beamforming and null steering. The interaction between the interelement spacing, the grating lobes and the mutual coupling had to be carefully studied and an optimal solution was to be reached at that meets all the specifications of the antenna array as described above. Directional beams, nulls along interference directions, low sidelobe levels, polarization, and operation along a wide bandwidth of 450-900 MHz were some of the key considerations. The major challenge was in the difficulty of satisfying all of these constraints simultaneously.

1.5 Outline of the thesis

Chapter 1 introduces the topic and discusses about passive radar. It also defines the problem, the aim of work and approach followed. Chapter 2 deals with the relevant theoretical background. It discusses the different kinds of array and related array antenna theory. The choice of circular array and the array architecture are explained. The phase mode theory of circular arrays and wideband beamforming and null steering theory are discussed. Chapter 3 describes the beamforming algorithms- the conventional ones and compares them. It also introduces the Bucci beamforming algorithm. Chapter 4 details the CORA radar system and the architecture of the antenna array. Chapter 5 presents simulation studies performed and design of the antenna array alongwith beamforming and null steering. The results of 4NEC2 and CST MWS are presented. Chapter 6 describes the experimental setup. Chapter 7 concludes by listing the prominent outcomes and possible suggestions for future work.

Chapter 2 – Theoretical background

The work presented here has scope across multiple dimensions. It involves the concepts in individual antenna element design to design of an array, while also covering the beamforming and null steering concepts. The theory to be dealt with spans across these domains.

2.1. Design of the discone antenna element

The Discone antenna element [8] for the array was chosen due to several reasons. Prominent among these were:

- The large bandwidth
- Omnidirectional coverage
- Low cost
- Ease of fabrication

A discone antenna is in principle a biconical antenna where one of the cones is replaced by a disk-shaped ground plane. The disk is mounted on top of the cone. This structure was first developed by Kandoian in 1945. Discones have linearly polarized radiation patterns like a monopole. Due to the strict vertical polarization of the Discone antenna, it exhibits higher cross-polarization. The radiation pattern is near omnidirectional in the azimuth plane for about one octave and the impedance bandwidth can be upto 10:1. In the elevation plane radiation pattern, it is toroidal shaped.

The Discone antenna has three components: the disk, the cone and the insulator as in Figure 5. The diameter of the top of the cone depends on the diameter of the coaxial cable used to feed the antenna. A coaxial line outer conductor is connected to the cone and the inner one is connected to the ground disk. The insulator keeps the disk and cone apart. The antenna's input impedance depends on the cone angle and disk to cone spacing.

Design rules

- The Length *l* of the cone elements should be a quarter wavelength of the minimum operating frequency.
- The diameter of the top of the cone depends on the diameter of the coaxial cable and determines the upper frequency limit of the antenna: the smaller the diameter the higher the frequency.
- The disk elements should have an overall length *r* of 0.7 times a quarter wavelength at the minimum frequency.
- The slant height of the cone is equal to a full free space quarter wavelength at the lowest frequency of interest.

The Discone antenna used in the scope of this project was designed earlier by the group [8] at Fraunhofer FHR to operate over a frequency range of 450 to 900 MHz for DVB-T system. It is a very small antenna, but very effective. This broadband antenna which has omnidirectional H-plane pattern and vertical polarization is meant to be element of the array.

The Discone antenna dimensions are shown in Figure 5 as derived in [9]

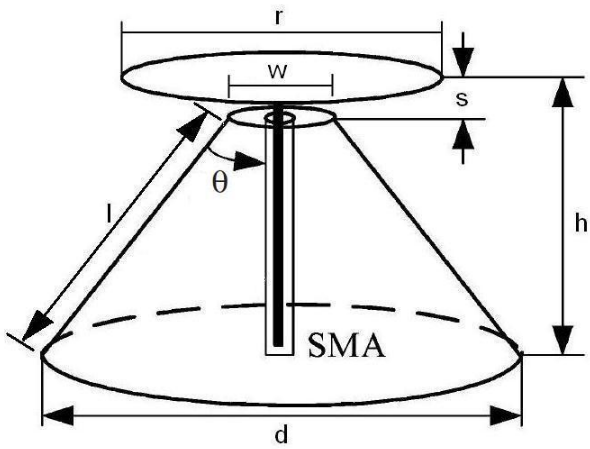

r=150 mm, *l*=210mm, *d*=194mm*, s*=8mm, *w*=20mm

Figure 5. Discone antenna and parameters [9]

The return loss (|S_{11}|) characteristics of the antenna are shown in Figure 6.

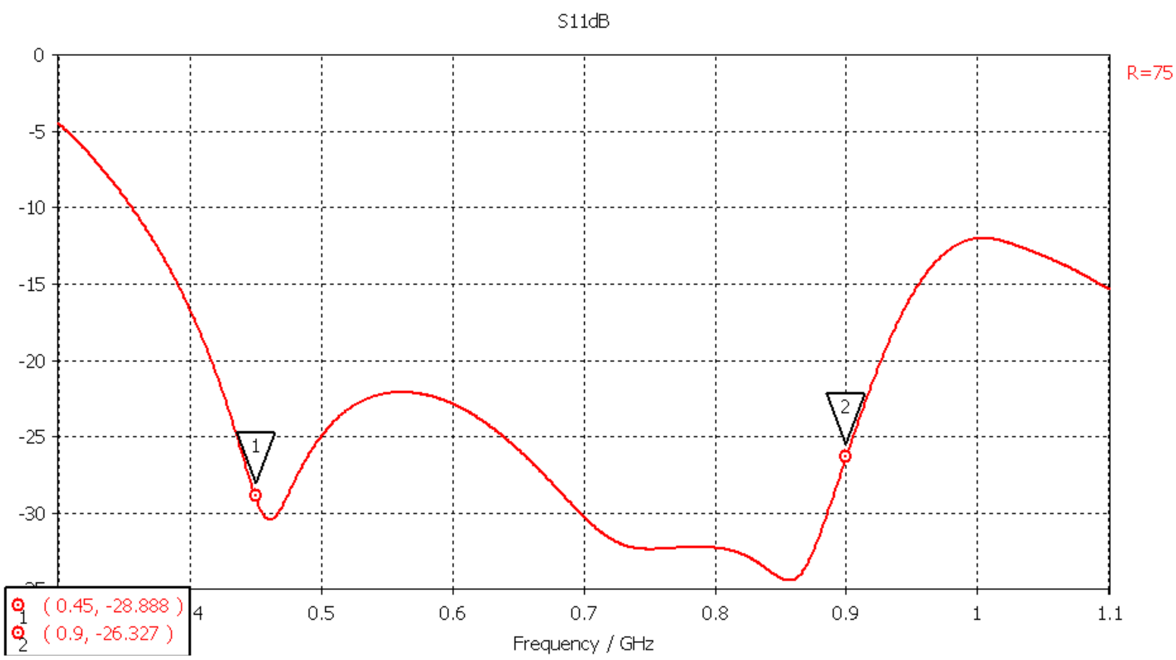

Figure 6. Return loss of the Discone antenna [9]

2.2 Array antenna theory

In this section a review of all the important and relevant topics related to antenna array theory is done. This includes the properties of linear array, phased array, planar array and the circular array.

Individual antennas generally have rather wide radiation patterns that lead to low directivity. Some applications like radar, radio links, remote sensing require high directivity beams and therefore need very directive antennas. There are two possibilities to achieve this:

1) Increasing the physical dimensions of the antennas such as a dipole antenna results in more directional beams. An increase in electrical size of the antenna generally results in directive beams
2) Arranging the single antennas in assemblies thereby generating a complex radiating structure called array antenna

Array antennas are arrangements of usually identical radiators assembled in a specific geometrical configuration to produce highly directive radiation.

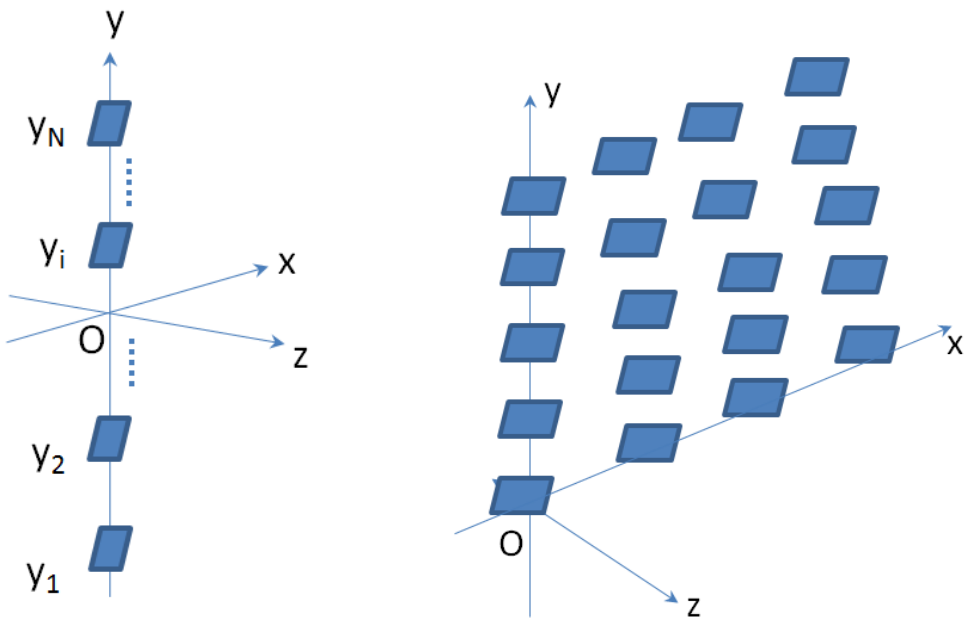

Figure 7. Linear and planar array depiction

The total field radiated by an array-antenna is the superposition of the fields radiated by the individual radiators. To produce high directivity the fields radiated by the individual radiators have to add up coherently in the desired direction and cancel out in the other directions [10]. Linear and planar arrays are depicted in Figure 7.

In order to achieve this high directivity there are several degrees of freedom that can be used. These are namely[10]:

- The relative displacement within the geometrical arrangement
- The excitation amplitude and phase
- The relative pattern of different elements

2.2.1 Two element array

Consider two infinitesimal dipoles aligned along the z axis excited with a phase difference of β radians as shown in Figure 8.

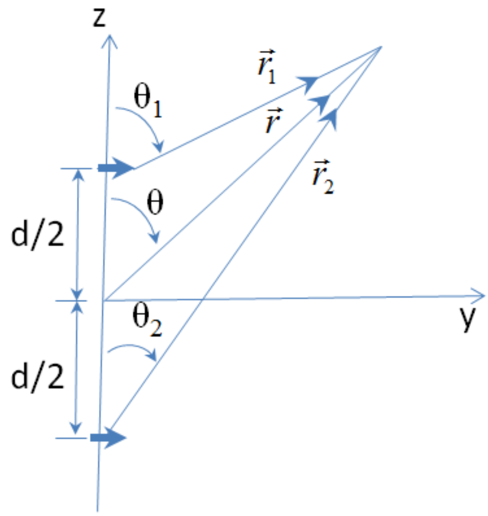

Figure 8. Two dipoles placed along the z axis

The total field in the *yz* plane is given by

$$\vec{E}_t = \vec{E}_1 + \vec{E}_2$$
$$\vec{E}_t = \hat{a}_\theta j\eta \frac{\kappa I_0 l}{4\pi}\left[\frac{e^{-j[kr_1-(\beta/2)]}}{r_1}\cos\theta_1\right] + \hat{a}_\theta j\eta \frac{\kappa I_0 l}{4\pi}\left[\frac{e^{-j[kr_2+(\beta/2)]}}{r_2}\cos\theta_2\right] \tag{1}$$

Under far field conditions $\theta_1 \cong \theta_2 \cong \theta$, as in Figure 9

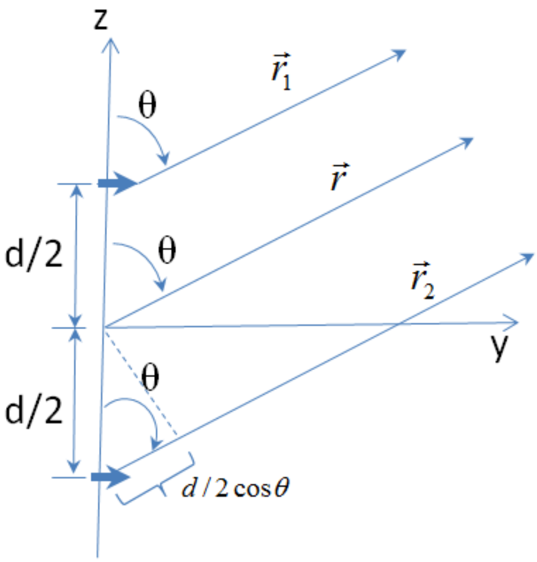

Figure 9. Two dipoles placed along the *z* axis under farfield condition

For the phase variations we have

$$r_1 \approx r - \frac{d}{2}\cos\theta \qquad (2)$$
$$r_2 \approx r + \frac{d}{2}\cos\theta$$

For the amplitude variations, under the assumption of Rayleigh distance criterion for far fields[10]

$$r_1 \approx r_2 \approx r \qquad (3)$$

The total field can now be approximated as [10]

$$\vec{E}_t = \hat{a}_\theta j\eta \frac{kI_0 l e^{-jkr}}{4\pi r}\cos\theta\left[e^{+j(kd\cos\theta+\beta)/2} + e^{-j(kd\cos\theta+\beta)/2}\right] \qquad (4)$$
$$\vec{E}_t = \hat{a}_\theta j\eta \frac{kI_0 l e^{-jkr}}{4\pi r}\cos\theta\left\{2\cos\left[\frac{1}{2}(kd\cos\theta+\beta)\right]\right\}$$

In a two element array of identical elements, the principle of pattern multiplication applies:

$$\vec{\mathrm{E}}_t = \vec{\mathrm{E}}_{\text{singleelement}} \text{ x Array factor (AF)} \qquad (5)$$

The pattern multiplication when performed for different *d* and *θ* values results in the following cases:

Case 1: d= λ/4, β=0

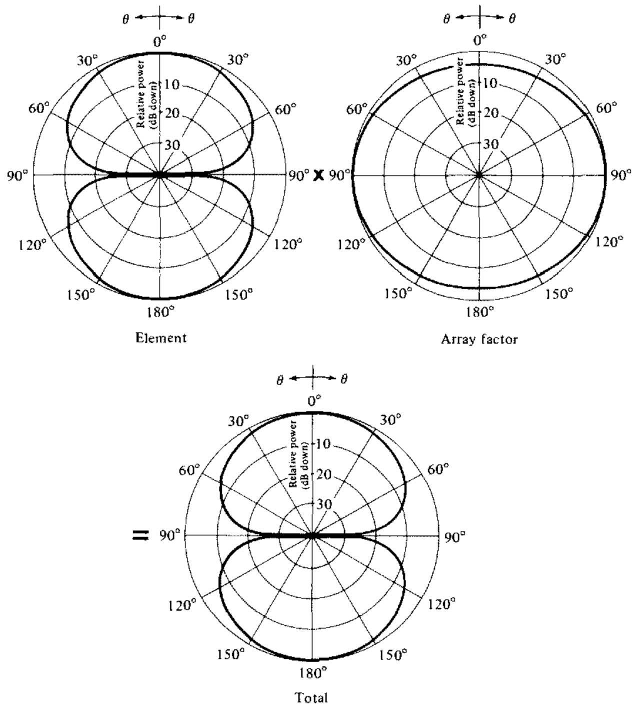

Figure 10(a). Illustration of principle of pattern multiplication when *d*= λ/4 and a) β = 0° [10]

Case 2: *d*= *λ*/4, β =90°

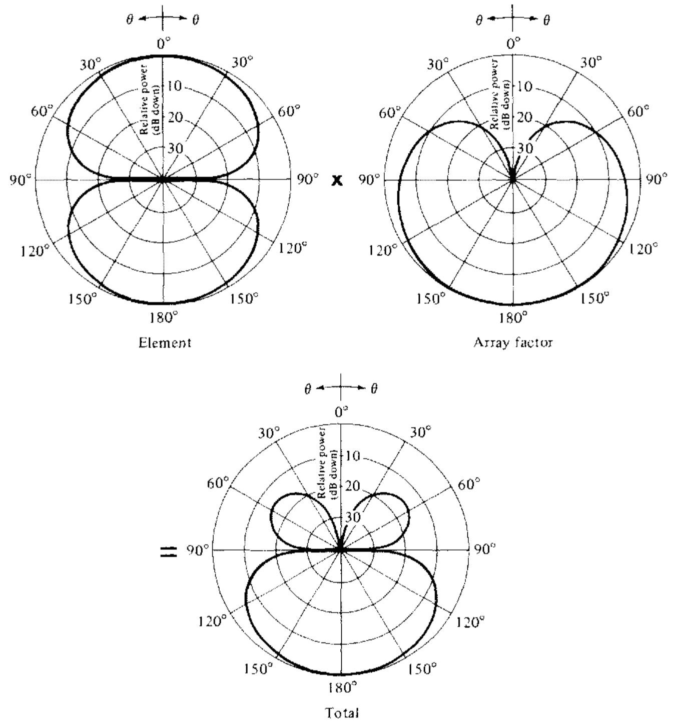

(b)

Figure 10(b). Illustration of principle of pattern multiplication when *d*= λ/4 and a) β = 90° [10]

Case 3: $d= \lambda/4$, $\theta= -90°$

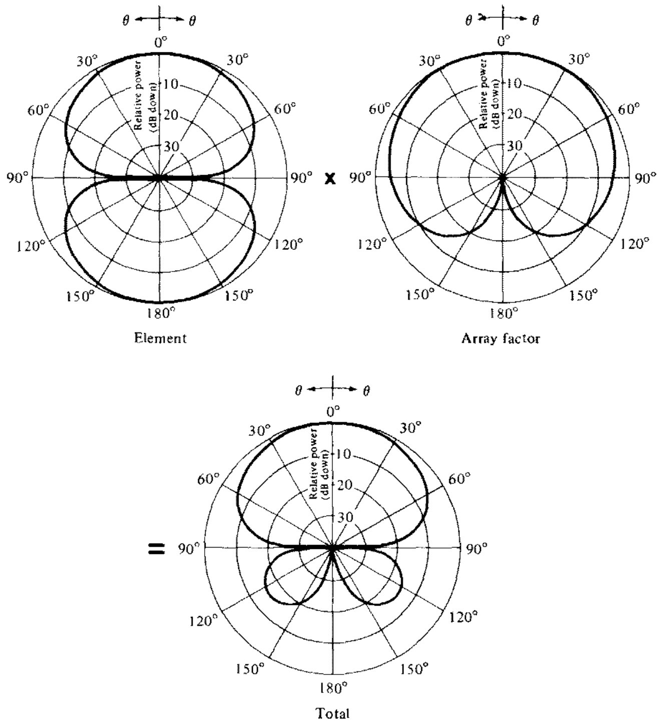

Figure 10(c). Illustration of principle of pattern multiplication when $d= \lambda/4$ and $\theta= -90°$ [10]

2.2.2 *N* element array

Consider N identicalelements aligned along the z axis at arbitrary locations $z_1, z_2, z_3, .. z_N$. The elements are fed with different amplitude and phase. Each element has a potentially different radiation pattern. The arrangement is shown in Figure 11

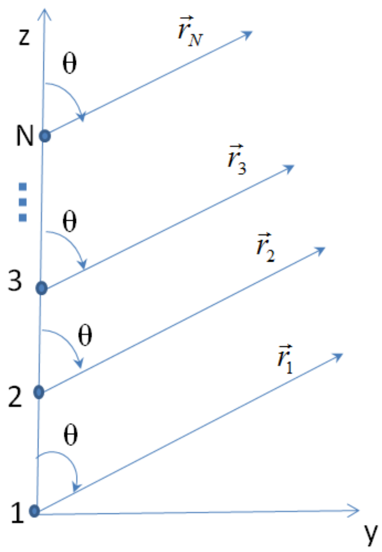

Figure 11. *N* element array

The total radiated field in the far zone is

$$\vec{E}_t(\theta,\phi) = \frac{e^{-jkr}}{4\pi r}\sum_{n=1}^{N} a_n \vec{f}_n(\theta,\phi) e^{j(kz_n\cos\theta+\beta_n)} \tag{6}$$

where $\vec{f}_n(\theta,\phi)$ is the electric field radiation pattern of the individual radiator

If the elementary radiators are identical[10]

$$\vec{E}_t(\theta,\phi) = \frac{e^{-jkr}}{4\pi r}\vec{f}(\theta,\phi)\sum_{n=1}^{N} a_n e^{j(kz_n\cos\theta+\beta_n)} \tag{7}$$

The term inside the summation is array factor (AF). The array factor would correspond to the normalized radiation pattern of the array if the identical individual antennas were isotropic radiators. The array factor is a function of the location of the antennas in the array and their amplitude and phase excitation coefficients [10].

$$AF(\theta,\phi) = \sum_{n=1}^{N} a_n e^{j(kz_n\cos\theta+\beta_n)} \tag{8}$$

Consider a uniform array, one in which the *N* identical elements are equally spaced, aligned and fed with identical amplitudes and progressive phase difference β as in Figure 12

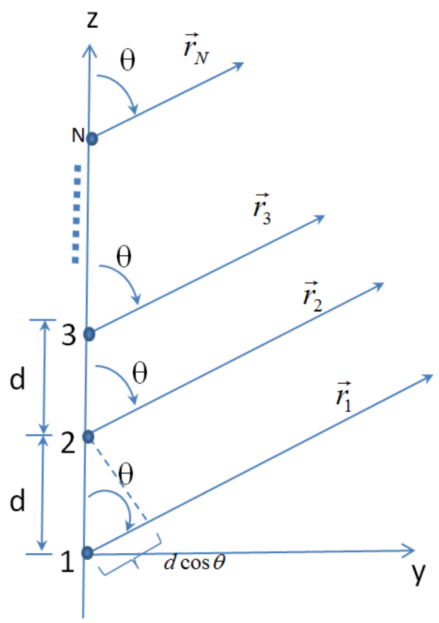

Figure 12. Uniform linear array

Considering the elements to be point sources

$$AF = 1 + e^{j(kd\cos\theta+\beta)} + e^{j2(kd\cos\theta+\beta)} + \ldots.. + e^{j(N-1)(kd\cos\theta+\beta)}$$
$$AF = \sum_{n=1}^{N} e^{j(n-1)(kd\cos\theta+\beta)} \tag{9}$$

The AF can be rewritten in the form

$$AF = \frac{\sin\left(\frac{N}{2}\psi\right)}{\sin\left(\frac{1}{2}\psi\right)} \tag{10}$$

After normalization this becomes

$$AF_n = \frac{1}{N}\left[\frac{\sin\left(\frac{N}{2}\psi\right)}{\sin\left(\frac{1}{2}\psi\right)}\right] \tag{11}$$

Array factor plot for *N*=10 is shown in Figure 13.

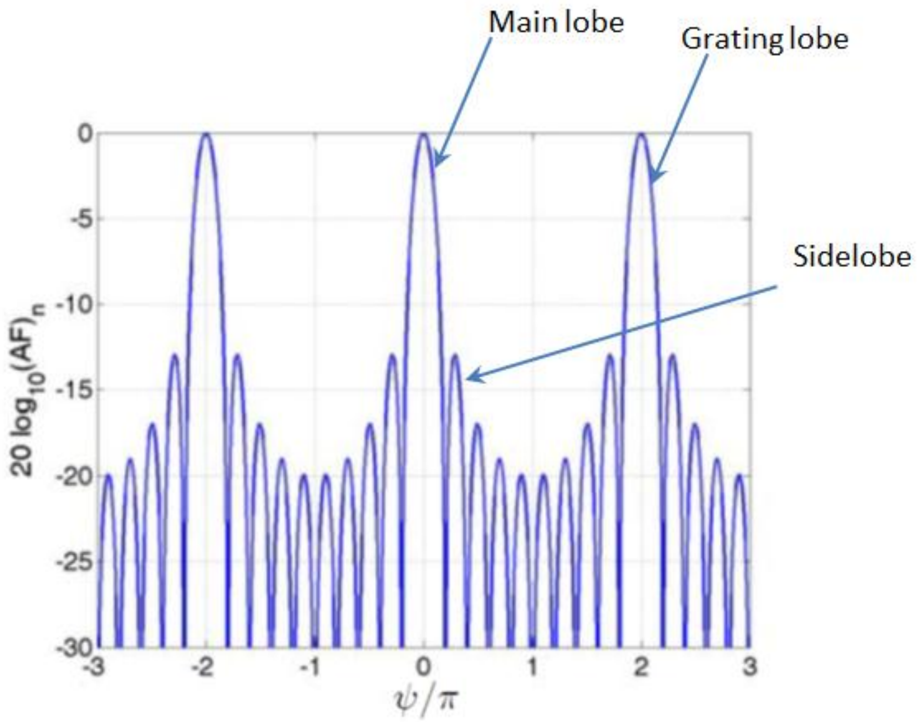

Figure 13. Array factor plot for *N*=10

The positions of the nulls are found for

$$\sin\left(\frac{N}{2}\psi\right) = 0 \tag{12}$$

$$\Rightarrow \theta_n = \cos^{-1}\left[\frac{\lambda}{2\pi d}\left(-\beta \pm \frac{2n}{N}\pi\right)\right] \tag{13}$$

The positions of the maxima are found for

$$\frac{\psi}{2} = \frac{1}{2}(kd\cos\theta + \beta) = \pm m\pi \tag{14}$$

$$\theta_m = \cos^{-1}\left[\frac{\lambda}{2\pi d}\left(-\beta \pm 2m\pi\right)\right] \tag{15}$$

By controlling the progressive phase difference between the elements it is possible to steer the maximum radiation in any desired direction θ_0

$$\theta_0 = \cos^{-1}\left[\frac{\lambda}{2\pi d}\left(-\beta \pm 2m\pi\right)\right] \tag{16}$$

$$\beta = -kd\cos\theta_0 \tag{17}$$

An example of phased array radiation pattern with $\theta_0 = 30^\circ$, $\lambda / d = 3.0$ and *N*=20 is shown in Figure 14

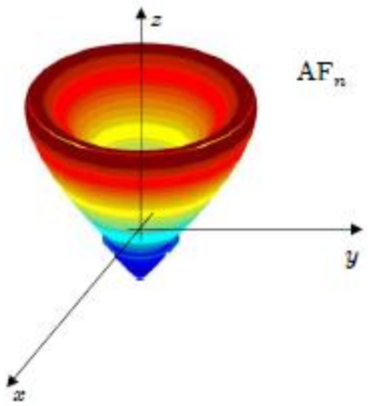

Figure 14. Phased array radiation pattern with $\theta_0 = 30^\circ$, $\lambda / d = 3.0$ and *N*=20 [39]

It is possible to reconfigure the radiation pattern by dynamically changing the feeding phase of the elements and point the maximum radiation in different directions.

A schematic representation of a phased array is shown in the figure 15:

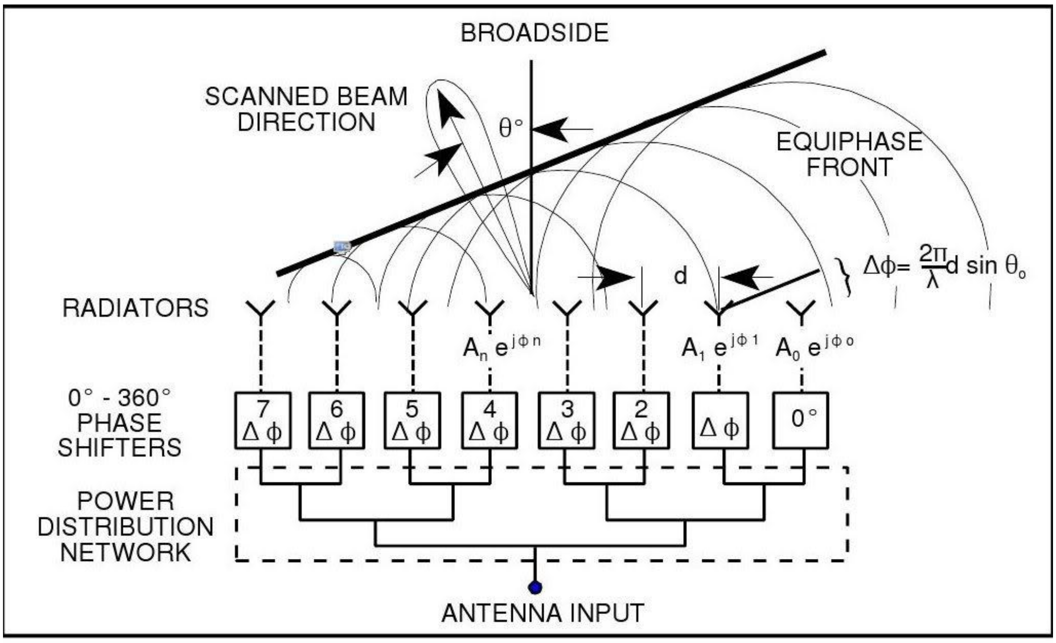

Figure 15. Schematic representation of phased array [33]

In a phase array antenna, each transmit-receive (TR) element is essentially a miniature radar antenna. The antenna computer then modulate individual TR power output and the entire system exploits the wave superposition principle to effect beamforming and to move or electronically 'sweep' the main beam by varying the phases at the individual antenna elements. The amplitudes and taper also influence the beam scanning. If the magnitudes of the excitation currents In are chosen to be tapered across the array instead of equal in magnitude, so that I_0 is largest and $I_{\pm n}$ decrease in magnitude, then θ must move farther from $\pi/2$ to obtain a pattern null than for the uniformly weighted array, and the main lobe is wider. In addition, the phasors add to a smaller value for the sidelobes, and the sidelobe level decreases [11].

Mutual coupling in antenna arrays:

The electromagnetic interaction between the antenna elements in an antenna array is called mutual coupling. The effect of mutual coupling is serious if the element spacing is small.
It will affect the antenna array mainly in the following ways:

1. Change the array radiation pattern
2. Change the array manifold (the received element voltages)
3. Change the matching characteristic of the antenna elements (change the input impedances)

The amount of mutual coupling depends on[10]

1. Radiation characteristics of each antenna
2. Relative separation between them
3. Relative orientation of each antenna

For most practical configurations mutual coupling is difficult to predict analytically but must be taken into account because of its significant contribution.

Isolated pattern and embedded element pattern:

An isolated pattern is the radiation pattern of an element alone without the influence of any neighboring antenna. It is the individual antenna radiation pattern, whereas the embedded element pattern is the radiation pattern in the presence of other antenna elements of the array when only the element under consideration is excited with other elements present passively around it in the array. It is therefore called the embedded element pattern.

Grating lobes in antenna arrays

If $kd > 2\pi$ then for θ large enough, $kd\cos\theta = 2\pi$ and we get another angle in addition to $\theta = \pi/2$ where all the phasors in the array factor sum are aligned, causing another pattern lobe with maximum amplitude. These are called grating lobes, and are usually undesirable. For an array with equal phase excitations, to avoid grating lobes the element spacing must be small enough that $d \le \lambda$. An array with widely spaced elements has many grating lobes, and the radiation pattern has strong peaks at many angles. Grating lobes can be eliminated by reducing the element spacing or suppressed by choosing an electrically large element with narrow radiation pattern [11].

If $d > \lambda$ then at some angle θ away from $\pi/2$, $kd\cos\theta = 2\pi$, and V_n = 1 for all n. The samples of the field at the array elements are too widely spaced to discriminate between the two different plane waves. In order to avoid grating lobes, the elements must be spaced more closely than one element per wavelength. For arrays with steered beams using progressive phase shifts of the element excitations, we must have $d \le \lambda/2$, or at least two elements per wavelength, to avoid grating lobes for all beam steering angles [11]. Since the array essentially samples the incident field at the element locations, grating lobes are simply a manifestation of aliasing.

2.2.3 Planar arrays

Consider a uniform planar array, with *M* elements along the *x* axis, *N* elements along the *y* axis with element spacing d_x, d_y.The feeding signals have uniform amplitude and progressive phase β_x, β_y as shown in the Figure 16.

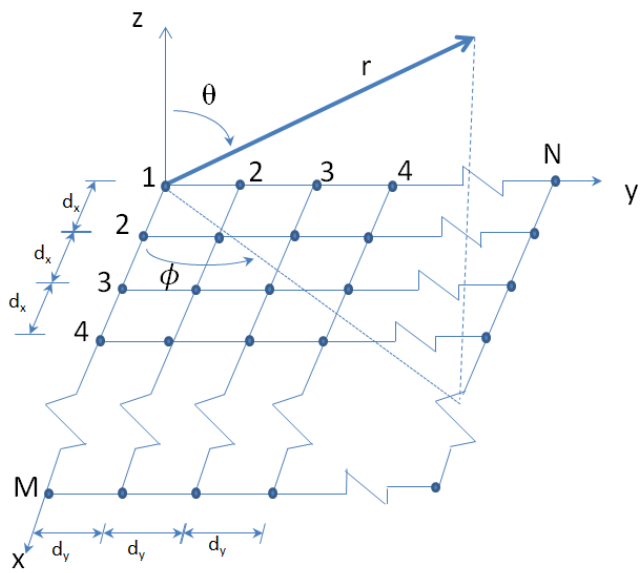

Figure 16. Planar array depiction

The uniform planar array, array factor (AF) is given by [10]

$$AF_n(\theta,\phi) = \left\{ \frac{1}{M} \frac{\sin(M\psi_x/2)}{\sin(\psi_x/2)} \right\} \times \left\{ \frac{1}{N} \frac{\sin(N\psi_y/2)}{\sin(\psi_y/2)} \right\} \tag{18}$$

With,

$$\psi_x = kd_x \sin\theta \cos\phi + \beta_x$$
$$\psi_y = kd_y \sin\theta \sin\phi + \beta_y$$

An example of a planar broadside array pattern with *M*=10, *N*=20, d_x=0.1, d_y=0.2, $\beta_x = \beta_y = 0$, *f*=1GHz is shown in Figure 17.

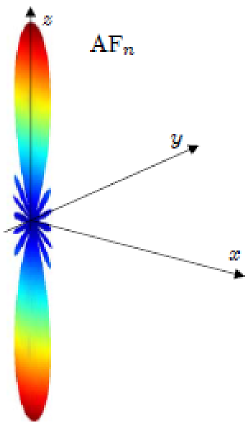

Figure 17. Planar broadside array pattern with *M*=10, *N*=20, d_x=0.1, d_y=0.2, $\beta_x = \beta_y = 0$, *f*=1GHz [39]

By controlling the progressive phase difference between the elements it is possible to steer the maximum radiation in any desired direction (θ_0, ϕ_0)

$$\beta_x = -kd_x \sin\theta_0 \cos\phi_0$$
$$\beta_y = -kd_y \sin\theta_0 \sin\phi_0$$

An example of a planar array pattern with beam along $(\theta_0, \phi_0) = (30^\circ, 45^\circ)$ is shown in Figure 18

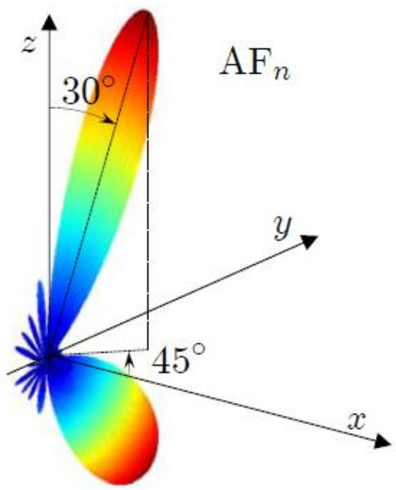

Figure 18. Planar array pattern with beam along $(\theta_0, \phi_0) = (30^\circ, 45^\circ)$ [39]

The maximum directivity than can be achieved in planar arrays is an important factor. It is given by

$$D_0 = \frac{4\pi[AF(\theta_0,\phi_0)][AF(\theta_0,\phi_0)]^*}{\int_0^{2\pi}\int_0^{\pi}[AF(\theta_0,\phi_0)][AF(\theta_0,\phi_0)]^* \sin\theta \, d\theta \, d\phi} \tag{19}$$

For large planar arrays with maximum pointed at small scanning angles the directivity is given by:

$$D_0 = \pi \cos\theta_0 D_x D_y \tag{20}$$

where D_x and D_y represent the directivities of broadside linear arrays of M and N elements respectively.

2.2.4 Circular array

Consider N equally spaced elements on a circular ring of radius a as shown in Figure 19

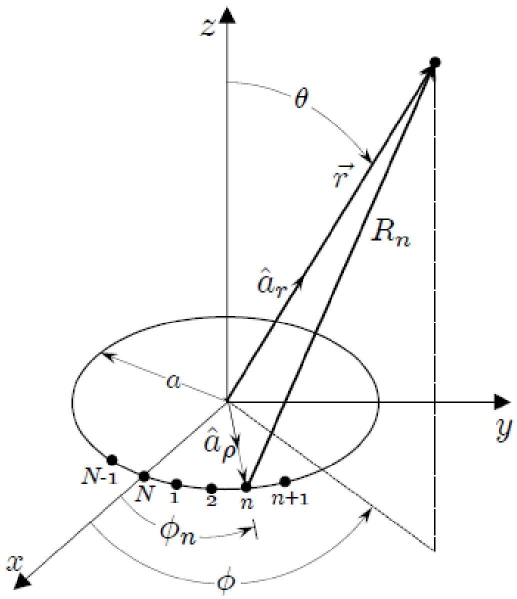

Figure 19. Uniform circular array [10]

The normalized total field is given by

$$E_n(r,\theta,\phi) = \sum_{n=1}^{N} a_n \frac{e^{-jkR_n}}{R_n} \tag{21}$$

a_n are the complex excitation coefficients.

The distance R_n between the n^{th} element and the observation point is:

$$R_n = \sqrt{r^2 + a^2 - 2ar\cos\psi_n} \tag{22}$$

For $r >> a$:

$$
\begin{aligned}
R_n &\cong r - a\cos\psi_n \\
&= r - a(\hat{a}_\rho . \hat{a}_r) \\
&= r - a\sin\theta\cos(\phi - \phi_n)
\end{aligned}
\tag{23}
$$

Where ϕ_n is the angular position of the n^{th} element.

For amplitude variations:

$$
\begin{aligned}
&R_n \cong r \\
&\Rightarrow E_n(r,\theta,\phi) \approx \frac{e^{-jkr}}{r}\sum_{n=1}^{N} a_n e^{+jka\sin\theta\cos(\phi-\phi n)} \\
&with \\
&a_n = I_n e^{j\alpha_n} \\
&\phi_n = 2\pi\left(\frac{n}{N}\right)
\end{aligned}
\tag{24}
$$

The farfield now becomes

$$
\begin{aligned}
E_n(r,\theta,\phi) &\approx \frac{e^{-jkr}}{r}\sum_{n=1}^{N} I_n e^{+j[ka\sin\theta\cos(\phi-\phi n)+\alpha_n]} \\
E_n(r,\theta,\phi) &\approx \frac{e^{-jkr}}{r}\left[AF(\theta,\phi)\right]
\end{aligned}
\tag{25}
$$

Where the array factor is

$$
AF(\theta,\phi) = \sum_{n=1}^{N} I_n e^{+j[ka\sin\theta\cos(\phi-\phi n)+\alpha_n]} \tag{26}
$$

The array factor depends on [10]

- The number of elements (*N*)
- Their excitations (I_n, α_n)
- The radius of the ring (*a*)

The main radiation beam can be directed towards (θ_0, ϕ_0) by setting the excitation phases to

$$
\alpha_n = -jka\sin\theta_0\cos(\phi_0 - \phi_n) \tag{27}
$$

The Array factor for a directional circular array becomes

$$
AF(\theta,\phi) = \sum_{n=1}^{N} I_n e^{jka[\sin\theta\cos(\phi-\phi_n)-\sin\theta_0\cos(\phi_0-\phi_n)]} \tag{28}
$$

One of the principal advantages of circular arrays is their ability to deflect beams electronically through 360 degree with little change of either beam width or sidelobe level. There has been a significant increase of interest in circular arrays for applications of direction finding and electronic support measures systems [12].

The most significant development was made in the 1960s when the concept of phase mode excitation was developed. The lack of applications in the past is due to the fact that the basic problems of exciting circular arrays with the correct values of amplitude and phase are in general more complex than for linear arrays. Also the electronic scanning of directional patterns for circular arrays may be difficult to implement and may require both the amplitude and phase of each element of the array to be changed.

Circular array applications have included Wullenweber arrays for direction finding [13], wide bandwidth HF communication arrays [14], wrap around antennas for ship borne communications [15], navigational aids, spacecraft antennas and null steering antennas for mobile communications applications [16]

The theory of the uniform circular array (UCA) is reviewed in this section[12]. This generic array has elements equally spaced along the periphery of a circle as in Figure 20(a), and the elements are excited with equal phase and amplitude. We will start by an analysis of the radiation in the plane that contains the array, which we refer to as the azimuth (or horizontal) plane. Local coordinates on the circle are (R, φ) , the radius and angle, respectively. Far-field coordinates are indicated by (r, θ , φ) as in Figure 20(b) . We consider element excitations (voltages or currents) as given or specified including the effects of mutual coupling. Limiting the analysis to the azimuth plane only makes the circular array problem a two-dimensional problem, that is, it has bearing on other two-dimensional problems like cylindrical array structures.

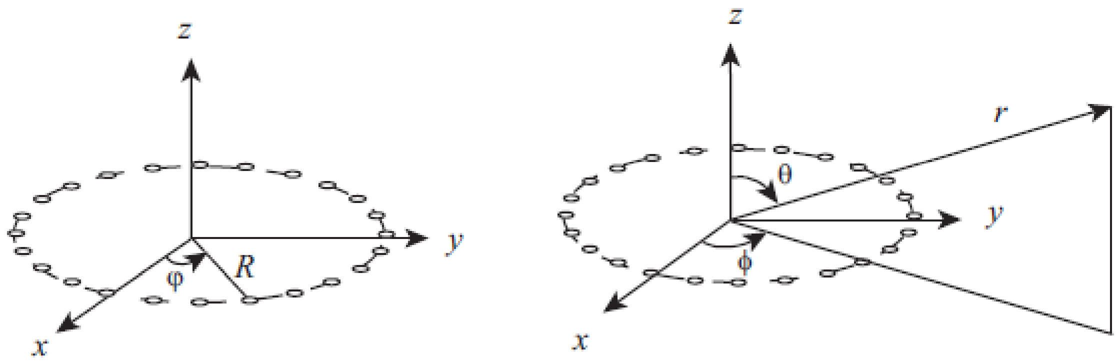

(a) (b)

Figure 20. Local and far field coordinates of the circular array [40]

There are some elementary differences between linear and circular arrays. For the linear array the radiating elements are identical, with equal spacing d, and they all point in the same direction. The far-field radiation function in the azimuth plane is, given by

$$E(\phi) = EL(\phi)\sum_n V_n e^{jknd\sin\phi} \tag{29}$$

where, V_n is the excitation amplitude of element n and k is the propagation constant, $k = 2\pi/\lambda$. The radiation pattern EL(φ) is common to all elements and was therefore brought outside the summation sign in this equation. The radiation function is the product of the EL(φ) and the array factor.
The corresponding far-field expression for the circular array shown in Figure 21, in the azimuth plane is

$$E(\phi) = \sum_n V_n EL(\phi - n\Delta\phi)e^{jkR\cos(\phi - n\Delta\phi)} \tag{30}$$

where the phase has been referenced to the center of the circle. The identical elements are spaced $R\Delta\varphi$ along the circle, each element pointing in the radial direction. The element function can, therefore, in general not be brought outside the summation, since it is a function of the element position; there is no common element factor. Consequently, we can, in general, not define an array factor as in linear and planar arrays, unless the elements are isotropic, that is, have isotropic (omnidirectional) radiation at least in the horizontal plane. A typical example of the latter is an array of vertical dipoles with their axes perpendicular to the array plane. A further difference compared to linear and planar arrays is found in the slightly more complicated phase expression because of the array curvature.

Equation (1) for the linear case is essentially a Fourier relationship between excitation and pattern functions. Much of the experience from Fourier analysis can be directly applied to linear (and planar) arrays, and there are several analogies with well-known time/frequency spectral relationships. Unfortunately, this knowledge is not so easily applied to the analysis of circular and conformal arrays.

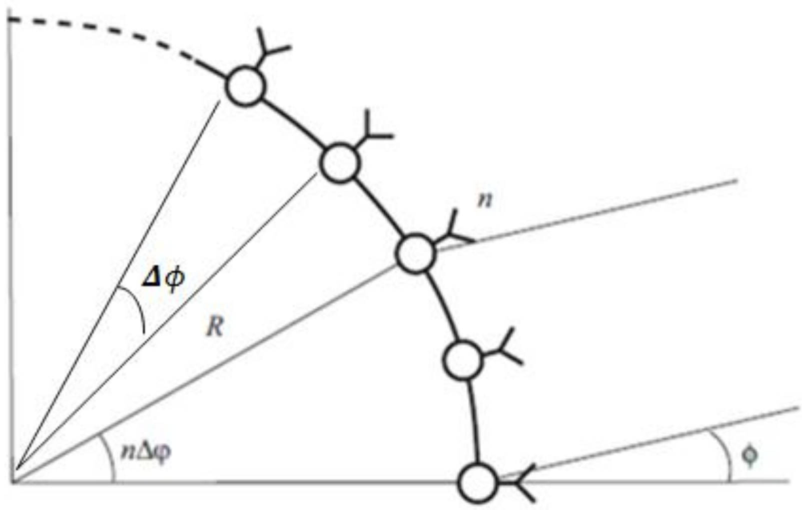

Figure 21. Part of circular array [40]

With the linear array, we can point a focused beam in a direction φ_0 by applying a linear phase shift ψ(n) to the elements along the array:

$$\psi(n) = -knd\sin\varphi_0 \tag{31}$$

With the circular array, we can similarly impose phase values to each element so that they add up coherently in the direction φ_0. We get the proper phase excitation for each element n by choosing

$$\psi(n) = -kR\cos(\varphi_0 - n\Delta\phi) \tag{32}$$

Thus, the radiation function for the focused, circular case becomes

$$E(\phi) = \sum_n |V_n| EL(\phi - n\Delta\phi) e^{jkR[\cos(\phi - n\Delta\phi) - \cos(\phi_0 - n\Delta\phi)]} \tag{33}$$

Sometimes, it is required to generate a beam with equal radiation in all directions in the azimuthal plane (an omnidirectional beam). Circular arrays are particularly suitable for this by virtue of their circular symmetry. We will now look more closely at circular array behaviour and investigate how performance can be optimized. Indeed, much better results can be obtained by proper choice of parameters.

Accordingly a parametric study was done on the inter-element spacing and grating lobe dependence using the uniform circular array factor definition using Matlab and with uniform excitation using eleven isotropic elements. Selected results are presented here for brevity. Consider for different inter-element spacing *d* as shown in Figure 22.

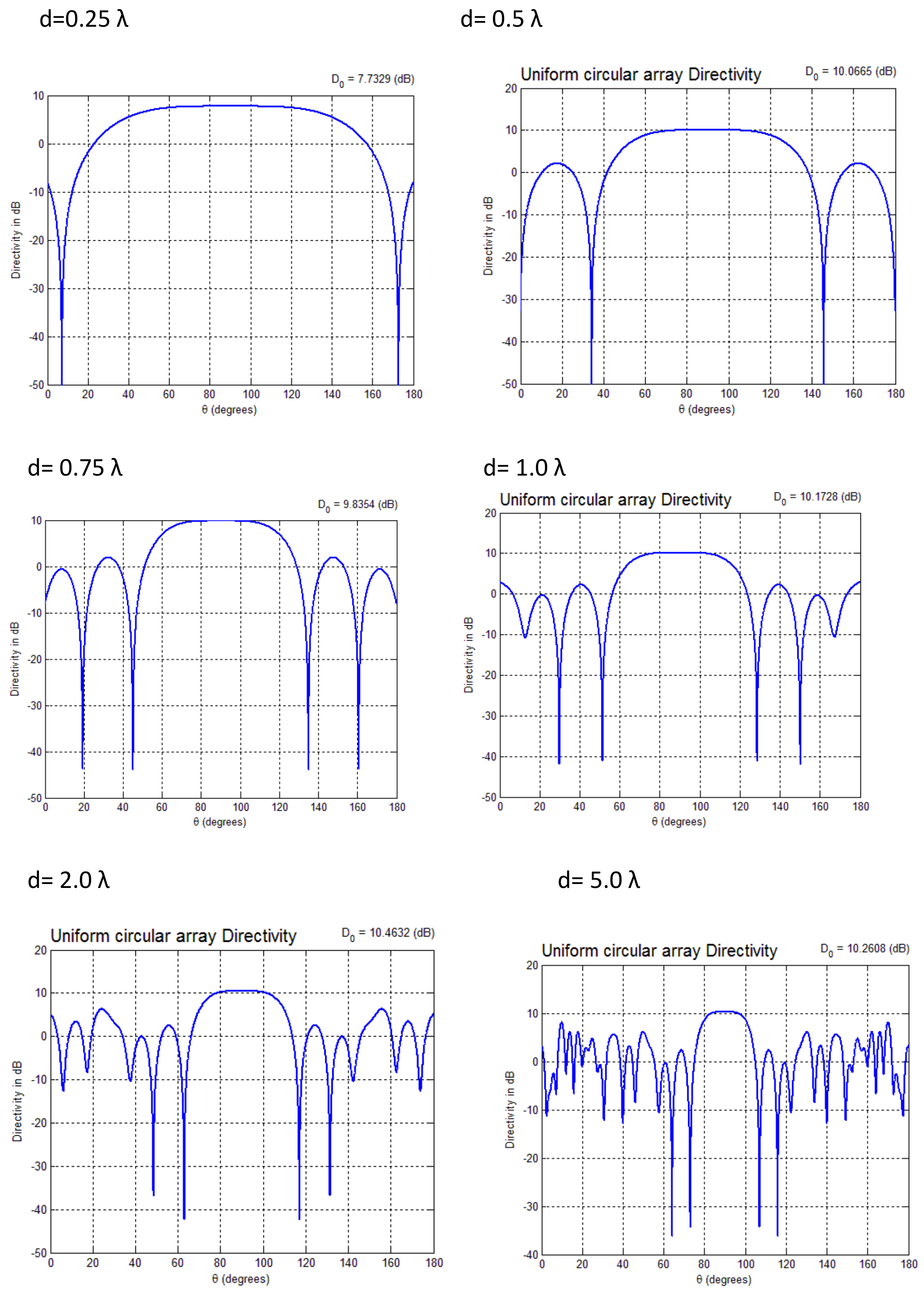

Figure 22. Grating lobes dependence on inter element spacing in a circular array of 11 isotropic elements

From the Matlab calculations above it can be concluded that the grating lobes, though difficult to locate in a circular array pattern, become dominant at spacing equal to or more than 1 λ. At spacing lesser than 0.5 λ the grating lobes are absent.

2.3 Wideband beamforming and null steering

The passive radar requires in its operation beam steering and null steering capabilities. These abilities are needed because it has to have antenna that can direct a main beam in the direction of signal of interest and a null in the direction of interference. The passive radar in which the designed antenna is deployed exploits DVB-T signal which is spread over the 450-900 MHz range. This beamforming has to therefore be accomplished over a wideband range of 450-900 MHz. This necessitates wideband beamforming and null steering.

Beamforming

'Beamforming' refers to the ability of the antenna array to focus energy toward a specific direction without the knowledge of the incoming signal's direction of arrival (DOA). Adaptive beamforming involves knowing the direction of desired signal and undesired signals and then adaptively calculating the array excitation coefficients to point directional beam along the desired direction in space and nulls in the undesired direction. It is often referred to as spatial filtering. It is one of the major areas of signal processing and has been studied extensively in the past due to its wide applications in various areas ranging from radar, sonar, microphone arrays, radio astronomy, seismology, medical diagnosis and treatment, to communications. It involves multiple sensors (microphones, antennas, etc.) placed at different positions in space to process the received signals arriving from different directions. An example for a simple array system consisting of four sensors with two impinging signals is shown in Figure 23 for illustrative purposes, [24] where the direction of arrival (DOA) of the signals is characterized by two parameters: an elevation angle θ and an azimuth angle ϕ .

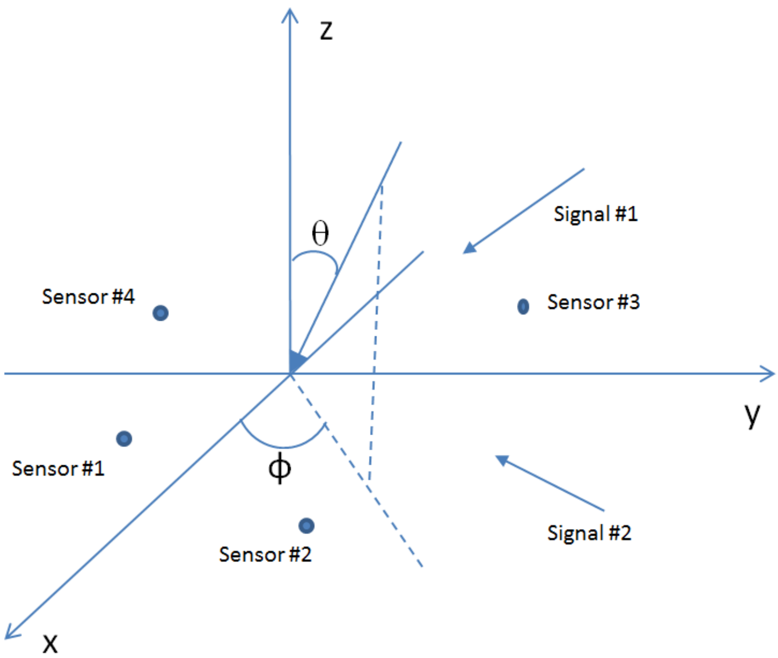

Figure 23. Array with four sensors and two impinging signals

For the impinging signals, we always assume that they are plane waves, i.e. the array is located in the far field of the sources generating the waves and the received signals have a planar wavefront.

Consider a plane wave with a frequency *f* propagating in the direction of the *z*-axis of the Cartesian coordinate system as shown in Figure 24.

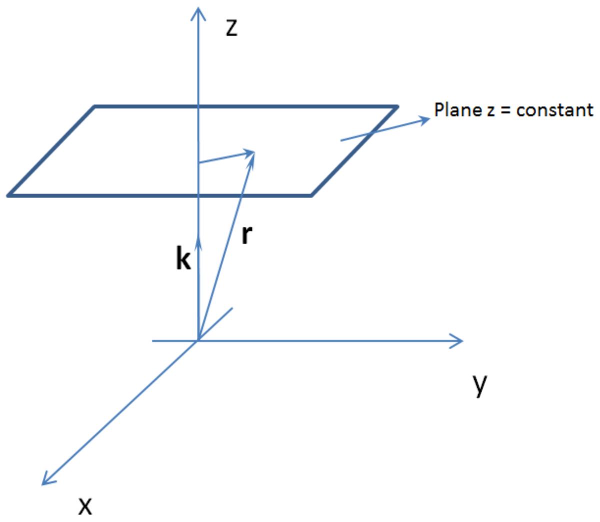

Figure 24. A plane wave propagating in the direction of *z* axis of Cartesian coordinate system.

At the plane defined by *z* = constant, the phase of the signal can be expressed as:

$$\phi(t,z) = 2\pi ft - kz \quad (34)$$

where t is time and the parameter k is referred to as the wavenumber and defined as

$$k = \frac{\omega}{c} = \frac{2\pi}{\lambda} \quad (35)$$

where ω is the (temporal) angular frequency, *c* denotes the speed of propagation in the specific medium and λ is the wavelength. Similar to ω, which means that in a temporal interval *t* the phase of the signal accumulates to the value ωt, the interpretation of *k* is that over a distance *z*, measured in the propagation direction, the phase of the signal accumulates to *kz* radians. As a result, *k* can be referred to as the spatial frequency of a signal [25].

Different from the temporal frequency ω, which is one-dimensional, the spatial frequency *k* is three-dimensional and its direction is opposite to the propagating direction of the signal. In a Cartesian coordinate system, it can be denoted by a three-element vector:

$$k = \left[k_x, k_y, \mathrm{k}_z \right]^T \quad (36)$$

with a length of:

$$k = \sqrt{k_x^{\ 2} + k_y^{\ 2} + k_z^{\ 2}} \quad (37)$$

This vector is referred to as the wavenumber vector. In the case shown in Figure 23, we have $k_x = k_y = 0$ and $k_z = -k$. Let $\hat{z} = [0,0,1]^T$ denote the unit vector along the *z*-axis direction, then we have $\mathbf{k} = \text{-k}\hat{\text{z}}$.

These two quantities are not independent of each other and are related by the following equation:

$$k = \frac{2\pi f}{c} \tag{38}$$

Any point in a 3-D space can be represented by a vector $r = \left[r_x , r_y , \mathrm{r}_z \right]^T$, where r_x, r_y and r_z are the coordinates of this point in the Cartesian coordinate system. With the definition of the wavenumber vector k, the phase function $\phi(t,\mathbf{r})$ of a plane wave can be expressed in a general form [25]:

$$\phi(t,r) = 2\pi ft + k^T\mathbf{r} \tag{39}$$

For the case in Figure 24, we have:

$$\mathbf{k}^T\mathbf{r} = -k(\hat{\mathbf{z}}^T\mathbf{r}) = -kr_z \tag{40}$$

Therefore, as long as the points have the same coordinate r_z in the z-axis direction, they have the same phase value at a fixed time instant t.

For the general case, where the signal impinges upon the array from an elevation angle θ and an azimuth angle ϕ, as shown in Figure 23, the wavenumber vector **k** is given by:

$$\mathbf{k} = \begin{bmatrix} k_x \\ k_y \\ k_z \end{bmatrix} = k \begin{bmatrix} \sin\theta\cos\phi \\ \sin\theta\sin\phi \\ \cos\theta \end{bmatrix} \tag{41}$$

Then the time independent phase term $\mathbf{k}^T\mathbf{r}$ changes to:

$$\mathbf{k}^T\mathbf{r} = k(r_x \sin\theta\cos\phi + r_y \sin\theta\sin\phi + r_z \cos\theta) \tag{42}$$

The wavefront of the signal is still represented by the plane perpendicular to its propagation direction.

Array signal processing involves [25]:

1. Detecting the presence of an impinging signal and determine the signal numbers.
2. Finding the DOA angles of the impinging signals.
3. Enhancing the signal of interest coming from some known/unknown directions and suppress the interfering signals (if present) at the same time.

The third area is the task of beamforming, which can be divided into narrowband beamforming and wideband beamforming depending on the bandwidth of the impinging signals.

<u>**Narrowband beamforming**</u>

In adaptive beamforming, we estimate the signal of interest arriving from some specific directions in the presence of noise and interfering signals with the aid of an array of sensors. These sensors are located at different spatial positions and sample the propagating waves in space. The collected spatial samples are then processed to attenuate/null out the interfering signals and spatially extract the desired signal. As a result, a specific spatial response of the array system is achieved with 'beams' pointing to the desired signals and 'nulls' towards the interfering ones.
Figure 25 shows a simple beamforming structure based on a linear array,

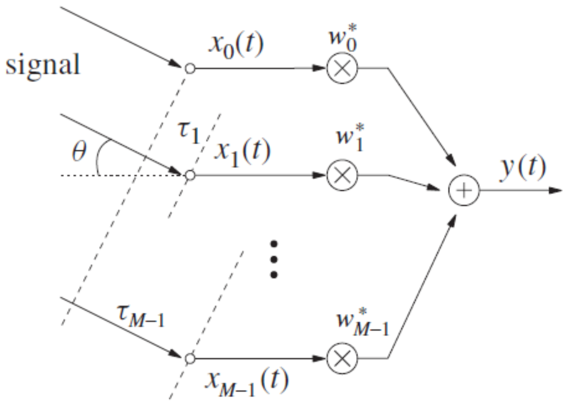

Figure 25. General structure of narrowband array architecture [24]

where *M* sensors sample the wave field spatially and the output *y(t)* at time *t* is given by an instantaneous linear combination of these spatial samples $x_m(t), m = 0,1,\ldots M-1$ as

$$y(t) = \sum_{m=0}^{M-1} x_m(t) w_m^* \tag{43}$$

The beamformer associated with this structure is only useful for sinusoidal or narrowband signals, where the term 'narrowband' means that the bandwidth of the impinging signal should be narrow enough to make sure that the signals received by the opposite ends of the array are still correlated with each other[26], and hence it is termed a narrowband beamformer.

Wideband beamforming

The beamforming structure discussed above works effectively only for narrowband signals. When the signal bandwidth increases, its performance will degrade significantly. This can be explained as follows.

Suppose there are in total M impinging signals $s_m(t)$, *m = 0, 1, . . . , M − 1,* from directions of θ_m, *m = 0, 1, . . . , M − 1*, respectively. τ_i is the propagation delay for the signal from sensor 0 to sensor m and is a function of θ. The first one $s_0(t)$ is the signal of interest and the others are interferences. Then the array's steering vector d_m for these signals is given by [25]:

$$d_m(\omega,\theta) = \begin{bmatrix} 1 & e^{-j\omega\tau_1(\theta_m)} & \ldots & e^{-j\omega\tau_{M-1}(\theta_m)} \end{bmatrix}^T \tag{44}$$

Ideally, for beamforming, we aim to form a fixed response to the signal of interest and zero response to the interfering signals. For simplicity, we do not consider the effect of noise here. This requirement can be expressed as the following matrix equation:

$$\begin{pmatrix} 1 & e^{-j\omega\tau_1(\theta_0)} & \ldots & e^{-j\omega\tau_{M-1}(\theta_0)} \\ 1 & e^{-j\omega\tau_1(\theta_1)} & \ldots & e^{-j\omega\tau_{M-1}(\theta_1)} \\ \vdots & \vdots & \ddots & \vdots \\ 1 & e^{-j\omega\tau_1(\theta_{M-1})} & \ldots & e^{-j\omega\tau_{M-1}(\theta_{M-1})} \end{pmatrix} \begin{pmatrix} w_0^* \\ w_1^* \\ \vdots \\ w_{M-1}^* \end{pmatrix} = \begin{pmatrix} \text{constant} \\ 0 \\ \vdots \\ 0 \end{pmatrix} \tag{45}$$

Obviously, as long as the matrix on the left has full rank, we can always find a set of array weights to cancel the *M − 1* interfering signals and the exact value of the weights for complete cancellation of the interfering signals is dependent on the signal frequency.

For wideband signals, since each of them consists of infinite number of different frequency components, the value of the weights should be different for different frequencies and we can write the weight vector in the following form:

$$w(\omega) = \left[w_0(\omega) \quad w_1(\omega) \quad \ldots, \quad w_{M-1}(\omega)\right]^T \tag{46}$$

This is why the narrowband beamforming structure with a single constant coefficient for each received sensor signal will not work effectively in a wideband environment.

While designing a wideband array, the array designer must balance avoiding undesired mutual coupling effects with eliminating grating lobes due to element spacing at the high end of the frequency band. This limits the array bandwidth to an extent.

The Bartlett beamformer was the first to emerge during World War II [17]. Later adaptive beam formers and classical time-delay estimation techniques were applied to enhance the ability to resolve closely spaced signal sources [18, 19]. The conventional beam former has some fundamental limitations connected to physical size of the array, available data collection time, and the signal to noise ratio (SNR).

Analog beamforming

The figure 26 depicts the radio frequency (RF) beamformer example for creating only one beam at the output [20]. RF beam formers can employ microstrip structures, transmission lines or microwave guides.

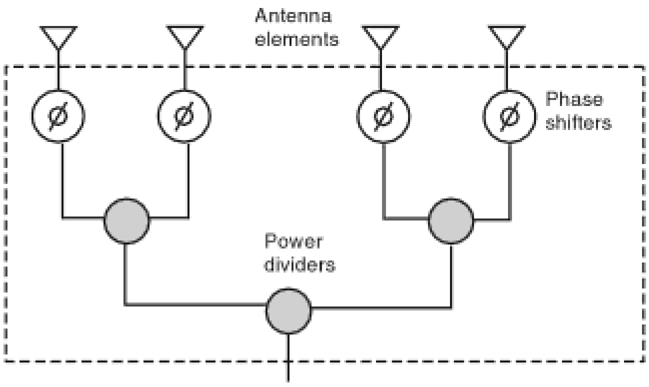

Figure 26. A simple on-beam RF beam former[20]

Multiple beamformers are more complex configurations, based mathematically on the beamforming matrix. The Butler matrix is the most well-known and widely used matrix [21, 22]. Typically the number of beams is equal to the number of antenna elements in the arrays. Although the Butler matrix was developed before the Fast fourier transform (FFT), they are completely equivalent. The Buttler matrix is used in analog beamforming , whereas FFT is used in digital beamforming.

Digital beamforming

The incident RF signal at each antenna element is converted in to two streams of binary complex baseband signals that represent the in-phase (I) and quadrature (Q) phase components. These weighted signals from each element are sampled, stored and beams are then formed summing the appropriate samples [23]. A digital beamformer of this form is shown in figure 27.

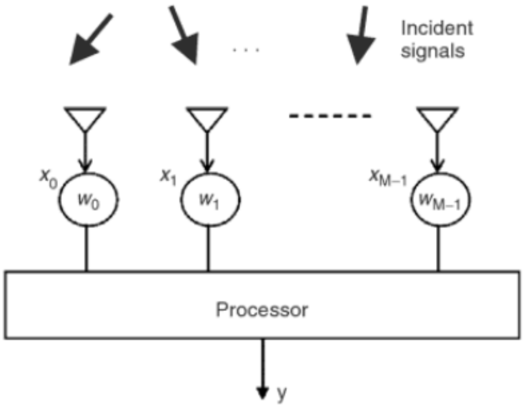

Figure 27. Digital beamformer architecture [24]

The array in Figure 27 has *M* elements. The output $y_n(\theta),(t = nT)$ is given by the sum of the sampled baseband data at *M* sensors given by

$$y_n(\theta) = \sum_{m=0}^{M-1} w_m^{\ *} x_m(n) \qquad (47)$$

Where x_m is the signal from the m^{th} element of the array,

$w_m^{\ *}$ is the weight applied to the antenna element m

'*' denotes the complex conjugate operation

The above equation can also be written as

$$y_n(\theta) = w^H \cdot x(n) \qquad (48)$$

Where H represents the Hermitian transpose.

The n^{th} sample of the output $y_n(\theta)$ is given by the array snapshot multiplied by a set of weights chosen to form a beam in desired direction θ. By choosing the appropriate weight vectors, beam steering, adaptive nulling and beam shaping can be achieved.

Null introduction and steering

The application for which the passive radar is built requires that a null is introduced in the direction of the direct signal in the presence of reflected signal from target. This calls for simultaneous existence of both aiding beam in one direction and canceling beam in the other direction. An illustration is shown in Figure 28. Dotted curve in the figure is pattern before beamforming. Solid curve in the figure is pattern after beamforming and nulling. The null as seen can be steered into any direction along the horizontal plane of the circular array. It can be rotated all around the circular array in a circle in any direction from 0 to 360 degrees.

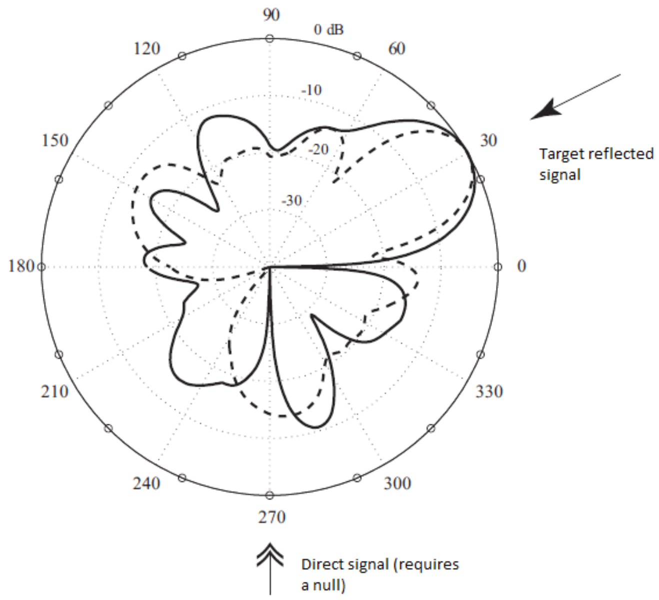

Figure 28. Illustration of null introduction and beamforming [40]

The introduction of a null is part of adaptive beamforming which involves estimation of direction of arrival/interference and calculation of optimum weights by using the concept of covariance matrix. Consider covariance matrix *R(t)*

$$R(t)=\begin{bmatrix} u_1^*(t)\cdot u_1(t) & u_1^*(t)\cdot u_2(t) & \dots & u_1^*(t)\cdot u_N(t) \\ u_1^*(t)\cdot u_1(t) & u_2^*(t)\cdot u_2(t) & & u_2^*(t)\cdot u_N(t) \\ \vdots & & \ddots & \\ u_N^*(t)\cdot u_1(t) & u_N^*(t)\cdot u_2(t) & \dots & u_N^*(t)\cdot u_N(t) \end{bmatrix} = \vec{u}^*\cdot\vec{u}^T \qquad (49)$$

Where $u_N(t)$ are the received signals in N^{th} antenna. The covariance matrix describes the correlation between the signals in different antennas. Then for the maximum signal to interference ratio (SIR) we have the array excitation coefficients given by

$$\vec{a} = (\mathrm{E} + \vec{u}^*\cdot\vec{u}^T)^{-1}\cdot\vec{a}_0 \qquad (50)$$

The null depth can be controlled by introducing a scaling factor α

$$\vec{a} = (\mathrm{E} + \alpha * \vec{u}^*\cdot\vec{u}^T)^{-1}\cdot\vec{a}_0 \qquad (51)$$

Chapter 3- Beamforming algorithms and their comparison

The beam former's coefficients often need to be adjusted according to the received array data in order to achieve an optimum solution to the specified scenario. When the environment keeps changing, the coefficients need to change too. This class of beamformers often employ all kinds of adaptive algorithms to update their coefficients. For block-based adaptation, we normally assume that the signals are relatively stationary for the duration of the received block of array data, so that the statistics of the signals can be estimated accurately for the block period to calculate the optimum solution. For a more time-varying environment or where the number of coefficients is too large, the coefficients are updated continuously, i.e. they are adjusted for each new set of signal samples. In this chapter the conventional beamforming algorithms are presented and compared for their complexities and then the Bucci beamforming algorithm and its advantage is presented.

3.1 Conventional beamforming algorithms

There are a lot many conventional algorithms that have been used frequently in beamforming applications. Prominent among them are the least mean squares, sample matrix inversion, normalized least mean squares and recursive least squares. These are discussed in detail in the section below.

3.1.1 Sample matrix inversion (SMI) algorithm

The SMI algorithm provides estimates for the array weights by replacing the correlation matrix $\hat{R}$ an estimate from multiple snapshots (N) of the array signal:

$$\hat{R} = \frac{1}{N}\sum_{n=1}^{N} x(n)x^{H}(n) \tag{52}$$

The estimate of $\hat{R}$ can be updated when new samples arrive:

$$\hat{R}(n+1) = \frac{n\hat{R}(n) + x(n+1)x^{H}(n+1)}{n+1} \tag{53}$$

Reed developed the sample matrix inversion technique for a fast adaptive beamforming scheme [27]

3.1.2 Least mean squares (LMS) algorithm

The LMS algorithm the most commonly used adaptive algorithm was developed by [18]. The LMS algorithm updates the weights at each iteration by estimating the gradient of the quadratic surface and then moving the weights in the negative direction of the gradient by a constant, referred to as "step" [21]. Let e(n) be the error function and E(x) be the 'expectation of x' then we have

$$\begin{aligned} \nabla(E(e(n)^2)) &= -e^{*}(n)\cdot x(n) \\ w(n+1) &= w(n) - step\cdot\nabla(E(e(n)^2)) \end{aligned} \tag{54}$$

From these two equations it can be seen that

$$w(n+1) = w(n) + step \cdot [e^*(n) \cdot x(n)] \quad (55)$$

When the step size is smaller than the maximum eigenvalue of the correlation matrix *R*, the algorithm is stable and the mean values of the estimated weights converge to the optimal weights. Since the sum of the eigenvalues of *R* is its trace, the step size is usually chosen as

$$0 < step < \frac{1}{Trace(R)} \quad (56)$$

The LMS algorithm does not require prior knowledge of the signal statistics [18]. The algorithm amounts to approximating the expected value by the product of the observation vector and the estimation error, a technique known as stochastic approximation. As the filter coefficients depend on new observations and are continuously updated via the estimate of the gradient, the LMS filter coefficients do not converge to a stable set of values even when the observation is stationary. Rather after an initial transient response to the set of observations, the coefficients settle towards a set of values and vary randomly to some degree. The variation of the filter's coefficients is related to the adaptation parameter "step" but in the opposite way to the settling time. A small value for the "step" results in slow convergence of the filter coefficients and their long term values do not vary greatly about the optimal values.

The LMS algorithm is the least computationally complex weight adaptation algorithm. The rate of convergence to the optimum weights depends on eigenvalues of correlation matrix *R*, that, is the power of the desired and interfering signals.

3.1.3 Normalized least mean squares (NLMS) algorithm

The LMS algorithm is a simple adaptive algorithm, but with data dependent behaviour. The influence of power of the input signal can be removed by normalization of the step size. This leads to the NLMS. In the LMS algorithm, the step size should never exceed its upper bound. In a non-stationary environment, the worst case has to be assumed and we have to choose a very small value for step size, which leads to a rather slow convergence rate for the algorithm. It is possible to normalize the step size to ensure an approximately constant rate of adaptation. Then a normalization of the step size is given by [25]:

$$\mu = \frac{\mu_0}{x(n)^H \cdot x(n)} \quad (57)$$

where μ_0 is the new step size. Substituting this equation into the LMS update equation yields a constant convergence rate independent of the power of the input signal **x**.

3.1.4 Recursive least squares (RLS) algorithm

In [28] it is shown that the weights can be calculated in a recursive manner

$$w(n+1) = w(n) + \frac{R^{-1}(n)e^{*}(n+1)x(n+1)}{\lambda + x^{H}(n+1)R^{-1}(n)x(n+1)}$$
$$R^{-1}(n+1) = \frac{1}{\lambda}\left[R^{-1}(n) - \frac{R^{-1}(n)x(n+1)x^{H}(n+1)R^{-1}(n)}{\lambda + x^{H}(n+1)R^{-1}(n)x(n+1)}\right]$$
$$R^{-1}(0) = \delta^{-1}I \quad (58)$$

Where δ is a small positive constant. The forgetting factor λ depends on the fading rate of the channel and the best value is close to 1. The RLS algorithm is extremely fast compared to the LMS algorithm and does not suffer from poor convergence in variance as with LMS, but requires several matrix multiplications at each iteration.

3.2 The Bucci beamforming algorithm

Of several beamforming algorithms available, the goal is to use an algorithm that has fast convergence and lower computational complexity. O. M. Bucci *et al.* [29] proposed a general projection method to array synthesis. This algorithm is discussed here.

An array factor synthesis procedure which allows to specify the side-lobe and shaped-zone ripple levels as well as the fall rate of the main lobe is proposed. The problem is formulated as the search of the intersection between two suitable sets and is solved by an iterative LMS projection method. The presence of excitation constraints can be very easily dealt with.

The array synthesis problem aims to compute the array excitations in order to satisfy the prescribed specifications. The array excitations are posed on the radiated field but also on the excitations themselves, at least in an implicit way.

Consider an array factor $F(u)$ of a linear equally spaced array of N+ 1 elements;

$$F(u) = \sum_{n=0}^{N} c_n e^{jnu} \quad (59)$$

$$\text{where } u = kd\sin\theta$$

The pattern mask can be prescribed as:

$$M_L(u) \le |F(u)| \le M_U(u) \quad (60)$$

where $M_L(u), M_U(u)$ are the lower mask and upper mask respectively.
Every feasible array pattern must lie within this mask. Two function sets can now be defined [29]

1) The set of all trigonometric polynomial which satisfy the excitation coefficients
2) The set of all functions which satisfy the pattern mask.

An array factor that belongs to the intersection of both the sets is a solution to the synthesis problem. The synthesis problem is therefore formulated as the search of the intersection of the two sets.

More specifically we are looking for the intersection of:

1) The set *M* of all functions which fit the assigned mask;
2) The set *B* of all array factors which can be radiated by a set of excitations satisfying the prescribed constraints.

The projector over *M* maps every function f onto the function $\bar{f}$ according to:

$$\bar{f}(u) = \begin{cases} M_U(u)\dfrac{f(u)}{|f(u)|} & |f(u)| > M_U(u) \\ f(u) & M_L(u) \le |f(u)| \le M_U(u) \\ M_L(u)\dfrac{f(u)}{|f(u)|} & |f(u)| < M_L(u) \end{cases} \qquad (61)$$

Figure 29 below shows the masks and the beamformed pattern.

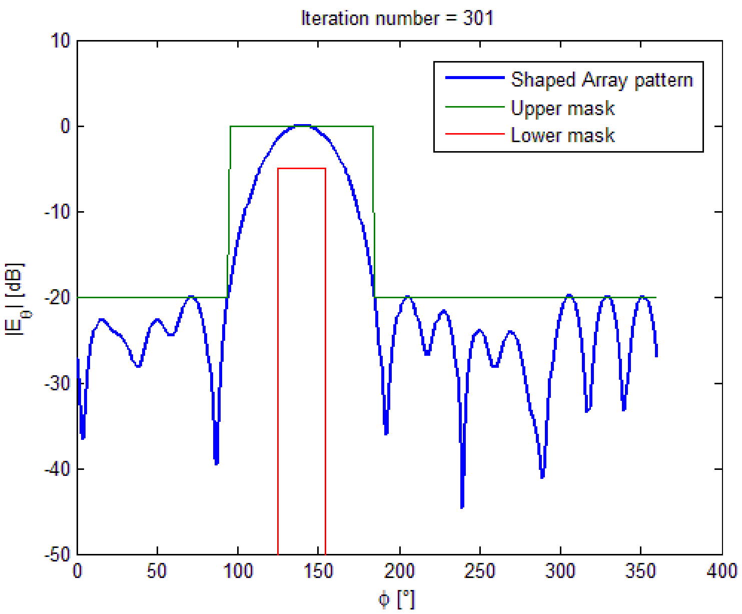

Figure 29. The masks and the beamformed pattern.

The projector over the set *B* is defined as a relation between Fourier coefficients [29].

The solution to this problem is found by the method of iterative LMS algorithm. For a dynamic range constraint we can start from a pattern whose amplitude is constant. The iterative LMS algorithm uses the principle of "pattern inversion" as discussed below.

$$\underbrace{\begin{bmatrix} e_{11} & e_{12} & \cdots & e_{1m} \\ e_{21} & e_{22} & & e_{2m} \\ \vdots & & \ddots & \vdots \\ e_{n1} & e_{n2} & \cdots & e_{nm} \end{bmatrix}}_{\mathrm{E}} \cdot \underbrace{\begin{bmatrix} c_1 \\ c_2 \\ \vdots \\ c_m \end{bmatrix}}_{\vec{c}} = \underbrace{\begin{bmatrix} f_1 \\ f_2 \\ \vdots \\ f_n \end{bmatrix}}_{\vec{f}} \qquad (62)$$

where *E* is the field matrix,

$\vec{c}$ is array coefficient, and
$\vec{f}$ is the electric field vector

The pattern inversion is done as:

$$\begin{aligned}
&E^T \cdot E \cdot \vec{\mathrm{c}} = E^T \cdot \vec{\mathrm{f}} \\
&[E^T \cdot E]^{-1} \cdot E^T \cdot E \cdot \vec{\mathrm{c}} = [E^T \cdot E]^{-1} \cdot E^T \cdot \vec{\mathrm{f}} \qquad (63) \\
&\vec{\mathrm{c}} = [E^T \cdot E]^{-1} \cdot E^T \cdot \vec{\mathrm{f}} \implies \mathrm{LMS\,solution\,(pseudo\,inverse)}
\end{aligned}$$

The pseudoinverse calculated using the LMS solution is then applied in multiple iterations until a pattern fitting into the prescribed mask is obtained following the projection rules described above and the corresponding array excitation coefficients are stored.

3.3 The advantage of Bucci beamforming algorithm

The Bucci beamforming algorithm has many advantages over the conventional approaches. Prominent among them being:

1) The whole method lends itself to a very efficient implementation.
2) The algorithm does not require phase information. It performs “Power synthesis”;
3) It uses iterative LMS method which is both simple and computationally efficient;
4) The projection of farfield onto prescribed masks gives control over varied beamshapes and sidelobe levels;
5) It has a fast convergence under physical limits;
6) The Algorithm uses the simple array factor in prescribing limits and this allows for a degree of freedom in having a tradeoff between the achievable beamwidth and sidelobe level.

Chapter 4- The CORA radar system and antenna array

4.1 Outline of the CORA radar system

Figure 3 shows the antenna, front-end and processing van of the DAB-DVB-T (Digital audio broadcast and Digital video broadcast-terrestrial) radar using the CORA system during the set-up for a measurement campaign in Germany in 2006. The digital waveforms employing COFDM modulation are noise-like. They have almost constant spectral amplitude within the band limits of 1.5 MHz (DAB) and 7.5 MHz (DVB-T). This provides a constant measurement quality at range resolutions of about 100m and 20 m, respectively [5]. This exceeds by far the range resolution of some km, which can be achieved using FM-radio emission. On the other hand, DAB stations transmit at much lower power than FM-stations; while the DVB-T transmit power levels are comparable to those of FM-radio [5].

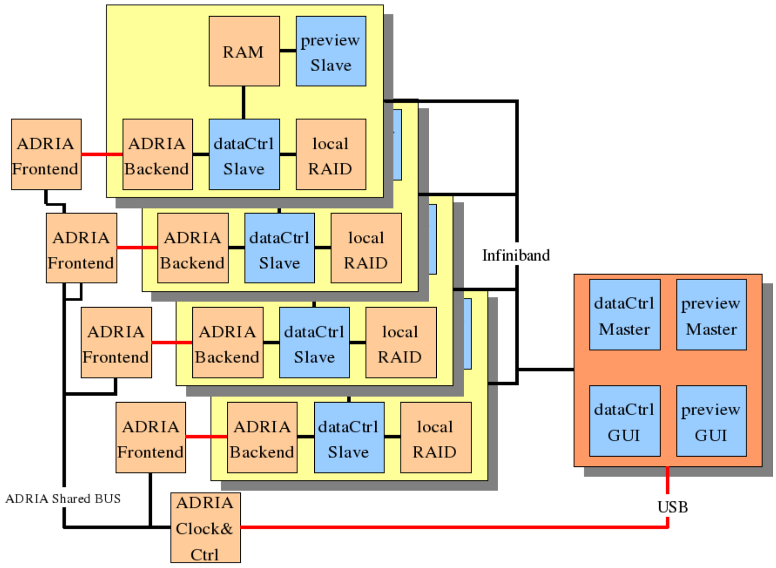

Figure 30 .CORA system architecture [30]

The HF-front-end consists of 16 equal receiver channels. Each of the receiver channels comprises of a LNA (low-noise amplifier), a tuneable or fixed filter and an adaptive gain control for optimum control of the ADC (Analog to Digital Converter). The LNAs have a noise figure of 1.1 dB and a gain of 40 dB. In the current configuration fixed DAB band-pass filters are being used with a pass band of 220 to 234 MHz. A chirp signal with a bandwidth of 1.536 MHz, centred around 227.36 MHz (226.592-228.128 MHz, channel 12C), generated by a separate signal generator and transmitted to the front-end by coaxial cable, is used for calibration. A bank of switches provides for calibration of each receiver channel chain from the LNA to the ADC, excluding only the antenna element.

A/D conversion is realised with 4 FPGA boards, each processing 4 receiver channels. The FPGAs currently provide only for serialising the 4 channels. Each FPGA board is equipped with 4 ADC-modules with 14 bit 100 Msamp/sec maximum sample rate ADC-chips. For the processing of DAB signals, a sample rate of 18.432Msamp/sec is used. It is matched to sample all sub-bands of TV-channel-12 and is also a multiple of 512 kHz, the basic clock rate of the DAB signal [30].

Each ADC output is fed to an electro-optic converter and linked to the signal and data processing unit via a fibre-optic cable. In the signal and data processing unit, the optical signals are converted back to digital data streams of 4 serial channels, each. Four high performance Quad-Opteron computers handle the four data streams. The opto-electric conversion and the feeding of the data to PCI-X-bus are performed on 64-bit-boards, hosting 4 FPGAs. The FPGAs can additionally be used for pre-processing the raw data. A data control process controls the storing of the raw data on two 1 TByte hard disc drives per Quad-Opteron and drives a FiFo RAM, which serves the 'pre-view' real time visualisation process. Hence, the signal and data processing unit provides 8 Tbyte of hard disc recording space. For further data storage a raid-array is used with 15.3 Tbyte hard disc space, where the measured raw data can be saved after each measurement sequence. In the visualisation master processor, which is served by the four data streams from the Quad-Opterons via 10 Gbit Infiniband links, performs the processing control, beam forming and detection processing. The 'pre-view' display is processed on a separate high performance computer in the signal and data processing unit [30].

The CORA-signal processing is based on determining the intersections of the RDEs and measuring the direction of the target echo. Here, too, the exact knowledge of the location of the transmitters is required to determine the RDEs and, together with the direction-of-arrival of the target echo, the true target range in order to separate false targets from true ones. Figure 30 shows the total system architecture of the CORA system.

4.2 The architecture of the array antenna

The Discone element being chosen to be the antenna array element, the next step in the antenna design was the requirement for the design of an antenna array. The antenna array had to be designed so that it supports several additional functionalities.

Choice of array geometry

Consider the scenario of unknown location of emitters/targets. In such a case equal performance of the array in all directions must be ensured. There is a need to introduce nulls in the direction of the direct signal and to be able to steer the main beam to any desired direction. When the direct signal and reflected signal from the target are received there is a need to attenuate the direct signal by several dB so as to make its magnitude comparable to the reflected signal form the target. For this purpose nulls are introduced in the direction of the direct signal. It should also be possible to steer this null in the entire azimuth plane for a 360 degree rotation. This can be achieved through the circular array configuration. The linear array fails to operate satisfactorily for the entire 360 degree rotation. Several other array configurations of the non-uniform nature were tried earlier which turned out to have non-satisfactory performance for the concerned application.

The basic symmetry of circular arrays offers a number of advantages. It has an ability to compensate for the effects of mutual coupling by breaking down the array excitation into a series of symmetrical spatial components. This gives rise to directional patterns that remain constant in shape over broad bandwidth. So the use of uniform circular array is self-evident.

The circular array thus chosen allows for beam steering and null steering capabilities in the entire 360 degree rotational plane.

Choice of number of elements in the array

The number of channels in the electronic components is 12. The signal processing involved for array signal processing has an advantage if there be a prime number of elements. The question to be investigated was, are 11 elements satisfactory.

The choice of 11 elements in the circular array can be explained based on two arguments:

1) The signal processing block that is used for the beamforming works best when the number of signal vectors are prime and this is fixed at 11 because of the number of available channels in the signal processing block.

2) Theoretically the number of elements in the Uniform circular array can be determined by taking the “ambiguity issues” into account. A radio direction finder is said to have a “rank-n” ambiguity if one steering vector is a linear combination of n other steering vectors. The minimal number of sensors in each array can be set initially to not less than 5 (justifying 11) to avoid the “rank-1” ambiguities [34].

The dipole element thus developed was used in a circular array of 11 elements.

Chapter 5 – Simulation studies on beamforming and null steering

The task of being able to steer the beam in the direction of Signal Of Interest (SOI) and to introduce a null in the direction of interference can be performed using a series of steps involving the computation of the array radiation patterns and post processing using Matlab. The step of computing the array radiation pattern proceeds by first computing the embedded radiation pattern of the element. The beam forming and null steering simulation results performed on 4NEC2 are presented in the following sections. The study was first done on 4NEC2 to avoid complexity of full wave analysis at first.

5.1 Preliminary studies with dipole circular antenna array

As mentioned above here we discuss the simulation results obtained using dipole as the antenna element in 4NEC2. Before embarking into explaining and presenting the results a brief section on the 4NEC2 and its operation is presented below:

5.1.1. Numerical Electromagnetics Code (4NEC2)

4NEC2 is based on a numerical solution of electromagnetic field integrals for thin, perfectly conducting wire segments using the Method of Moments (MoM). Such segments can be freely arranged in three-dimensional space and excited in different ways. To calculate the electromagnetic properties of antennas there are different analysis functions available [31].

The task of determining the current distribution on a wire antenna resulting from an arbitrary excitation may be put in terms of an integral equation problem. The formulation begins with the development of an integral expression which defines the electric field resulting from an arbitrary current distribution on the wire. The integral expression will employ a Green's function which relates the electric field at an arbitrary observation point to the current at an arbitrary source point. The integral equation problem then employs the integral expression to relate known electric field boundary conditions to an unknown current distribution on the wire. A well known formulation for simple wire antennas is Pocklington's integral equation. The MoM applies orthogonal expansions to translate the integral equation statement into a system of circuit like simultaneous linear equations[37].

The software Numerical Electromagnetics Code (NEC-2) has been developed in the 1970s in the Lawrence Livermore Laboratory in Livermore, California. The program has later been released as Public Domain and is available today in many different versions for almost all operating systems and CPU platforms. 4NEC2 is a completely free windows based antenna modeling tool developed by the Dutch radio amateur Arie Voors [31].

A NEC-2 input file consists of a number of commands specifying the geometry of a problem, the excitation and the output data to be calculated. The usage of the different commands and the different parameters is explained in a detailed Handbook, the complete NEC-2 Manual is available over the internet [32]. For wire geometries some design criteria have to be considered. To obtain accurate and reliable results, certain rules for the dimensions and alignment of the wires must be observed [31]:

Segment length: l < λ/10
Segment radius: r < λ/100, r < l/8

4NEC2 is an efficient tool to compute radiation pattern of electrically large structures such as arrays. This feature of 4NEC2 was exploited to make parametric studies on deciding on the array radius of the final array geometry.

5.1.2 Design of the dipole element

As an example the dipole was designed for operation in the center frequency of at 675 MHz. The dipole single arm length has to be λ /4 that turns out around 11cm. The radius of wire is less than λ/30 =0.01, λ =0.44m. The radius was kept to 1/10 of a mm. The number of segments was adjusted to 7 to get impedance near to the ideal dipole impedance of 73 ohms. The current distribution was sinusoidal. The dipole antenna is shown in Figure 31.

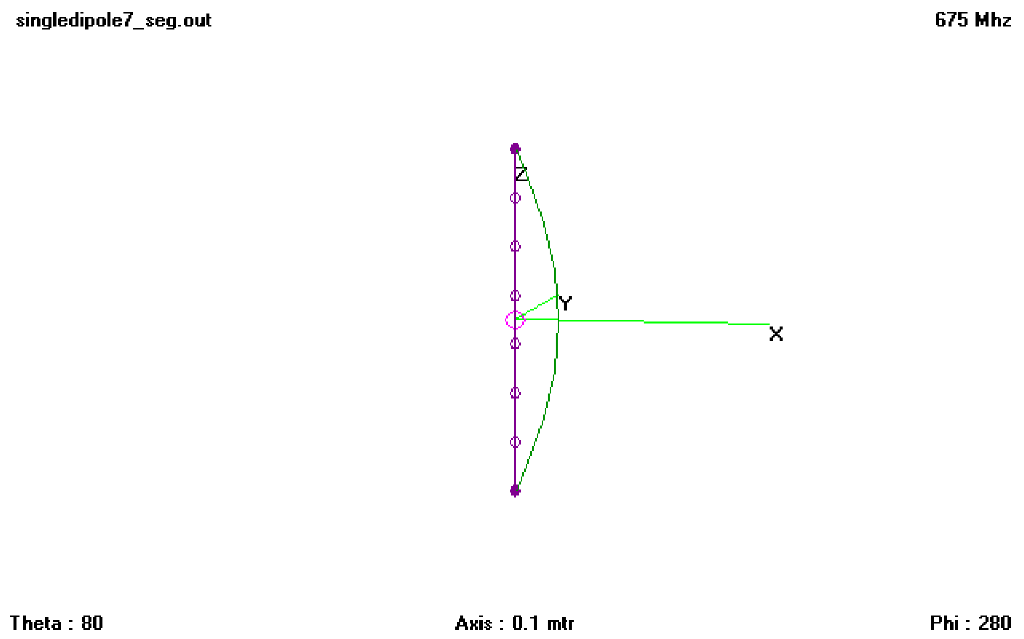

Figure 31. Dipole antenna designed in 4NEC2. Pink line is the dipole and the green curve shows the sinusoidal current distribution along the wire

The return loss and VSWR characteristics of the dipole are shown in the Figure 32:

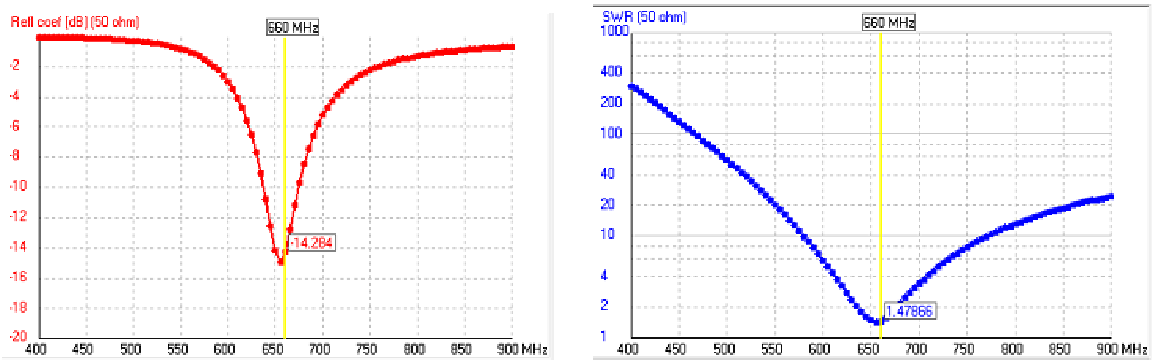

Figure 32. Return loss (S11) and VSWR of the designed dipole element.

It can be seen from Figure 31 and Figure 32 that the dipole element designed has a sinusoidal current distribution and resonates around the center frequency of 675 MHz with a good return loss greater than 10 dB. The VSWR is also less than 2. These results will further improve if normalization is done to 73 ohm than 50 ohm. The radiation pattern of the dipole along the horizontal and vertical plane is shown next in Figure 33.

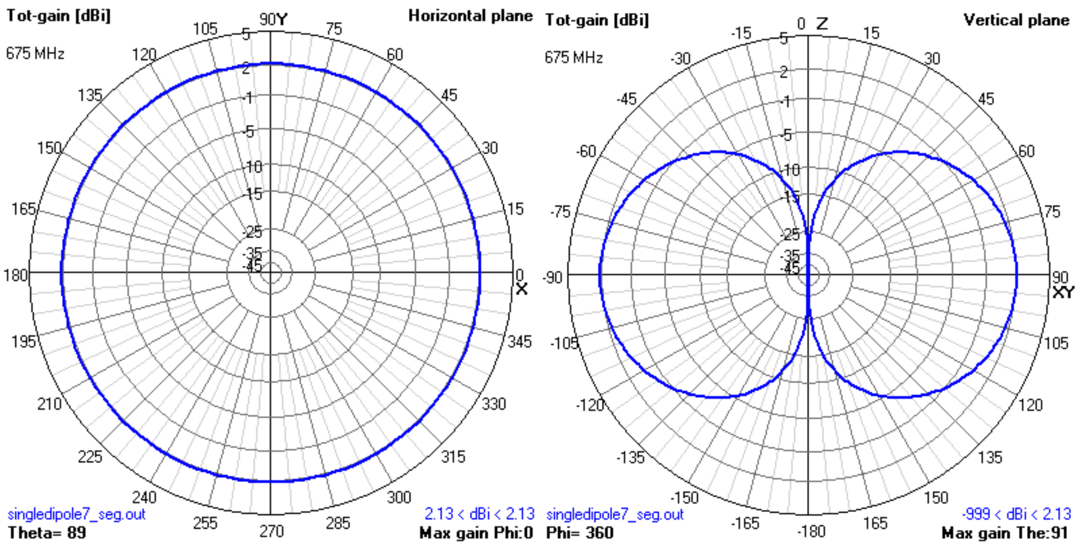

Figure 33. Horizontal and vertical patterns of the designed dipole element.

The 3D radiation pattern of the dipole element is shown in Figure 34.

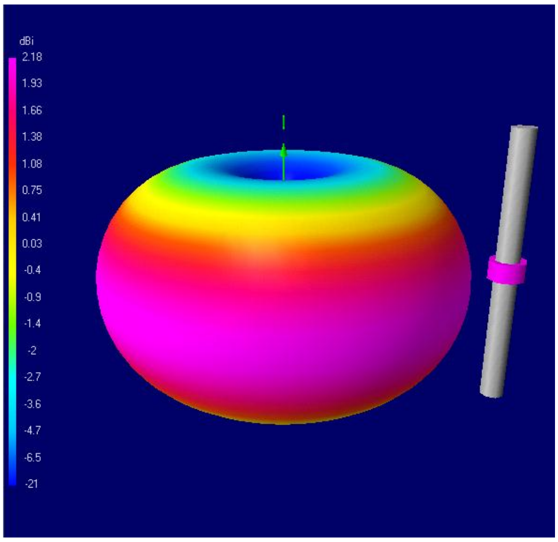

Figure 34. 3D radiation pattern depicting the total gain in dBi of the designed dipole element.

From Figure 32 and 33, it can be seen that the radiation pattern obtained is omnidirectional, which is the requirement in our current scenario of beamforming. The pattern is almost circular in the azimuthal plane which is an added advantage.

The circular dipole array simulation results are next presented.

5.1.3 Design of the dipole circular array

The design of the dipole circular array needs the following important steps to be performed in order for successful operation.

1) Decision on the number of elements in the array (Explained above)
2) Decision on the right inter-element spacing to reduce mutual coupling
3) Decision on the array radius to be able to avoid grating lobes.

Keeping the above criteria in focus the circular array antenna was designed and the array simulation results are presented next.

In the array a single element is excited with a voltage source and the other 10 elements are retained in a passive way as shown in Figure 35. The radiation pattern thus obtained is called the “embedded radiation pattern” as in Figure 36 and 37

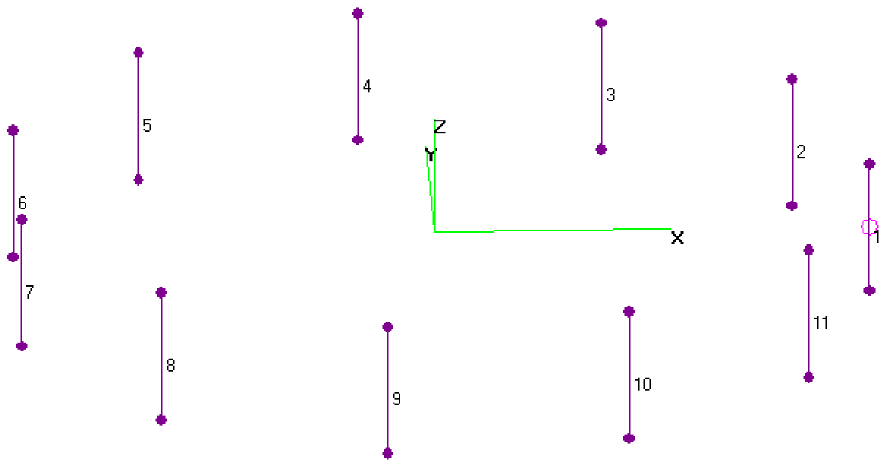

Figure 35. Geometry of 11 element circular array built in 4NEC2 with 0.5 λ inter-element spacing

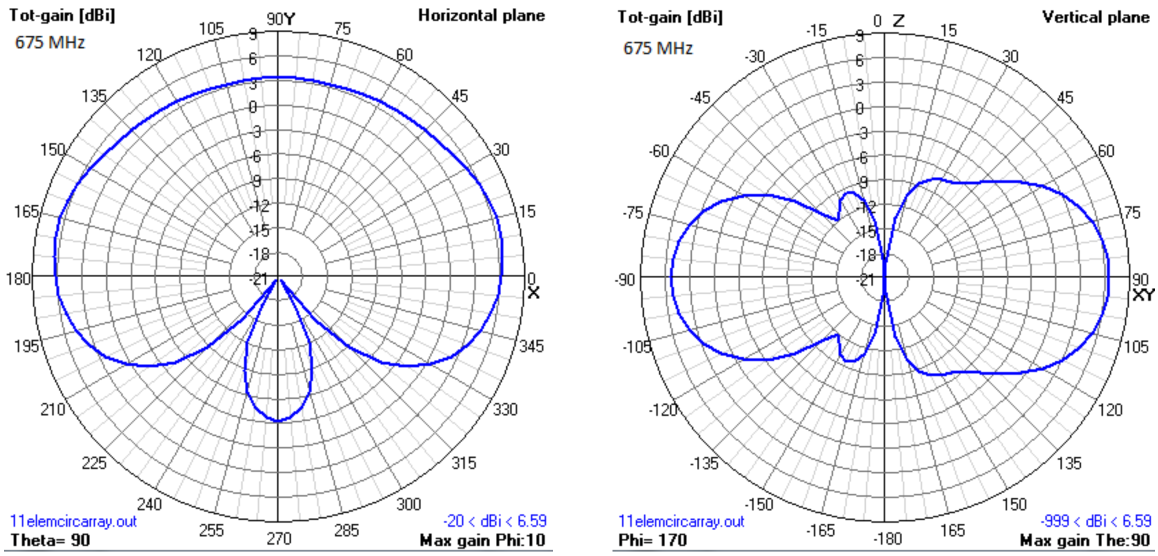

Figure 36 Radiation pattern in the horizontal $(\theta = 90^{\circ}, 0 < \phi < 360^{\circ})$ **and vertical plane** $(\theta = 0^{\circ}, 0 < \phi < 360^{\circ})$ **at the center frequency**

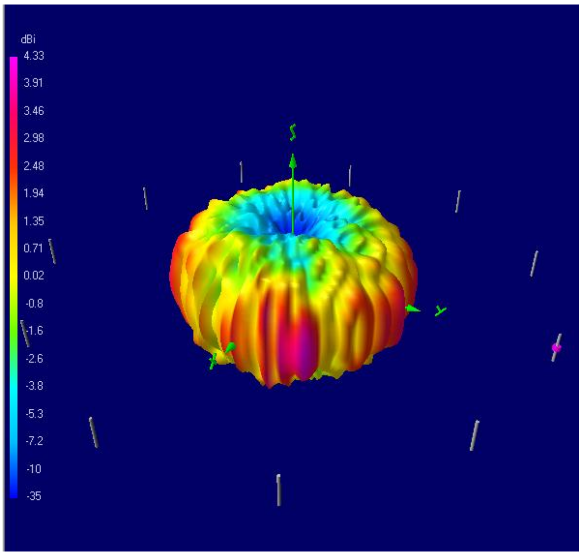

Figure 37. 3D embedded radiation pattern

The embedded radiation pattern, which is the radiation pattern of the excited element when the other elements of the array are passively located around it along the circle, is omnidirectional as desired. The embedded element pattern takes into account the effect of the coupling between the excited element and the passively located elements. . The embedded radiation pattern of a single element is then used in generating the “array manifold” matrix of the entire array by rotating and superposing the embedded element pattern 11 times. This array manifold matrix is then used in the signal processing steps. This leads to beamforming and null steering which is discussed in the next section.

5.1.4 Beamforming using the dipole circular array

The circular array geometry has rotational symmetry. This property can be exploited by calculating the embedded radiation pattern of a single element and using the same to generate the embedded radiation of other elements in the array by simple rotation and then superposing all the patterns to get the array manifold. The array manifold matrix thus generated is then processed in Matlab for beamforming and null steering.

One method of beamforming is the maximum gain method where the goal is to maximize the gain along the desired direction while keeping the gain along other directions relatively low.

Steps involved in maximum gain method beamforming

Algorithm

1) Import the embedded element pattern from 4NEC2 to Matlab (Figure 38)
2) Calculate the array manifold using the embedded element pattern.(Figure 39)
3) The array manifold matrix is obtained by rotation and superposition of the embedded element pattern 11 times. (Figure 40)
4) Calculate the array excitation coefficients using the following method
   “The array excitation coefficients are the conjugate transpose of the row corresponding to the desired phi direction in the Array manifold matrix”

5) Calculate the far field as a matrix multiplication of the Array manifold matrix with the array excitation coefficients a_i

6) The total field is given by $E_{total} = \sum_{i=1}^{N} a_i \cdot E_i(\phi)$

7) Maximum gain for direction φ_0 is obtained for array excitation coefficients a_i

8) Get the corresponding radiation pattern.

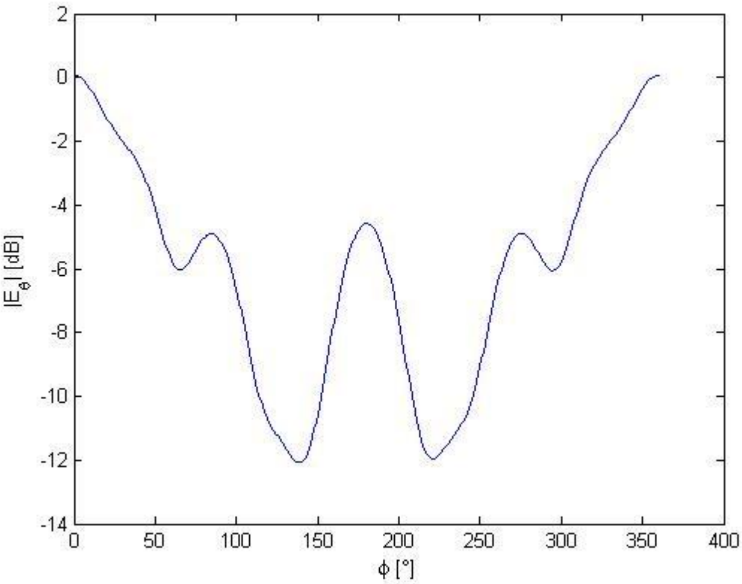

Figure 38. Embedded element pattern (Pattern on excitation by a single embedded element). The numerical value of the electric field represents the E-theta component of the Electric field in dB.

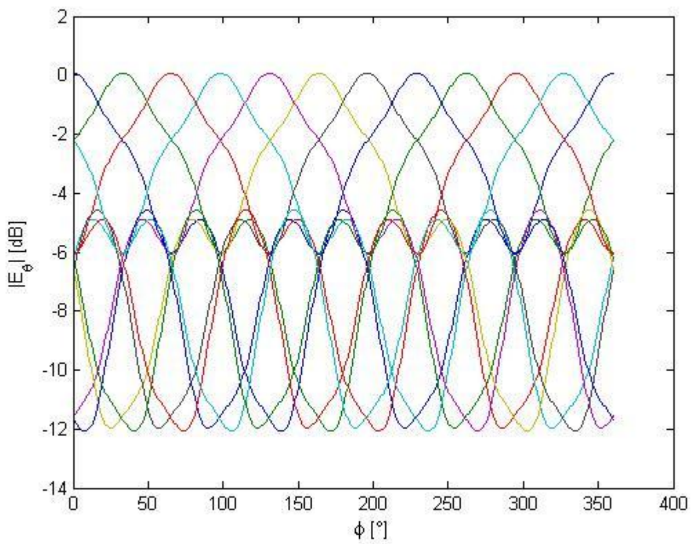

Figure 39. Superposition of fields due to rotation of the element pattern.The E-theta component of the electric field is plotted against the azimuthal angle for all the 11 elements.

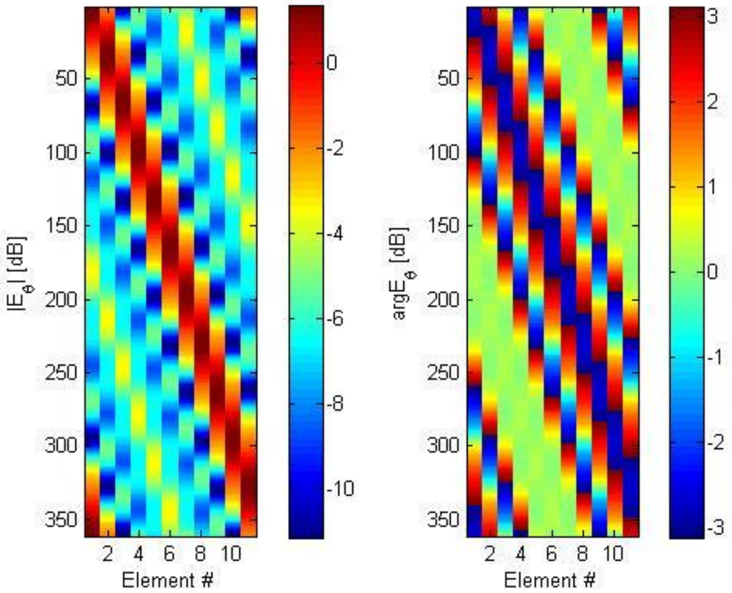

Figure 40. Array manifold for half lambda spacing (Amplitude and phase vs element).

In figure 40 on the left is the plot of the amplitude of *E*-theta component vs element number. It can be seen that there is a progressive rotational shift in the radiation pattern on moving sequentially along the number of element. The figure on the right is a plot of the phase shift in radians vs. element number. It can be seen that there is a progressive rotational shift in the phases on moving sequentially along the number of element. The scaling has been chosen so as to accommodate a grading between the maximum and minimum values in the picture.

The maximum gain method described above is employed in steering the main beam (that is obtained from the array manifold matrix) in the direction of interest of maximum gain. Presented in Figure 41 are main beams steered to 56 and 206 degrees.

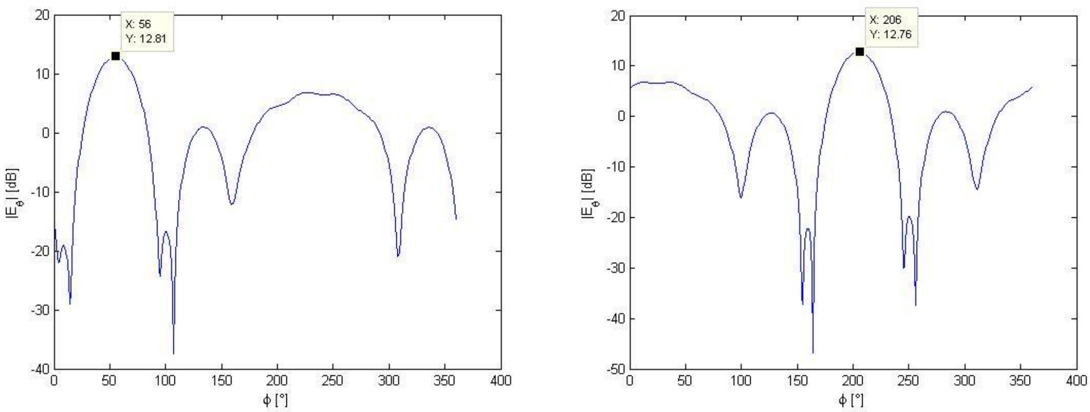

Figure 41. Main beams steered along 56 and 206 degrees using the maximum gain method. The E-theta component of the electric field is plotted against the azimuthal angle

The algorithm described above can be used to steer the main beam along any direction. However there is no control over the sidelobe levels. An algorithm that can direct main beams along particular directions with fixed sidelobe levels is developed using the generalized Bucci projection method. The

Bucci algorithm was discussed in detail in chapter 3. Here the results of Bucci beamforming are presented.

The sidelobe level that can be obtained from a given radiation pattern has a physical limit. The sidelobe level attainable is a tradeoff with the required beamwidth. The wider the beamwidth the lower is the sidelobe level. In the Bucci beamforming performed on the Dipole array at 675 MHz a sidelobe level of 20 dB was aimed at. The results are shown in Figure 42.

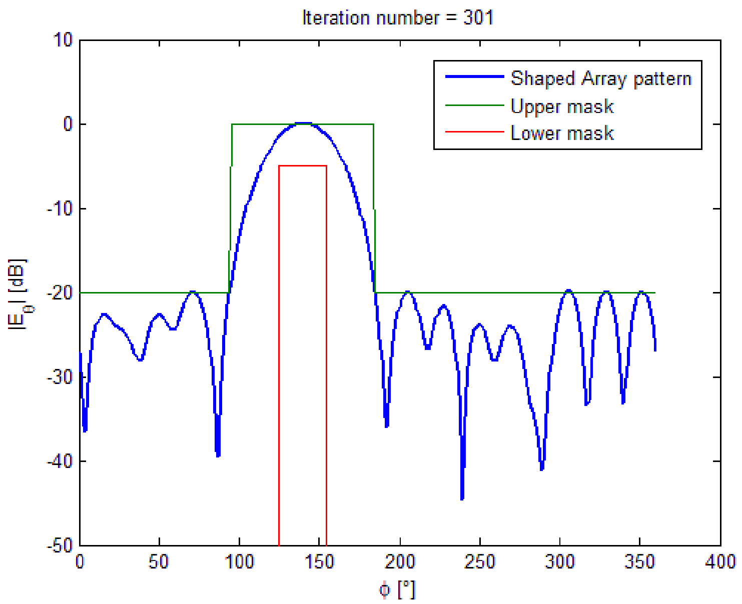

Figure 42. Bucci beamforming performed on the circular dipole array at 675 MHz

The upper mask defines the beamwidth and the location of the main lobe and the lower mask is introduced to get a pattern nearing a flat table top pattern. The extent to which this can be achieved depends on the physical limits controlled by the array radiation pattern.

5.1.5 Null introduction and steering

Using the null steering principles discussed in section 2.3 the null was introduced and steered along the desired sidelobe level as shown in the Figure 43 below:

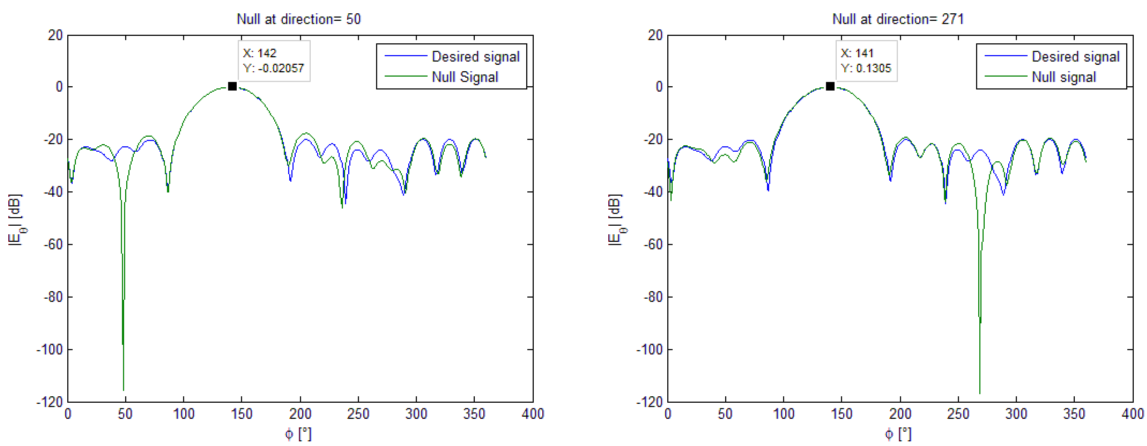

Figure 43: Null introduced at 50 and 271 degrees at the desired sidelobe level of 20 dB

- The null can only be present in directions other than the direction of the received signal i.e in the direction of the direct signals in other directions.
- The introduction of nulls seems to depend on frequency of operation. A study of this is presented in the section on the actual Discone antenna array.
- The null depth can be easily controlled by the above method by just introducing a proper weight and scaling it in the formula.

5.2 Uniform Circular Array of Discone antennas

The design of the Discone antenna element was discussed in chapter 2. The Discone antenna model in 4NEC2 library was used for the initial simulation studies. The Discone antenna model available in the library was designed for operation around 7 MHz. This antenna had to be scaled down for operation in the 450-900 MHz range. The Discone antenna element thus designed was adapted into the circular array antenna of 11 elements. The 4NEC2 simulation results of the same are presented. The Discone antenna model in 4NEC2 is shown in Figure 44.

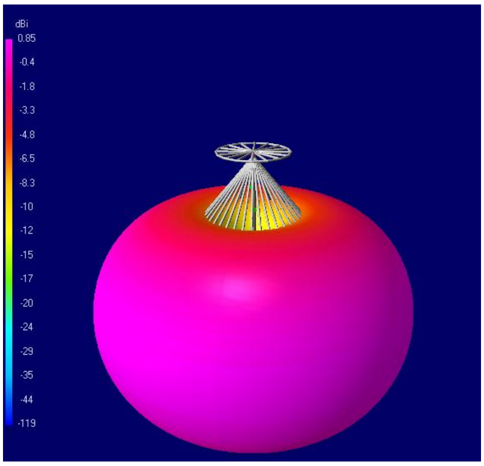

Figure 44. The wire model and the 3D radiation pattern of Discone antenna used in 4NEC2

The radiation pattern of the Discone antenna in the horizontal and vertical plane is shown in Figure 45 and the E_θ and E_ϕ polarization components are shown in Figure 46.

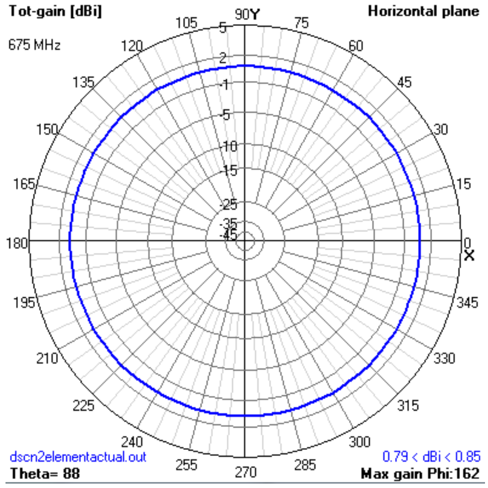

Figure 45. The horizontal and vertical radiation pattern of the Discone antenna at the center frequency of 675 MHz.

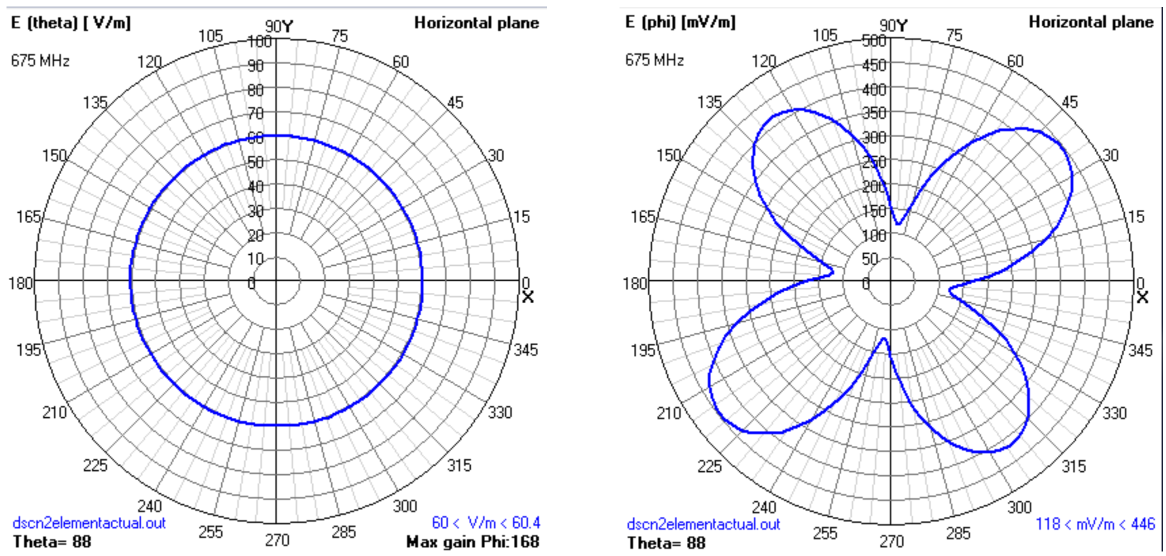

Figure 46. The E_θ and E_ϕ polarization components of the Discone antenna at the center frequency of 675 MHz.

It can be seen from figures 44 and 45 that the Discone antenna element exhibits omnidirectional pattern characteristics as desired. The return loss characteristics of the embedded Discone antenna element are shown in Figure 47.

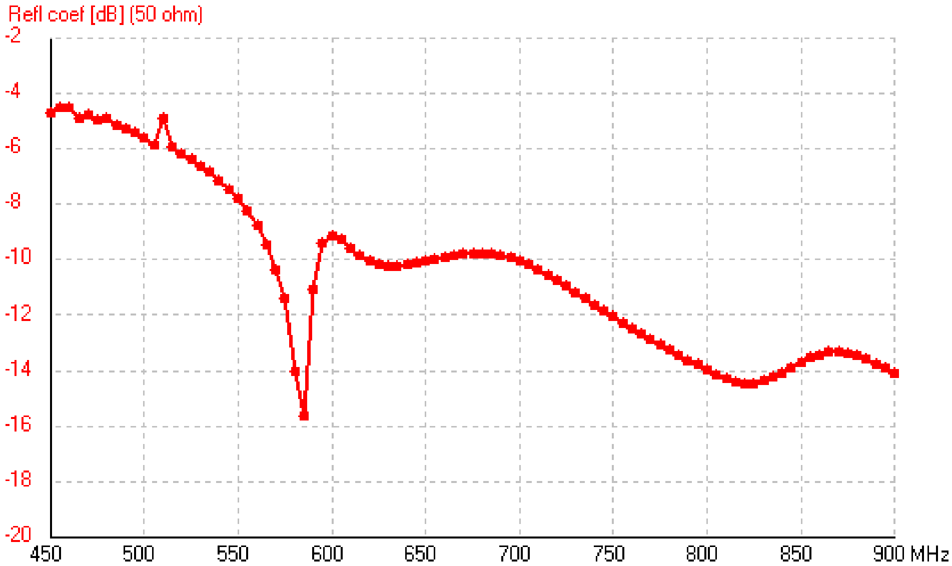

Figure 47. The return loss characteristics of the embedded Discone antenna element

The characteristics of the 4NEC2 model of the Discone meet the required criteria and therefore it was used in a uniform circular array system. The top view of the Discone array system is shown in Figure 48.

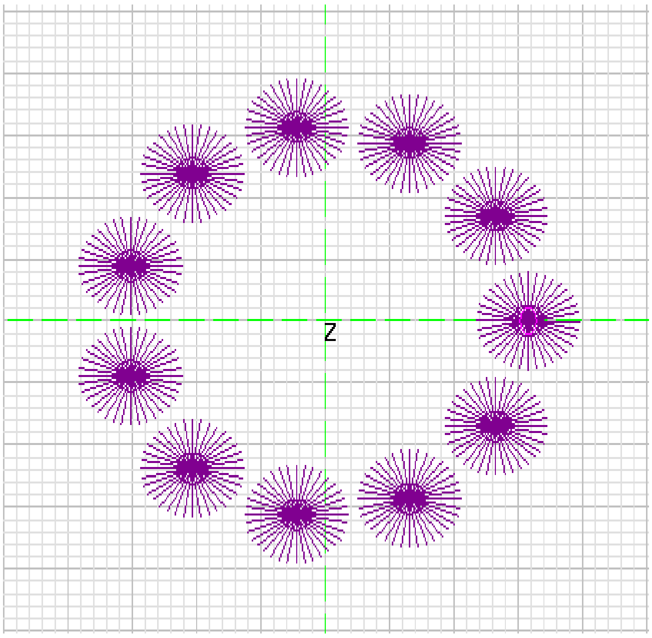

Figure 48. Figure depicting the top view of the Discone circular array model with the inter element spacing = 22 cm, and array radius of 77 cm derived through parametric studies, corresponding to center frequency of 675 MHz. Desired operational band is 450-900 MHz.

5.3 Beamforming and null steering in 4NEC2

The array thus modelled in 4NEC2 was simulated and the embedded radiation pattern obtained for all frequencies in steps of 25 MHz between 450 MHz and 900 MHz. The embedded radiation pattern was then used in generating the array manifold matrix in Matlab. Post processing in Matlab was performed to achieve beamforming and null steering. The Bucci algorithm described earlier was applied to obtain the required beamwidth and sidelobe levels. The beamforming at various frequencies is shown in Figure 49.

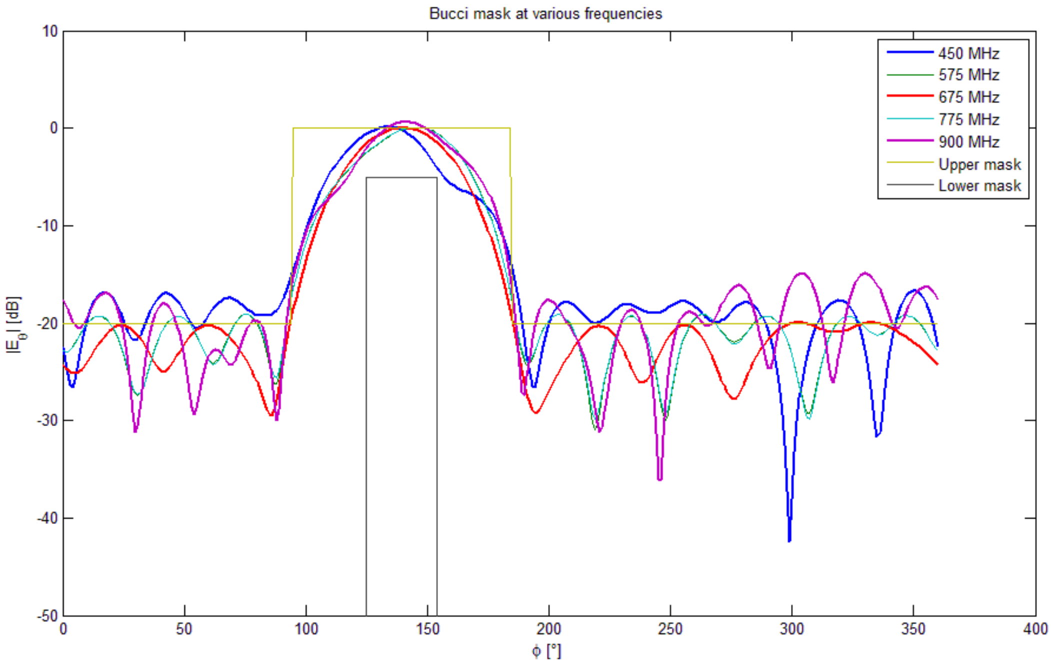

Figure 49. Bucci beamforming performed at selected frequencies.

It can be seen from Figure 49 that the beamforming is more accurate around the center frequency than at the extremes, this can be attributed to the fact that the inter-element spacing was set corresponding to the enter frequency.

1) It is seen that the inter-element spacing corresponding to half lambda is good enough for the Bucci algorithm to converge on a wide bandwidth i.e 450-900 MHz.
2) There are no grating lobes present at this spacing.
3) The convergence is very sharp at the 675 MHz operation as expected. This is because the spacing corresponds to half wavelength at 675 MHz.
4) The spacing could not be set corresponding to 900 MHz (the highest frequency) because of the limitation of the Discone element dimensions. The interelement spacing turns out much smaller than the realizable center to center spacing between the discone elements.

The Bucci beamforming algorithm involves calculating array excitation coefficients that generate the required shaped radiation pattern. The algorithm runs in iterations before it converges to a good solution (fitting the mask). The array excitation coefficients were calculated at each frequency between 450-900 MHz in intervals of 5 MHz and the sidelobe level was set to 20 dB. The results of such wideband beamforming performed are shown in Figure 33.

It can be seen that the beamforming maintains an almost constant sidelobe level of 20 dB throughout the band except at the extreme ends. This can be attributed to the physical limits set on the radiation pattern due to the interelement spacing. It can also be seen form Figure 47 that a prominent main beam with a fixed beamwidth is set for the entire frequency range from 450-900 MHz. The main beamwidth can be changed to any desired value by setting masks and so is the corresponding sidelobe level. There is a trade-off between the two. In general the wider the beamwidth the lower the sidelobe level (SLL).

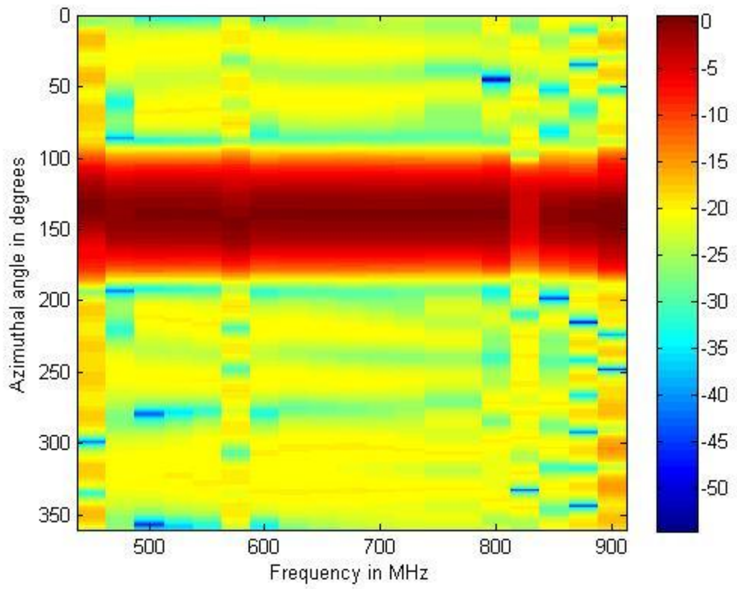

Figure 50. Bucci beamforming performed over the wideband from 450-900 MHz in steps of 5 MHz.

As stated earlier it is the requirement of the DVB-T based passive radar to have ability to introduce null in a particular direction and be able to steer it. The nulls as explained earlier are introduced by the covariance matric concept and the same was applied to the Discone antenna element array .The results are shown in Figure 51.

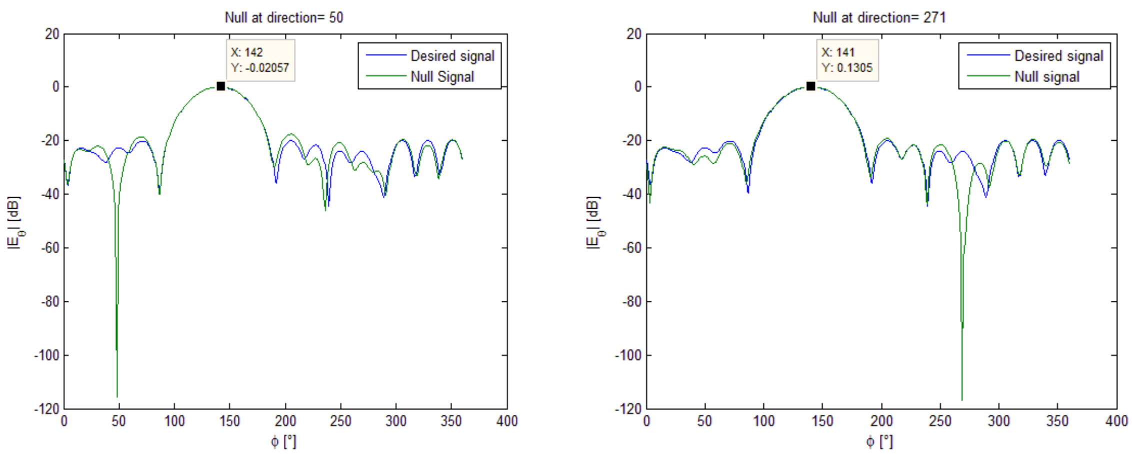

Figure 51. Null steering performed on the Discone antenna array at 50 and 271 degrees.

The null introduced at a particular frequency generated array excitation coefficients at that particular frequency. It is of interest to see if the same array excitation coefficients generated, at the center frequency (675MHz) can be used in applying nulls at other frequencies. This gives rise to a study on the null dependence on frequency. The result of this study is shown in Figure 52.

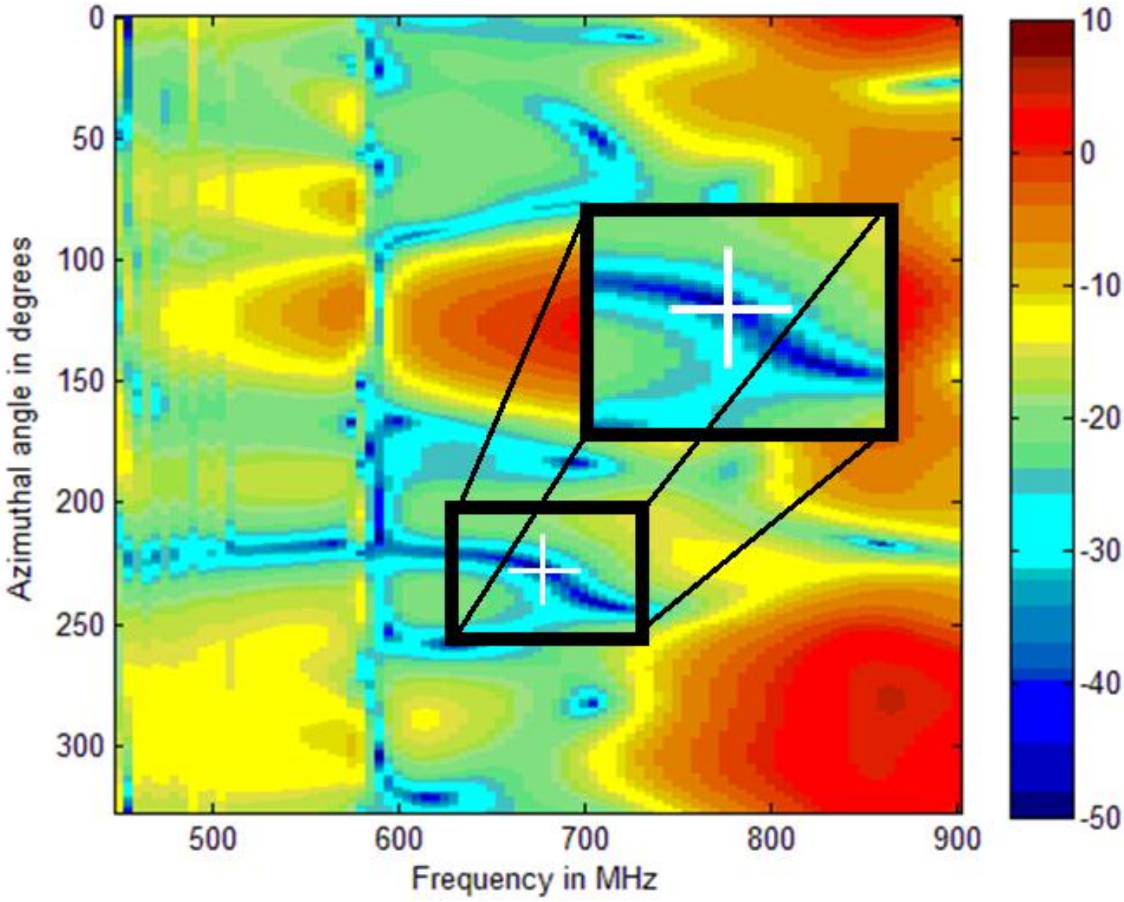

Figure 52. Null dependence over frequency with coefficients calculated for 675MHz applied over the 450-900 MHz band. Null position at 230°/675 MHz.

It can be seen from Figure 35 that the null bandwidth does not operate over the entire range when the same coefficient is used for other frequencies. The null is displaced from its location partially when approaching the frequencies lower than 675 MHz and the null gradually disappears for frequencies higher than 675 MHz.

The array excitation coefficients that are generated by the Bucci algorithm have their relative amplitudes and phases dependent on the beam direction. For example consider the beam direction along 140° at 675 MHz. The array excitation coefficients amplitude and phase is plotted vs the elements in Figure 53.

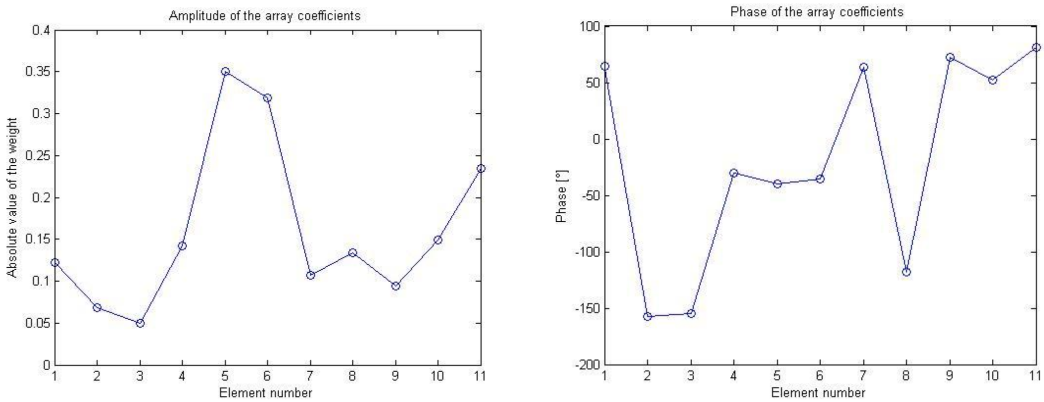

Figure 53. Array coefficients amplitude and phase.

As seen in Figure 53 the amplitude of the array coefficients is maximum along the element number 5 which corresponds to scan direction ϕ=140° as shown in Figure 54.It can be seen that the Bucci masking essentially results in dominant array elements along the desired direction and receded ones along the other directions in case of a circular array.

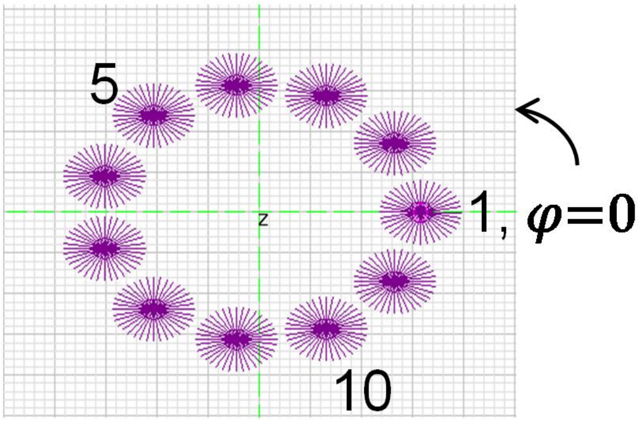

Figure 54. 11 element circular array

The embedded element radiation pattern when plotted vs the 450-900 MHz shows a 'blind spot' around 600 MHz as shown in Figure 55. Since this is due to the limit of the 4NEC2 wire grid model, it will be compared with full wave analysis of the same in the next section.

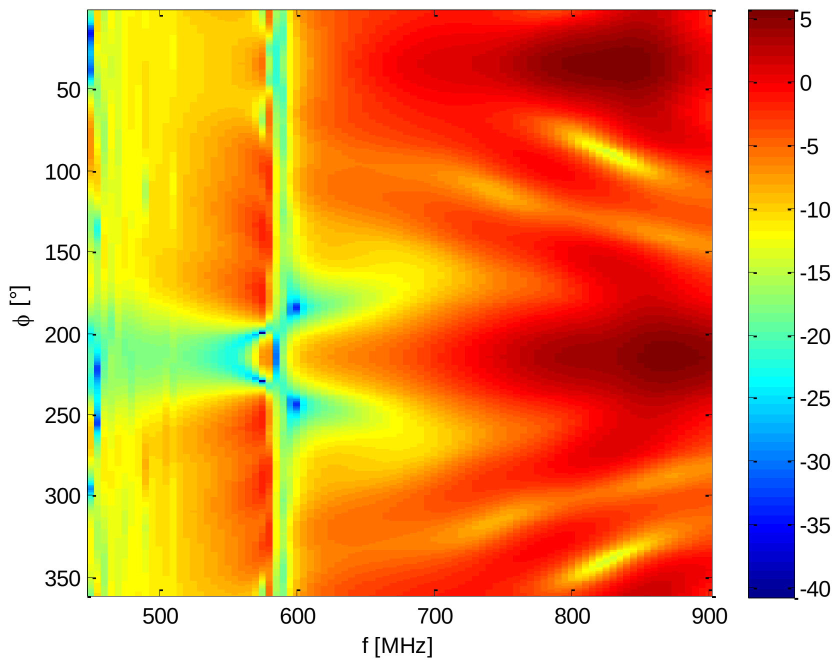

Figure 55. Embedded radiation pattern of element vs frequency

5.4 Need for CST Microwave studio validation

As discussed in the sections above the wideband array antenna has been designed using 4NEC2 and beamforming and null steering performed on it. The array design procedure is operational with wideband beamforming and null steering capabilities. Simulation has considered the EM characteristics of the Dipole and Discone via the 4NEC2 software including mutual coupling. Inter-element spacing corresponding to half lambda (at 675 MHz) is good enough for the Bucci algorithm to converge on a wide bandwidth i.e 450-900 MHz and there are no grating lobes present at this spacing. However there is a “blind spot” at around 600 MHz as in Figure 38. The existence of which has to be checked with full wave analysis using CST Microwave studio. CST Microwave studio provides better options for modeling the Discone antenna when compared to 4NEC2. 4NEC2 Discone antenna model is a wire grid model and is only an approximation to the actual solid Discone antenna. The solid Discone antenna model can be more realistically designed and simulated in CST Microwave studio.

The 4NEC2 Discone antenna model is an approximate model to the actual Discone antenna discussed in chapter 2. Therefore an actual model of the Discone antenna built in CST Microwave studio will be used in further studies.

In view of the above two requirements the Discone antenna model was used in CST Microwave studio and the beamforming and null steering studies were performed on it. The CST Microwave studio simulation results and analysis is presented in the next section.

5.5 CST Microwave studio analysis

In any design the ability to have a superior and user friendly Graphical User Interface (GUI) always aids the design process and allows for better handling of the structure in the CAD tool. CST

Microwave studio is a CAD tool that combines the power of efficient EM solvers with extremely user friendly GUI.

CST MICROWAVE STUDIO 2012 is a full-featured software package for electromagnetic analysis and design in the high frequency range. It simplifies the process of inputting the structure by providing a powerful solid 3D modelling front end. Strong graphic feedback simplifies the definition of your device even further. After the component has been modeled, a fully automatic meshing procedure is applied before a simulation engine is started [36].

CST MICROWAVE STUDIO is part of the CST DESIGN STUDIO suite [35] and offers a number of different solvers for different types of application. Since no method works equally well in all application domains, the software contains four different simulation techniques (transient solver, frequency domain solver, integral equation solver, eigenmode solver) to best fit their particular applications.

A brief description of the four solvers as defined by CST Studio Suite is given below [35]

- **Transient solver**: This is a very flexible time domain simulation module that is capable of solving any kind of S-parameter or antenna problem. It will stimulate the structure at a previously defined port using a broadband signal. Broadband stimulation enables you to receive the S-parameters for your entire desired frequency range and, optionally, the electromagnetic field patterns at various desired frequencies from only one calculation run.
- **Frequency Domain Solver**: Like the transient solver, the main task for the frequency domain solver module is to calculate S-parameters. Due to the fact that each frequency sample requires a new simulation run, the relationship between calculation time and frequency steps is linear unless special methods are applied to accelerate subsequent frequency domain solver runs. Therefore, the frequency domain solver usually is fastest when only a small number of frequency samples need to be calculated. Hence, a broadband S-parameter simulation with adaptively chosen frequency samples is performed to minimize the number of solver runs. Especially for lower frequency problems with a small number of mesh cells (e.g. 50,000) the frequency domain solver may be an interesting alternative to the transient solver.
- **Eigenmode Solver**: In cases of strongly resonant loss-free structures, where the fields (the modes) are to be calculated, the eigenmode solver is very efficient. This kind of analysis is often useful for determining the poles of a highly resonant filter structure. But of course there are different applications for the eigenmode solver: with periodic boundaries and a non-zero phase shift for instance, the eigenmodes are traveling waves. The eigenmode solver directly calculates the first N frequencies for which fields may exist in the structure, and the corresponding field patterns.
- **Integral Equation Solver**: The areas of application for the integral equation solver are S-Parameter and Farfield/ RCS calculations. The integral equation solver is of special interest for electrically large models. The discretization of the calculation area is reduced to the object boundaries and thus leads to a linear equation system with less unknowns than volume methods. The system matrix is dense. For calculation efficiency the equation system is solved by the Multi Level Fast Multipole Method (MLFMM). The integral equation solver is available for plane wave excitation and discrete face ports. Electric and open boundaries are supported. Far field monitors and surface current monitors can be set in the Frequency Domain Solver with surface mesh.

The most flexible tool is the transient solver, which can obtain the entire broadband frequency behavior of the simulated device from only one calculation run (in contrast to the frequency step approach of many other simulators). It is based on the Finite Integration Technique (FIT) introduced in electrodynamics [36]. This solver is efficient for most kinds of high frequency applications such as connectors, transmission lines, filters, antennas and more. For the current array antenna purpose the Time Domain solver was used.

The General CST simulation workflow is listed below:

- Define the Units
- Define the Background Material: The background material has to be set. For an antenna problem, these settings have to be modified because the structure typically radiates in an unbounded/open space or half-space.
- Modelling the Structure
- Define the Frequency Range
- Define Ports: The ports define the excitation to the structure. The correct definition of the port is essential to get accurate S parameters.
- Define Boundary and Symmetry Conditions: The ability to define symmetry planes is very useful especially when there is a large structure with large number of mesh cells.
- Set Field Monitors: To calculate the farfield at desired frequencies field monitors have to be set at those frequencies.
- Start the Simulation

When the simulation run completes successfully the output data such as the far field patterns at the field monitors and the calculated S parameters are available for analysis and interpretation.

5.6 Discone antenna array designed using CST Microwave Studio

The Discone antenna array was designed in CST MWS 2012. The Discone antenna model described in chapter 2 was used in the array design. The array antenna was built with a diameter of 77 cm as found by 4NEC2 simulations. One of the Discone antennas was excited with a waveguide port and the rest of the antenna ports were matched terminations. As the number of mesh cells obtained for such an antenna was very large - 90 million cells, a symmetry plane was defined to ease the computation load. The antenna array structure is shown in Figure 56.

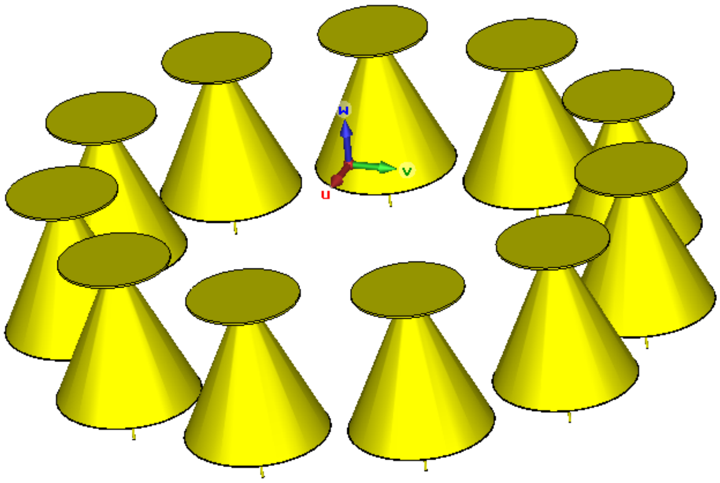

Figure 56. Discone antenna array model designed in CST MWS. Array diameter is 77 cm. The type of feeding is coaxial feed from bottom of Discone. The center frequency of operation is 675 MHz.

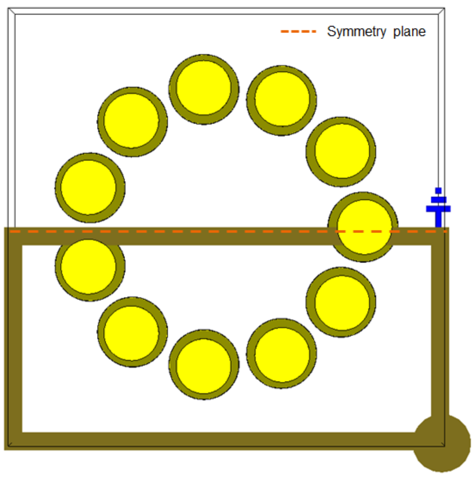

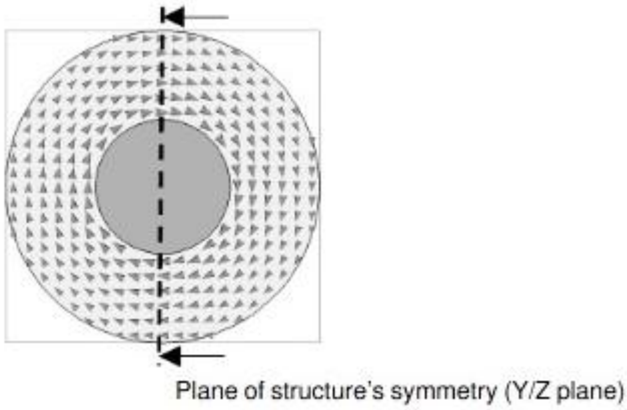

Figure 57(a). Top view of the array antenna showing a magnetic symmetry plane passing through the center of the array along its diameter.(b) The magnetic field in the fundamental mode of coaxial cable

As in Figure 57(a) the symmetry plane chosen was a magnetic one and it passes right through the antenna that is excited thereby dividing the array into two symmetrical halves. The decision on the magnetic symmetry plane was made on the fact that the single antenna is excited by a coaxial cable and the excitation of the field will be performed by the fundamental mode in the coaxial cable for which the magnetic field is shown in Figure 57(b).The magnetic field has no component tangential to the plane of the structure's symmetry. The electric fields are parallel to the boundary and magnetic fluxes are normal to the boundary. Thus the symmetry plane chosen was magnetic. The definition of such a symmetry plane reduced the computational effort on the CPU by almost half.

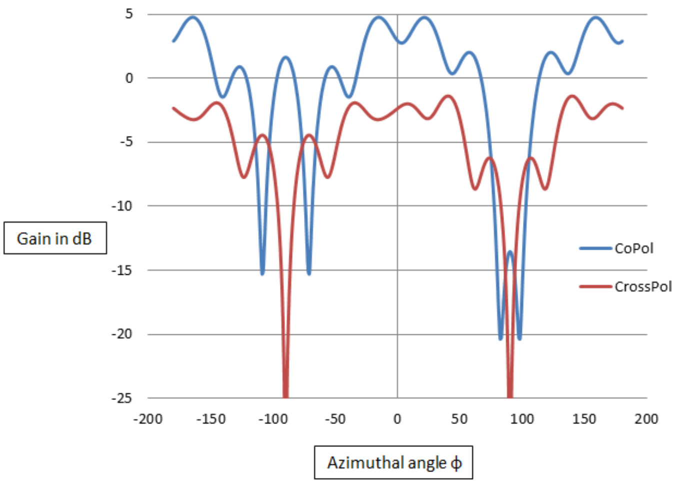

(a)

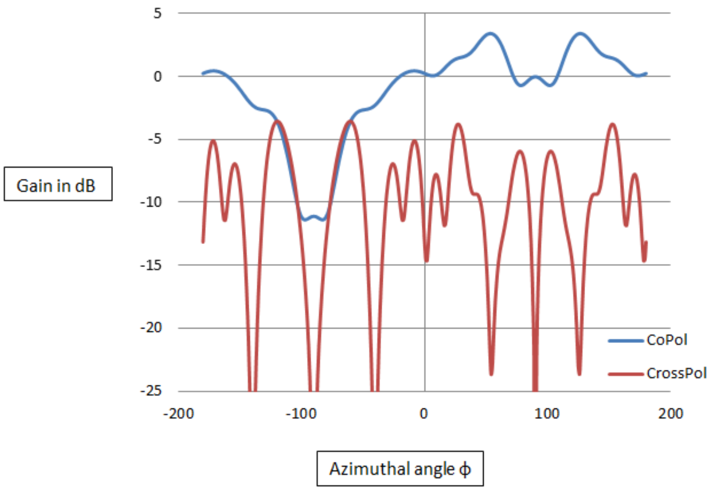

(b)

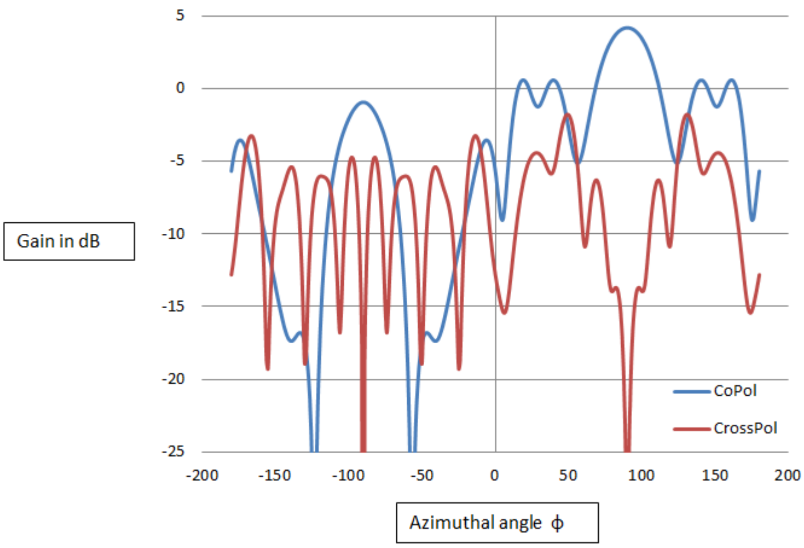

(c)

Figure 58. The embedded radiation pattern of the single element antenna along the azimuthal plane $(\theta = 90^{\circ}, 0 < \phi < 360^{\circ})$ **at 450, 675 and 900 MHz with the Co and Cross polarization levels is shown in (a), (b) and (c) respectively.**

The embedded radiation pattern of the array antenna has omnidirectional characteristics in the azimuthal plane and it is seen for all the three frequencies of 450,675, and 900 MHz in Figure 58.

The embedded radiation pattern of the array antenna is read from CST into Matlab and then the post processing is performed in Matlab. The embedded array pattern is rotated and superposed to obtain the array manifold matrix. The array manifold amplitude and phase plotted against the element number at the center frequency of 675 MHz is shown in Figure 59.

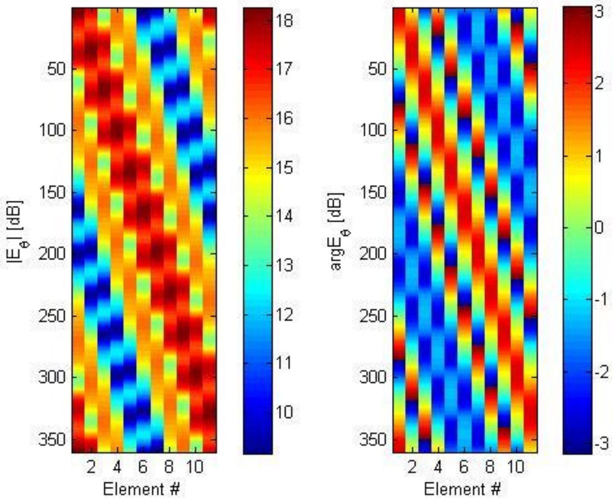

Figure 59. The array manifold amplitude and phase plotted vs the element number. The rotation of the filed amplitudes and phases along with the element number is clearly seen. The rotation is bin steps of 360/11 degrees.

The array manifold matrix derived using the procedure described above is then subject to Bucci beamforming by setting masks and projecting the farfields onto this mask in an iterative fashion as shown in Figure 60

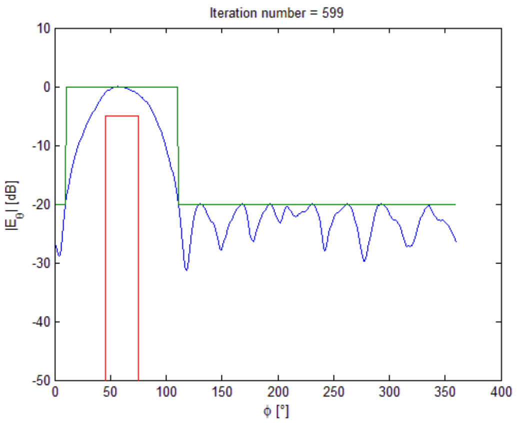

(a)

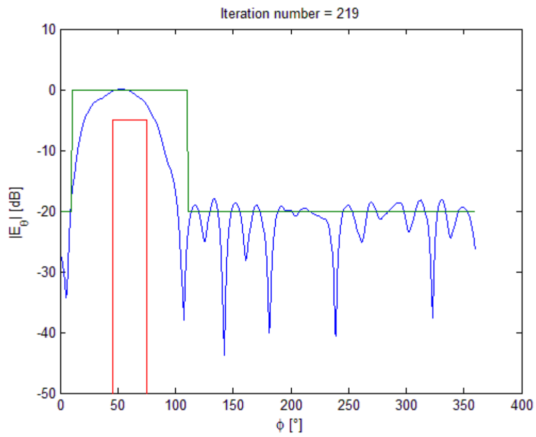

(b)

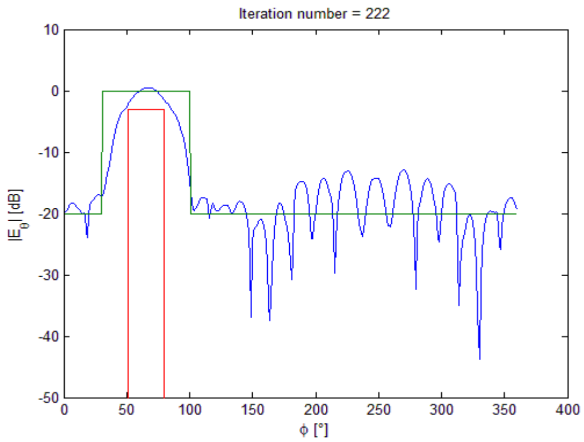

(c)

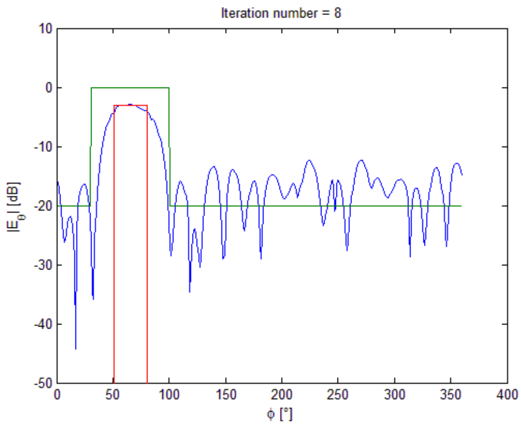

(d)

Figure 60. a,b,c and d show the Bucci beamforming performed using embedded element pattern obtained using CST MWS at 450, 675, 875and 900 MHz respectively

The Bucci beamforming algorithm involves calculating array excitation coefficients that generate the required shaped radiation pattern. The algorithm runs in iterations before it converges to a good solution (fitting the mask). The array excitation coefficients were calculated at each frequency between 450-900 MHz in intervals of 25 MHz and the sidelobe level was set to 20 dB. The results of such wideband beamforming performed are shown in Figure 58.

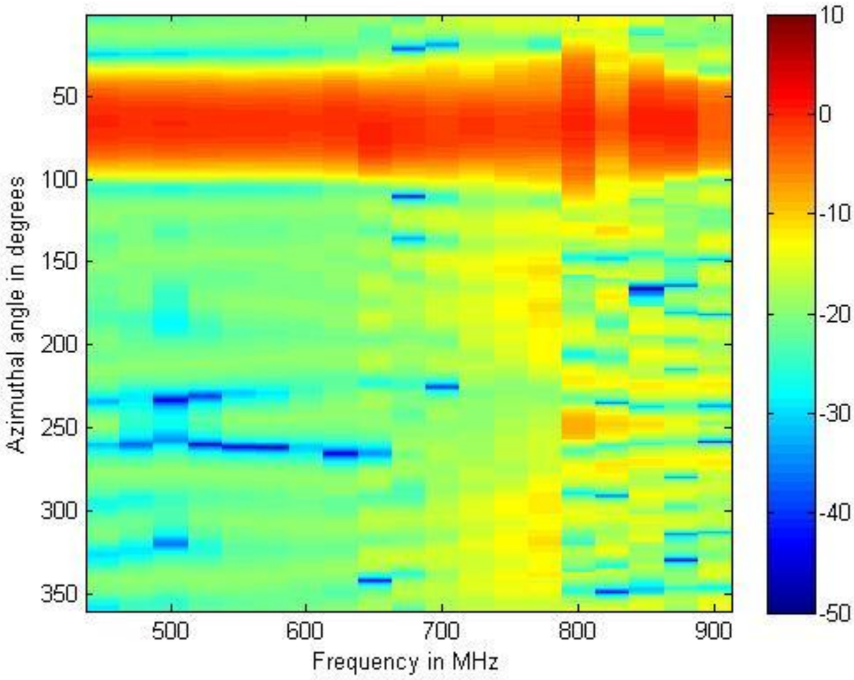

Figure 61. Bucci beamforming performed over the wideband from 450-900 MHz in steps of 25 MHz.

It can be seen from Figure 61 that the beamforming performs good at all frequencies except around the higher frequencies where though the required main beam is obtained in the desired direction, the sidelobe levels (SLL) are a bit high. This can be attributed to the physical limits set on the array due to its inter element spacing. However the sidelobe levels can be made lower by increasing the beamwidth at higher frequencies.

The nulls as explained earlier are introduced by the covariance matrix concept and the same was applied to the Discone antenna element array. Two typical null steering examples are shown in Figure 62.

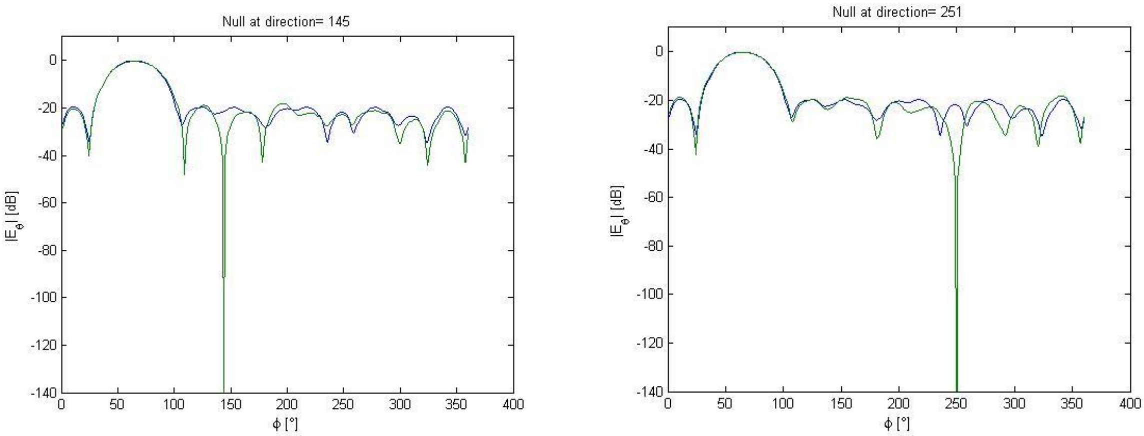

Figure 62. Null steering performed on the Discone antenna array at 145 and 251 degrees using CST MWS radiation patterns

As seen in the post processing results performed using 4NEC2 the embedded element radiation pattern vs frequency exhibited a' blindspot' at around 600 MHz. When the post processing was performed using the CST MWS embedded element pattern the 'blindspot' at 600 MHz was no longer seen. The results are shown in Figure 63. This can be explained by attributing the appearance of 'blindspot' in 4NEC2, to the approximation done in 4NEC2 modeling of the Discone antenna as a wire grid model. The 'blindspot' is often caused by array mutual coupling, which tends to direct the radiation in the plane of the array, rather than as a wave propagating away from the array. Careful design of the array element shape, size, and spacing can prevent the occurrence of blind spots [38]. Since the Discone antenna array is in free space, there is little scope for the existence of surface waves, which hints that there should be no 'blindspot' expected. Thus the existence of blindspot in 4NEC2 could be a numerical artefact and this had to be investigated further using CST Microwave studio. The Discone antenna could be modeled more accurately in CST MWS. CST MWS models and solves the array in a different manner using FIT (Finite integration technique). The much more accurate Discone model designed in CST explains the disappearance of the 'blindspot' in CST MWS. It can also be seen from the CST pattern, Figure 63(b), that there is a more directive pattern at high frequency.

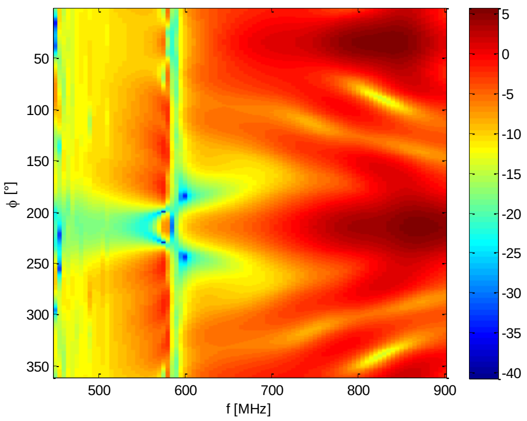

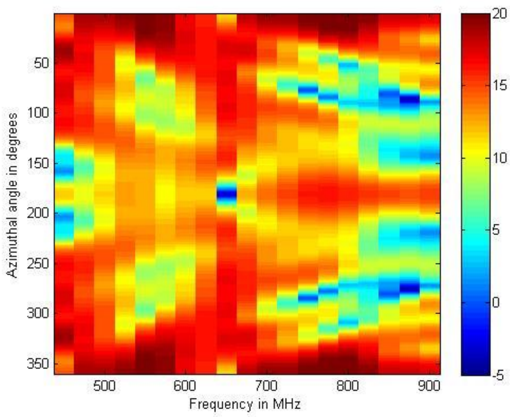

(a) (b)

Figure 63. (a) 'Blindspot' seen around 600 MHz using 4NEC2 embedded pattern. (b) The 'Blindspot' disappears around 600 MHz on using CST MWS embedded pattern.

5.7 Supporting structure and its influence on the antenna performance

The wideband array antenna designed above needs a supporting structure to rest on. This supporting structure is expected to have influence over the radiation pattern. Therefore the supporting structure was designed using CST MWS and its effect on the radiation pattern and mutual coupling was studied. In addition to the aluminium support rods arranged radially along the array, the support structure consists of a central mast that extends from the array to the ground. Since the mast is long, the cylindrical space around it with diameter equal to the array diameter takes up quite a lot of volume and thus leads to huge number of mesh cells which makes it impossible to solve on the CPU.
However it is well known fact that the mast should not have much influence on the operation as it is anyway located along the nulls of the radiation pattern. For this reason the studies were done without the mast and consisting of the support structure only. A single element of the support structure is shown in Figure 64.

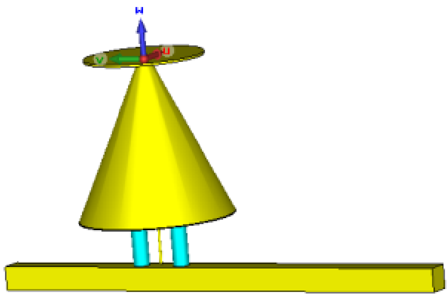

Figure 64. Single element of the support structure with parallelopiped aluminium supports and PVC connectors from Discone to aluminium support.

The support structure designed using the element in Figure 64 is shown in Figure 65.

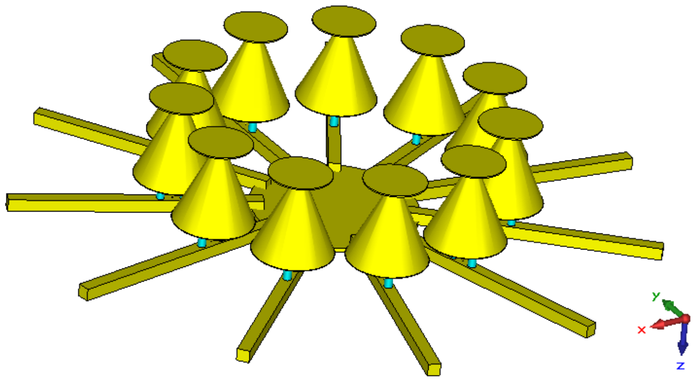

Figure 65. Support structure for the array antenna built using element in Figure 64.

The 3D radiation pattern with the support structure is shown in Figure 66. The computation was highly intensive and it was solved using GPU acceleration. Time taken to solve using GPU was 15 hrs.

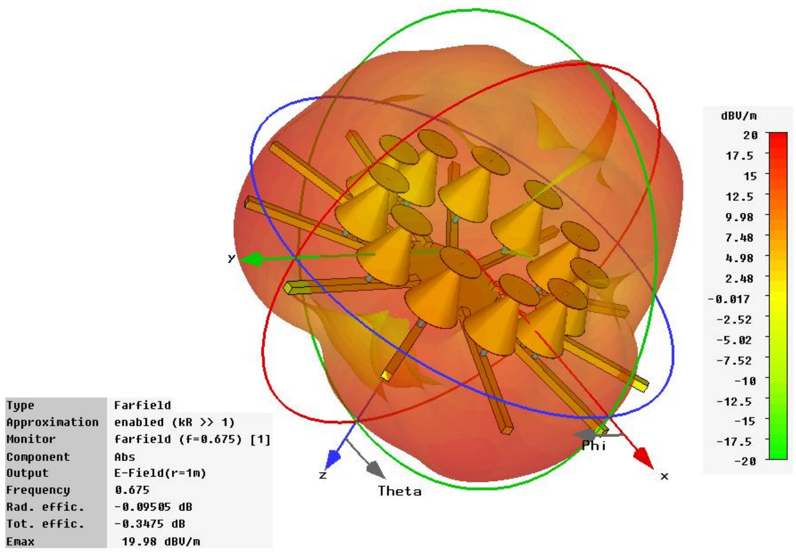

Figure 66. 3D radiation pattern of the array antenna with support structure

In order to assess the coupling effects of the aluminium support rods on the antenna pattern, a full wave solution of the antenna array with the supporting structure is required. However this is difficult to compute on the CPU due to memory limits. Therefore a section of the array was considered to study mutual coupling effects. The section consists of 5 antennas with the center antenna fed and the mutual coupling along the other antennas on either side studied. This was performed with and without the supporting structure to see its influence. The results are shown in Figure 67 and 68. It can be seen from the figures 67 and 68 that the supporting structure does not much influence the coupling.

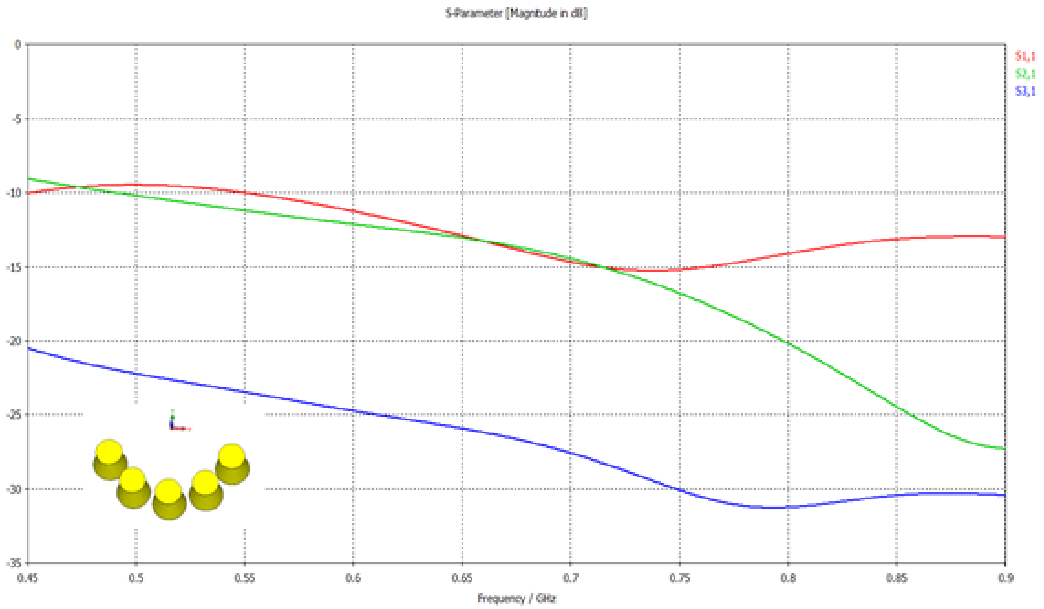

Figure 67. The S11, S12 and S13 for a section of the array without the supporting structure.

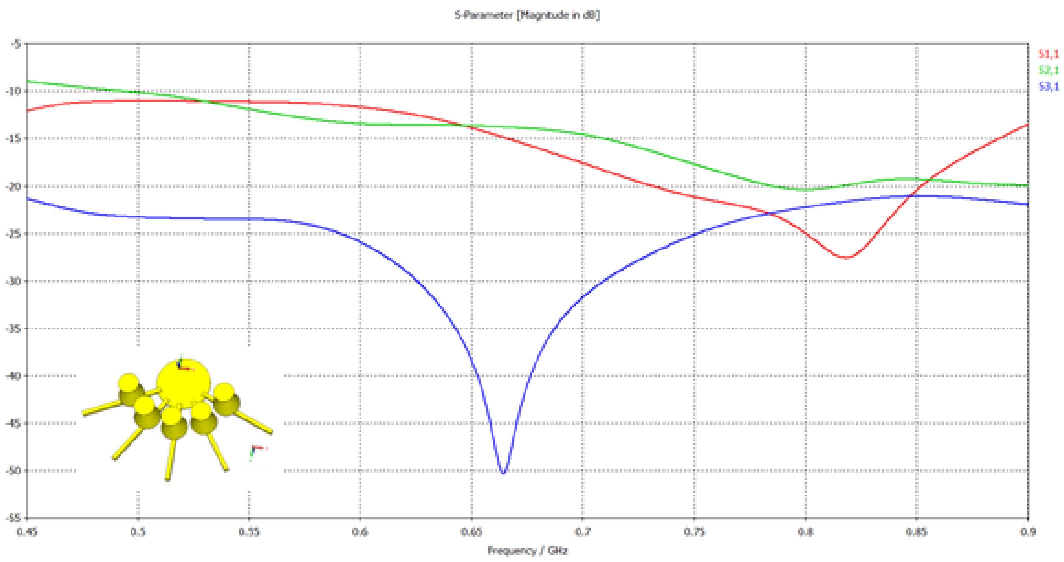

Figure 68. The S11, S12 and S13 for a section of the array with the supporting structure.

It now follows to compare the radiation pattern for this section at different frequencies with and without the support structure. A comparison of the radiation pattern is presented at 450,675 and 900 MHz in Figure 69.

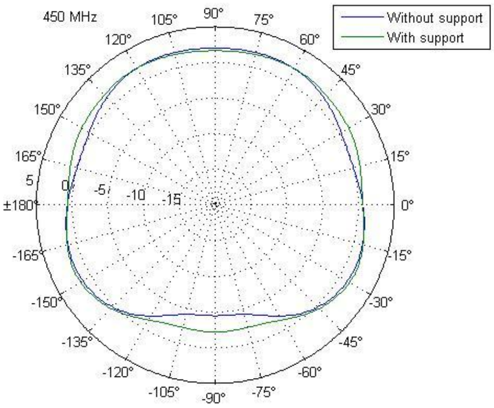

(a)

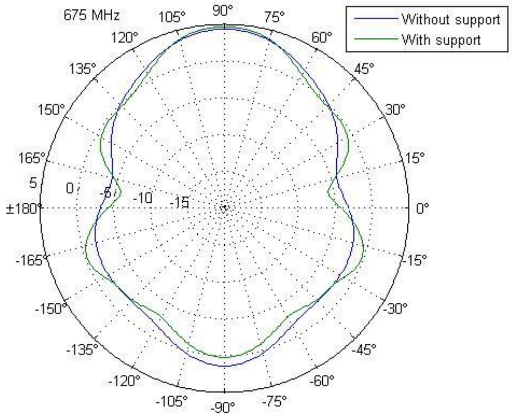

(b)

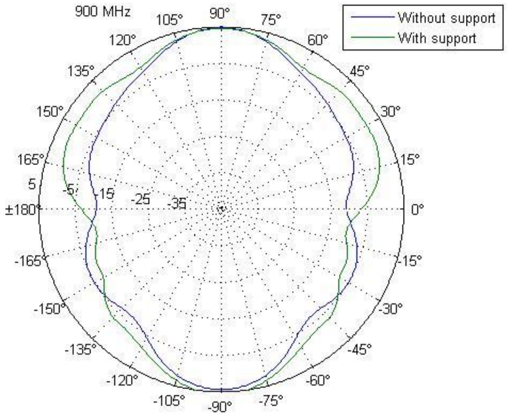

(c)

Figure 69. Comparison of the radiation patterns without and with the support structure at a) 450 MHz b) 675 MHz and c) 900 MHz. It can be concluded that the radiation pattern is comparable and does not deviate much from its normal pattern when a support structure is used.

5.8 Polarimetric beamforming

The DVB-T signals are mostly vertically polarized. The reception of these vertically polarized signals by the antenna becomes a crucial factor in deciding the polarization purity of the received signals. The antenna has to have very low levels of cross polarization and good co-polarization patterns. The beamforming performed keeping in consideration the polarization aspects of the received signals is called polarimetric beamforming.

The polarimetric beamforming was realized as detailed below:

Beamforming involving, applying the same array excitation coefficients, generated for the copolarization patterns, on the cross polarization patterns too. The results of such beamforming done on the Discone antenna array is shown in Figure 70.

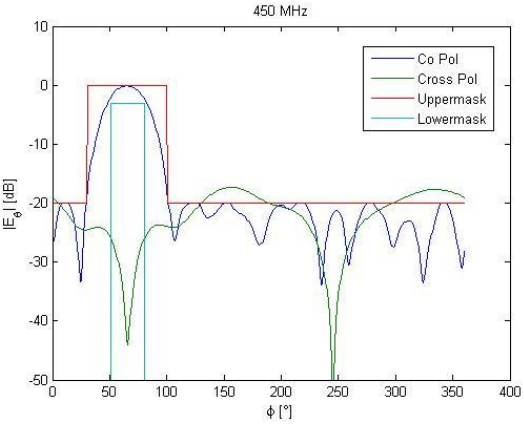

(a)

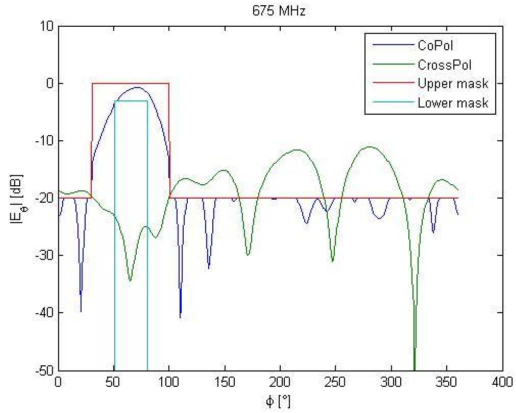

(b)

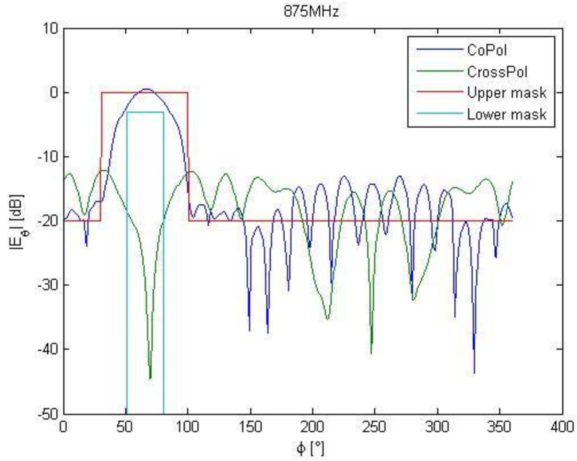

(c)

Figure 70. Polarimetric beamforming with same array excitation coefficients for Co-polar and Cross polarizations at a) 450 MHz b) 675 MHz c) 875 MHz

Polarimetric beamforming involving concatenation of the copolar array manifold matrix with the cross polar array manifold matrix and then applying masks for both together and doing iterative Bucci beamforming. The results of such beamforming is shown in Figure 71

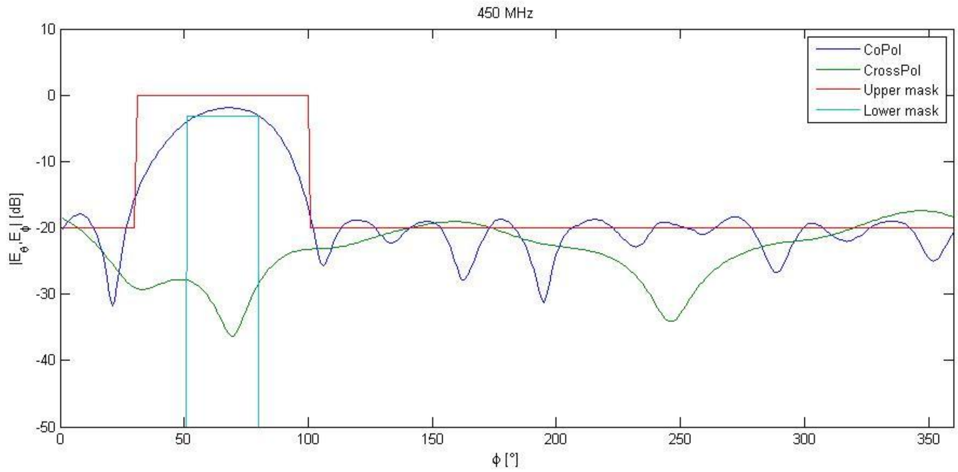

(a)

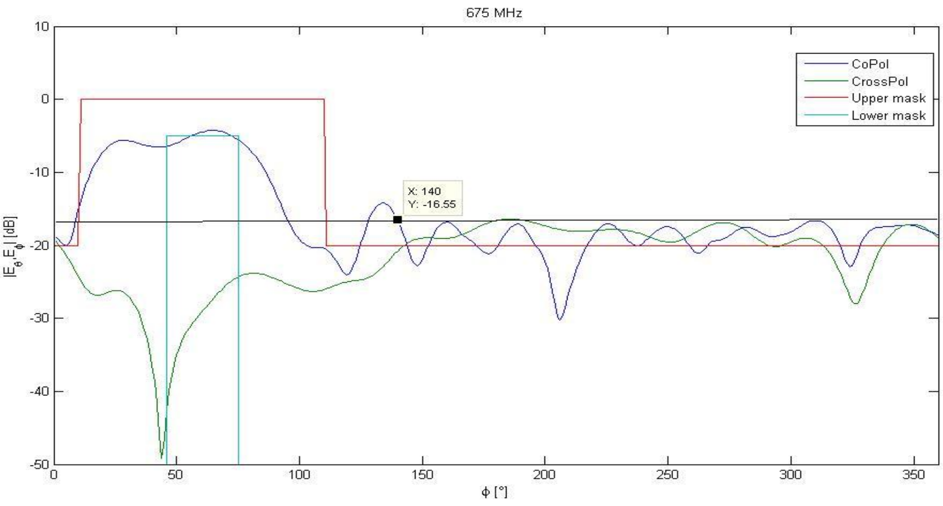

(b)

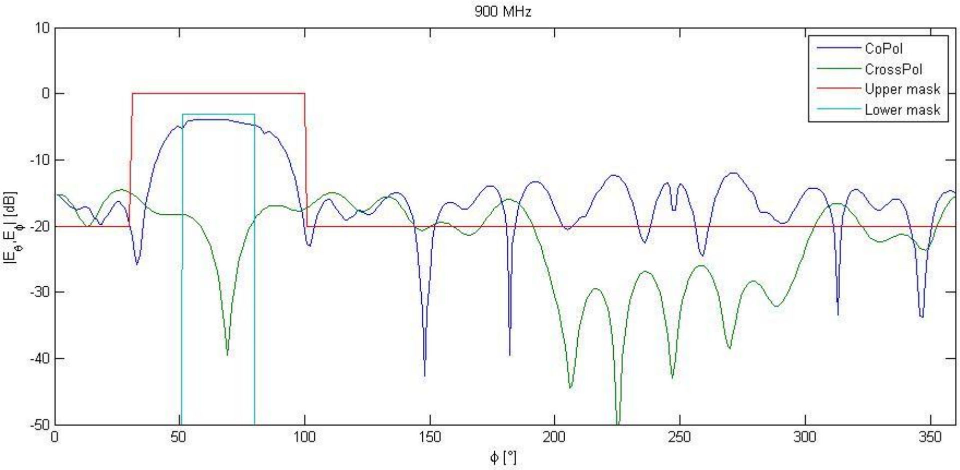

(c)

Figure 71. Polarimetric beamforming involving concatenation of the copolar array manifold matrix with the cross polar array manifold matrix for frequencies a) 450 MHz b) 675 MHz c) 900 MHz

On comparison between Figure 70 and 71 it can be seen that the polarimetric beamforming involving concatenation of the copolar array manifold matrix with the cross polar array manifold matrix works better at the desired frequencies though the performance is satisfactory at higher frequencies.

Chapter 6- Experimental validation

6.1 Measurement results of Discone antenna

The Discone antenna elements were fabricated and measured individually for their performance characteristics. The measurement results of these are presented in this section.

The fabricated Discone antenna is shown in Figure 72.

Figure 72. The fabricated Discone antenna

The construction and design rules for these Discone antennas have already been presented in section 2.1.The measured antenna input reflection coefficient for two different feeding mechanisms is shown in Figure 73. Type A is for top feeding connector and Type is for bottom feeding connector. It can be seen that the return loss is well below 10 dB throughout the desired range.

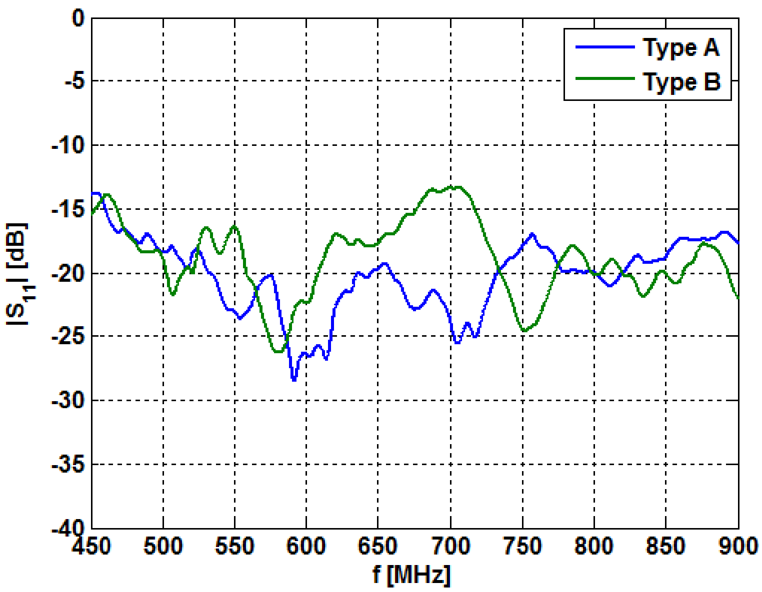

Figure 73. The measured return loss characteristics of the antenna [8]

The measured antenna radiation pattern in the elevation plane for Discone with Vertical Polarization is shown in Figure 74 for three different frequencies.

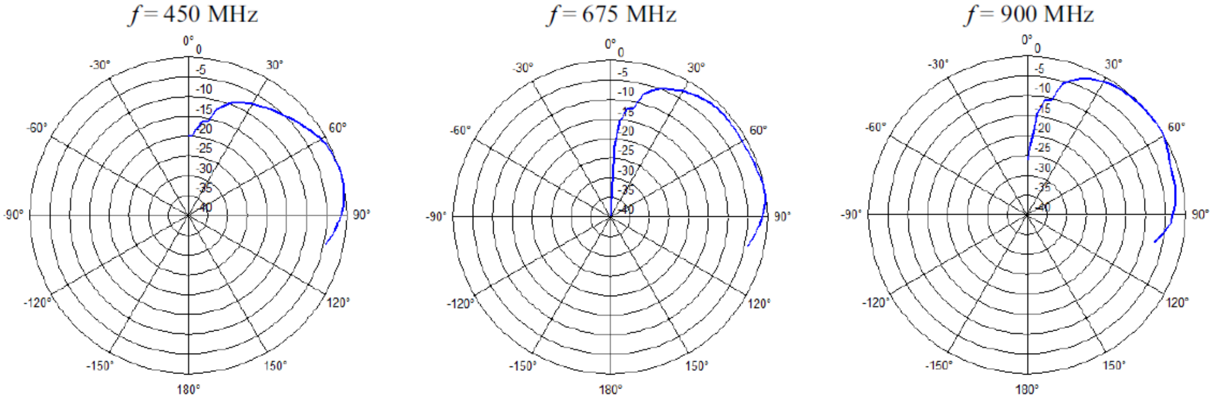

Figure 74. The measured antenna radiation pattern in the elevation plane for Discone with Vertical Polarization at three different frequencies [8].

6.2 Experimental set up

The fabricated Discone antenna array along with the supporting structure is placed in the anechoic chamber for measurement of far field patterns. A log periodic antenna will be used as probe to evaluate the near fields of the antenna array and the far fields are calculated from them by a transformation. The probe antenna is able to scan the array along azimuthal and elevation directions. The transmitting and receiving antennas namely the probe and the antenna array can be used to calculate the gain of the antenna array too by applying well known Friis formula or modified version of it:

$$\frac{P_r}{P_t} = G_t G_r \left(\frac{\lambda}{4\pi R} \right)^2 \qquad (64)$$

where P_r is the power available at the input of the receiving antenna, P_t is the power at the transmitting antenna and G_t, G_r are gain of antennas at transmitter and receiver respectively and R is the distance between the antennas.

The antenna can also be checked for beamforming capabilities by exciting the individual Discone antenna elements with different voltages one at a time and then superposing the patterns and performing Bucci masking. At the time of writing of the thesis the supporting structure for the array was being built. So a picture showing the 11 manufactured Discone antenna elements arranged in a circle is presented in Figure 75. The antenna anechoic chamber for the setup is shown in Figure 76. Figure 77 shows the control room for the anechoic chamber.

Figure 75. 11 Discone antenna elements

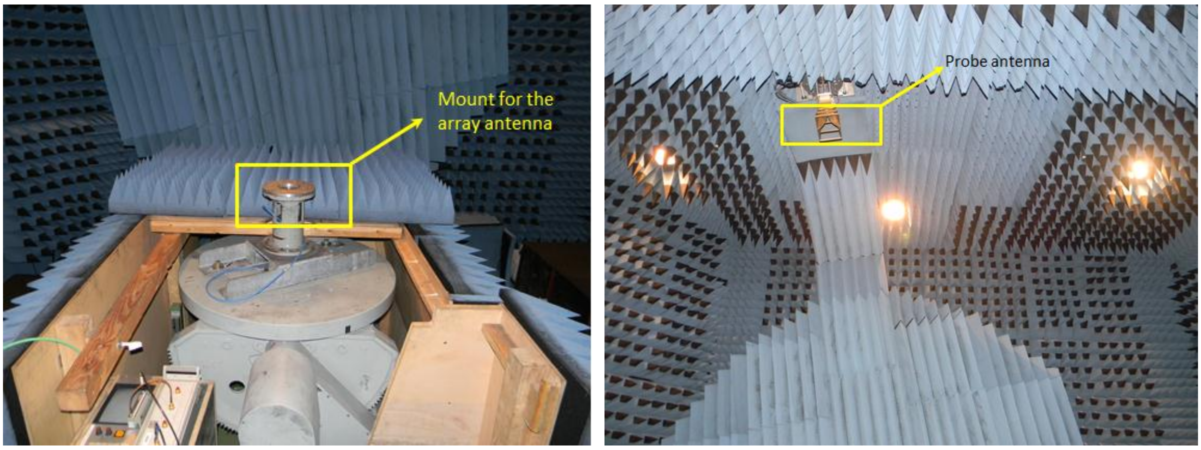

(a) (b)

Figure 76 (a). Mount for the array antenna in the anechoic chamber (b) The probe antenna

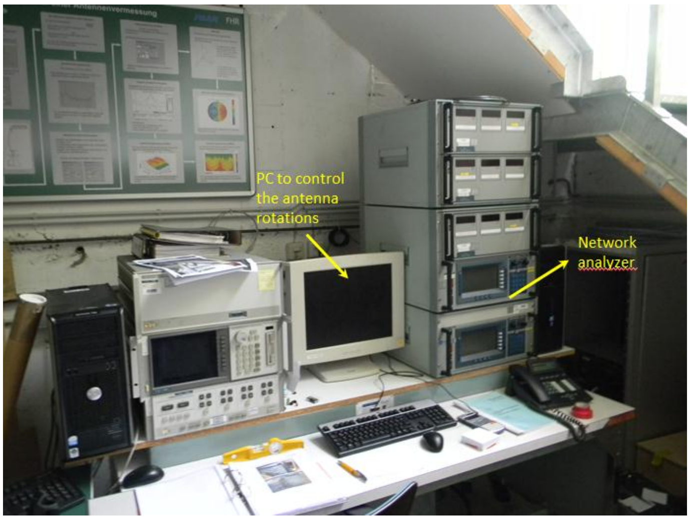

Figure 77. Control room for the anechoic chamber.

Chapter 7-Conclusions and future work

7.1 Conclusions

The goal of this work was to design and develop a wideband antenna array for application in the DVB-T passive radar with necessary algorithm implementation. The design of the wideband antenna array was successfully carried out with wideband beamforming and null steering capabilities. The design studies were started with a dipole antenna array. Several parametric studies were made to decide on the appropriate inter-element spacing between the elements of the array taking into account the interaction between the grating lobes and mutual coupling. A full wave EM analysis was conducted and using these results , later the Discone antenna element was used for the actual design of the antenna array. The embedded Discone antenna element pattern was used in generating the array manifold matrix and beamforming and null steering were performed. The phenomenon of occurrence of "blindspot" usually observed in arrays was thoroughly investigated using both 4NEC2 and CST microwave studio and it was concluded through simulations that the "blindspot" does not actually exist in the designed array.

Extensive simulation studies were performed on the designed antenna array to test its performance when a main beam and a null are introduced in different directions. Studies were done taking into account the polarization aspect and correspondingly polarimetric beamforming was performed. The beamforming done with the Bucci algorithm has shown good results over a wide range of frequencies around the center frequency. However at the upper and lower end of the frequency range some problems with high side lobes are seen. - There may be several possible explanations for this behavior: On one hand side, the antenna elements have a half-wavelength spacing only around the center frequency of 675 MHz. For lower frequencies where the wavelength increases, the antenna array becomes electrically small and can hardly satisfy the given main lobe width and side lobe level requirements. At the upper frequencies where the wavelength is smaller, the spacing between neighboring antenna elements becomes larger and effects similar to the grating lobes of linear / planar arrays may occur.

On the other side is the strong increase of cross polarization due to the effects of mutual coupling. The close inter-element spacing causes strong coupling which affects the current distribution on the discone antennas and alters the embedded element radiation pattern. It is shown in section 5.6 that the amount of horizontal polarization in the far-field increases and that, for some directions, it is in the same order of magnitude as the main polarization. This deteriorates the quality of the far-field radiation patterns and makes beamforming more difficult, since both orthogonal polarizations must be controlled with the same number of degrees of freedom, i.e. antenna excitation coefficients.

An additional issue is the beamforming method itself. The projection method proposed by Bucci has the advantage of a relatively fast convergence but may not necessarily find the best solution physically possible. Since its original publication several modifications to the algorithm have been proposed. Also beamforming methods based on global optimization techniques may provide better results, e.g. Genetic Algorithms. In the scope of the present thesis it was, however, not possible to test the performance of other beamforming methods. The simulation results indicate that the performance of the antenna array will be sufficiently high for the major part of the DVB-T frequency range and that passive radar operation will be possible.

Despite the issues mentioned above, the following were the major outcomes of the thesis work:

1) Design of an algorithm to steer the null to any desire direction along the azimuthal plane in a circular array. The algorithm helps to steer a null of fixed beamwidth throughout the 360 degree azimuthal range while maintaining the same sidelobe level. (the sidelobe levels raise when the null is in the direction of the main beam which is not relevant for practical experiments or applications). It involves first performing the beam shaping by introducing masks and then introducing the null for steering which also maintains the required sidelobe levels.
2) Array topology optimization (radius and inter-element spacing) for UWB digital beamforming realized with Bucci algorithm.
3) Study of null dependence on frequency over the operating range.
4) Study of mutual coupling impact on performance of the wideband antenna element (Discone) to be fully operable on the wideband and the corresponding inter element spacing when used in an array.
5) Investigation of the influence of the support structure on the array performance.

7.2 Future work

The wideband antenna array was designed and its operation was verified through simulations. The actual implementation of the designed array antenna in the CORA radar system and its performance with respect to beamforming and null steering will be performed in the near future. The performance of the array antenna will be first checked in the anechoic chamber and field measurements will be done.

Another significant step is the calibration of the array where the antenna is connected to the RF components of the CORA system. By measuring each channel against a pre-defined reference signal, fabrication tolerances of the antennas and variations between individual channels of the electronic back-end may be characterized and compensated for. These data are important for the calculation of the correct array excitation coefficients and will be stored in the system memory.

As for the beamforming procedure itself, it is recommended to compare the Bucci projection method used in the present thesis to other methods which may provide better radiation pattern results, as indicated above.

Bibliography

[1] Robert Watson-Watt, “Three Steps To Victory”, Odhams Press, London, 1958.

[2] S. S. Swords,” Technical history of the beginning of radar”, The institute of engineering and technology 1986

[3] D.Freeman, “the Silent Sentry System”, in AoC 5th Multinational Conference of Passive Covert Radar, November 2007

[4] M.Tobias and A.D.Lanterman, “A probability hypothesis density based multitarget tracker using multiple bistatic range and velocity measurements”. Proc. 36th Southeastern Symp. on System Theory, Atlanta, GA, March 2004, pp. 205–209

[5] H. Kuschel and D. O'Hagan, "Passive radar from history to future,"11th international Radar symposium, pp.1-4, June 2010

[6] LTJ Thornton,“ Passive and Low-Frequency Radar: Theory in Detection of Stealth Aircraft”

[7] M.Conti, F.Berizzi, D. Petri, A.Capria and M. Martorella, "High range resolution DVB-T Passive Radar," Radar Conference (EuRAD), 2010 European , vol., no., pp.109-112, Sept. 30 2010-Oct. 1 2010

[8] P.Knott, T.Nowicki, H.Kuschel , "Design of a disc-cone antenna for Passive radar in the DVB-T frequency range," *Microwave Conference (GeMIC), 2011 German* , pp.1-4, March 2011

[9] T.Nowicki , Internship report, “Discone antenna– element for circular array construction”, August 2011

[10] C. A. Balanis,” Antenna Theory - Analysis and Design” 3rd Edition, John Wiley & Sons, 2005

[11] K.F.Warnick,”Antennas and Propagation for Wireless Communications”,2005

[12] A.W.Rudge, K. Milne , A.D. Olver and P.Knight, “ The handbook of antenna design Vol 2”, IET 1983

[13] P.J.D Gething, “High frequency direction finding”,Proc IEE, 113,Jan 1966

[14] J.T. Starbuck ,” A multiple beam HF receiving aerial system”, Radio Electron Engr, April 1969

[15] J.E.G. Wyatt,” The design of an omnidirectional UHF wrap around antenna”, Journal of Royal Naval Scientific Service, pp 251-258

[16] D.E.N.Davies and M.S.A.S Rizk,” A broadband experimental null steering antenna system for mobile communications”, Radio Electron Engr,48 , Oct 1978, pp 511-517

[17] M.S.Bartlet, “An introduction to Stochastic process” , Cambridge university press, Cambridge, UK 1956

[18] B. Widrow, P.E Mantey, L.J Griffiths and B.B.Goode, “Adaptive antenna systems”, IEEE proc, vol 55,No 12, December 1967

[19] S.P. Applebaum, “Adaptive arrays”, IEEE Transactions on Antenna propagation, Vol 24, No 5, September 1976

[20] L.C. Godara,”Application of antenna arrays to mobile communication”,Proc IEEE,Vol 85,pp1195-1245, August 1997

[21] J. Butler and R.Lowe,”Beamforming matrix simplifies design of electronically scanned antennas” Electron design ,April 1961.

[22] J.P. Shelton and K.S.Kelleher, “ Multiple beams from linear arrays”, IRE transactions Antennas propagation, March 1961.

[23] R.G Pridham and R.A.Mucci ,” Digital interpolation beamforming for low pass and bandpass signals” ,Proc IEEE,Vol 67,No 5 ,1979

[24] S.Anderson, M. Millnert, M.Viberg ,”An adaptive array for mobile communication systems”, IEEE transactions on Vehicular technology, Vol 40,No 2,1991

[25] Wei Liu, Stephan Weiss, ”Wideband beamforming concepts and techniques”, Wiley series 2010

[26] R.T .Compton ,”Adaptive Antennas: Concepts and Performance”, Prentice-Hall, Englewood Cliffs, NJ, USA, 1988

[27] I.S.Reed, J.D.Mallett and L.E.Brennan, ”Rapid convergence rate in adaptive arrays”, IEEE Transactions, AES, Vol 10, pp 853-863, 1974

[28] S.Haykin,”Adaptive filter theory”, Prentice Hall, Englewood Cliffs, NJ, 2002

[29] O.M.Bucci ,G.Franceschetti,G.Mazzarella, G.Panariello,”A general projection approach to array synthesis”,1989 Antennas Propagation symposium, San Jose, USA June 1989

[30] J.Heckenbach and H.Kuschel,” Exploitation of DVB-T signals for passive radar”, Internal report, Fraunhofer FHR

[31] Peter Knott, ”Tutorial wire antennas”, Antenna Engineering

[32] NEC-2 User Manual, ftp://ftp.qsl.net/pub/wb6tpu/NEC/nec2prt1.pdf

[33] http://www.microwaves101.com/encyclopedia/phasedarrays.cfm

[34] I.Liberal, D.Caratelli and A. Yaravoy , “Conformal antenna array for ultra-wideband direction-of-arrival estimation”, International Journal of Microwave and Wireless Technologies, 2011

[35] CST Studio Suite 2012 , Online guide

[36] Peter Knott, ”Tutorial patch antenna design”, Antenna Engineering

[37] W.D.Rawle,” The MoM: a numerical technique for wire antenna design”, High frequency design

[38] A. J. Fenn , D. H. Temme , W. P. Delaney and W. E. Courtney "The development of phased-array radar technology", *Lincoln Lab. J.*, vol. 12, pp.321 2000

[39] M.Simeoni, ” Antenna systems” , ET4015 , TU Delft

[40]L.Josefsson and P.Persson,”Conformal Array Antenna Theory and Design“, IEEE Press Series on Electromagnetic Wave Theory, Wiley-IEEE Press, 2005

Publication

D.W.O'Hagan, V.Basavarajappa, P.Knott, H.Kuschel, M.Ummehofer and M.Simeoni , "*A wideband antenna array for DVB-T based passive bistatic radar applications*" , Accepted in the IET Radar conference, Glasgow, UK, October 2012